The occurrences of ultramafic pegmatites at Dwarsrivier Mine, Lower Critical Zone, Eastern Bushveld Complex, South Africa.

By

CHRISTOPHER SBUSISO LETSOELE

Dissertation submitted in partial fulfillment for the requirements of the degree

MAGISTER SCIENTIAE (MSc.)

In

Geology

In

The Faculty of Natural and Agricultural Sciences

At the

University of Pretoria

Pretoria

July 2017

Supervisor: Prof R.K.W Merkle.

THIS PROJECT REPRESENTS THE ORIGINAL WORK OF THE AUTHOR

EXCEPT WHERE SCIENTIFIC ACKNOWLEDEMENT

IS MADE TO THE WORKS OF

OTHER SCIENTISTS

Page number

DECLARATION.

I**,** Christopher Sbusiso Letsoele, declare that this thesis/dissertation, which is submitted for the partial fulfilment of the degree Magister Scientiae: Applied Mineralogy at the University of Pretoria, is my own unassisted work and has not been previously submitted for the attainment of any degree at this or other tertiary institution.

SIGNATURE

DATE…….July 2017…….

ABSTRACT.

This study presents a detailed petrological and geochemical investigation of the concordant ultramafic pegmatites of the Lower Critical Zone at Dwarsrivier Mine, in the eastern Bushveld Complex. The pegmatites are coarse-grained and of variable size and mineralogy. They occur within the LG-6 chromitite layer as well as in the silicate rocks of the Rustenburg Layered Suite. Field observations into their occurrence, and their association with the LG-6 chromitite layer, suggest that the pegmatites intrude, deform and disrupt the LG-6 chromitite. The mineralogy of the pegmatites is similar as the surrounding pyroxenite rocks, although they are texturally different from the surrounding pyroxenite host rocks. They comprise variable amounts of clinopyroxene, orthopyroxene, olivine, plagioclase, biotite and accessory amphiboles. Based on dominant mineralogy, the pegmatites can be grouped into clinopyroxene-, orthopyroxene- and olivine-rich pegmatites.

The major and trace element composition of the pegmatites is different from the surrounding pyroxenite host rocks. The whole rock geochemistry of the pegmatites indicate that the pegmatites have a slightly higher concentration of incompatible trace elements compared to the pyroxenite host rocks, although compositional overlaps exist. Whole rock Mg# and trace element ratios suggests that the pegmatites are the products of less fractionated liquid(s) than their surrounding pyroxenite rocks.

When the whole rock geochemical data of the pegmatites are compared to other similar concordant pegmatites in the eastern Bushveld Complex, as well as the discordant pegmatites from the western Bushveld Complex, it is established that the pegmatites at Dwarsrivier mine are not genetically related to the discordant, intrusive iron-rich pegmatites. They are also different from the concordant pegmatites found elsewhere in the eastern Bushveld Complex.

The pegmatites are interpreted as the products of a volatile-rich melt which promoted the recrystallization or sub-solidus enlargement of the pyroxenes. The occurrence of cumulus olivine at the stratigraphic position of the Lower Critical Zone is exceptional. Olivine crystalized as a result of continuous phase shifts within the pegmatite melt. Some of the pegmatites are serpentinised by late hydrothermal fluids. The olivine-rich pegmatites display the most prominent serpentinisation, and are composed of a mineral assemblage dominated by serpentine and magnetite.

ACKNOWLEDGEMENTS.

I would like to thank my beautiful wife Nomalizo for her steadfast and unwavering support throughout this project. The many words of encouragements have now borne fruit!

Furthermore, my sincerest gratitude goes to Professor R.K.W Merkle who supervised and guided this project. He has been with me all the way since the beginning of the project. At times I wanted to quit, but I thank him for his encouragements!

Many thanks to Jeanette Strydom at the University of Pretoria Analytical Facilities for performing the XRF analyses of the samples that formed the basis of this project.

This work was funded by a grant from Assmang Dwarsrivier Mine, and I specially thank the management for their financial contribution to the project, notably, Mthi Mtshengu (Former Senior General Manager) and Silas Hlapolosa (Head of Department) for motivating for the financial assistance. The geology and laboratory departments at Dwarsrivier Mine, especially Moses Magakwe and Patience Sedidi are highly appreciated for assistance with sample collection, in the former, and for sample preparation, in the latter.

LIST OF FIGURES

Figure 3.19: Photographs of two separate borehole cores. (A) Borehole DCD 11 and (B) borehole DWR155 showing the intersection of pegmatitic mafic/ultramafic rocks. Note the similarities with regards to the layering, the veins and the colour of the serpentinised pegmatite. A graphical representation of the borehole cores is presented in Figure 3.20 below.

Figure 3.20: A section along A-B showing the boreholes that have intersected the serpentinised pegmatites. The serpentinised pegmatites are intersected at various stratigraphic levels.

Figure 3.21: A sketch depicting an underground section, where a large pegmatite (approximately 100 m) was encountered. The serpentinised pegmatite occurs within the LG-6 chromitite layer, and such a pegmatite will affect mining, resulting in the abandonment of the area. The letters on the plan indicate the position of the cross sections presented in Figure 3.22.

Figure 3.22: Cross sections of various parts of the serpentinised pegmatite shown in Figure 3.16. The LG-6 chromitite layer is deformed by the serpentinised pegmatite. In some instances, the chromitite forms depression structures into the underlying pegmatite (b and f).

Figure 3.23: A schematic cross section showing a reef roll structure. Note the synchronous rolling of the hanging and footwall pyroxenite.

Figure 4.1: Photomicrograph of a fresh, coarse-grained clinopyroxene-rich pegmatite showing euhedral to subhedral clinopyroxene (Cpx) with orthopyroxene (Opx) crystal. Photomicrograph taken in cross-polarised light (XPL). Alteration in the fresh pegmatites is minimal, as can be seen in this photograph.

Figure 4.2: Photomicrograph of the clinopyroxene-rich pegmatite showing orthopyroxene exsolution in primary clinopyroxene. Secondary clinopyroxene develops when olivine is in contact with plagioclase. Photomicrograph taken in cross-polarised light (XPL).

Figure 4.3: Photomicrograph of an orthopyroxene-rich pegmatite showing euhedral to subhedral orthopyroxene in textural equilibrium with clinopyroxene. The orthopyroxene crystals are slightly smaller than the clinopyroxene crystals. Photomicrograph taken in cross-polarised light (XPL).

Figure 4.4: Photomicrograph of an orthopyroxene-rich pegmatite showing orthopyroxene crystals in textural equilibrium with the clinopyroxene. No alteration of either minerals is visible. Photomicrograph taken in cross-polarised light (XPL).

Figure 4.5: An orthopyroxene-rich pegmatite, where orthopyroxene (Opx) coexists with intercumulus plagioclase (Plag) and olivine (Ol). Biotite (Bt) occurs in association with plagioclase. The photomicrograph was taken under crossed polarised light (XPL).

Figure 4.6: Photomicrograph of an orthopyroxene-rich pegmatite showing phlogopite which occurs in association with plagioclase. Photomicrograph taken under XPL.

Figure 4.7: Photomicrograph of an orthopyroxene-rich pegmatite, where orthopyroxene coexists with plagioclase (Plag), olivine (Ol) and clinopyroxene (Cpx). Photomicrograph taken in cross-polarised light (XPL).

Figure 4.8: Photomicrograph of an olivine-rich pegmatite, in which subhedral olivine crystals are poikilitically enclosed by a clinopyroxene crystal. The olivine crystals are well rounded and show evidence of moderate alteration to serpentine, whereas the orthopyroxene crystal does not show alteration. This is common in olivine-rich pegmatites. Photomicrograph taken in cross-polarised light (XPL).

Figure 4.9: A photomicrograph of an olivine-rich pegmatite, where olivine (Ol) crystals occur within a large orthopyroxene crystal. Also in the thin section, there is chromite (Cr) occurring in association with orthopyroxene (Opx). Chromite crystals were observed in the olivine-rich pegmatites only. The olivine shows moderate alteration. Photomicrograph was taken under crossed polarised light (XPL).

Figure 4.10: A photomicrograph of an olivine-rich pegmatite in which serpentine (Serp) replaces olivine. The olivine poikilitically enclosed by clinopyroxene (Cpx) and orthopyroxene (Opx), is almost completely altered to serpentine. Both the clinopyroxene and the orthopyroxene are moderately altered. This is common in olivine-rich pegmatites, where the olivine is almost completely replaced by serpentine. Photomicrograph was taken under crossed polarised light (XPL).

Figure 4.11: A photomicrograph of an olivine-rich pegmatite showing serpentine (Serp) pseudomorphs after olivine. The olivine in this sample is completely replaced by serpentine. Olivine-rich pegmatites show the most severe alteration. Photomicrograph was taken under crossed polarised light (XPL).

Figure 4.12: A photomicrograph of an olivine-rich pegmatite showing that olivine is preferentially altered along crystals fractures to produce magnetite. This is typical of olivine-rich pegmatites. Photomicrograph was taken under crossed polarised light (XPL).

Figure 4.13: A photomicrograph of a moderately altered orthopyroxene-rich pegmatite showing calcite (Cc) and dolomite (Dol) in association with orthopyroxene (Opx). Photomicrograph was taken under crossed polarised light (XPL).

Figure 4.14: A photomicrograph of an altered orthopyroxene-rich pegmatite showing calcite (Cc) in association with orthopyroxene (Opx). The carbonates are a post magmatic replacement feature. Photomicrograph was taken under crossed polarised light (XPL).

Figure 4.15: A photomicrograph of an altered clinopyroxene-rich pegmatite showing prismatic clinozoisite in association with clinopyroxene (Cpx). When the clinopyroxene alters, it produces clinozoisite. Photomicrograph was taken under crossed polarised light (XPL).

Figure 4.16: A photomicrograph of an altered clinopyroxene-rich pegmatite, showing clinozoisite and epidote (Ep) in association with clinopyroxene (Cpx) and orthopyroxene (Opx). The clinozoisite and epidote are common alteration mineral assemblages in the clinopyroxene-rich pegmatites. Photomicrograph was taken under crossed polarised light (XPL).

Figure 5.1(a-c): Binary variation diagrams of major elements showing CaO vs MgO for the pegmatites and their pyroxenite host rocks. The data indicate that the pyroxenite host rocks have lower CaO content than the pegmatites due to the modal abundance of clinopyroxene.

Figure 5.1 (d-f): Binary variation diagrams of major elements showing FeO vs MgO for the pegmatites and their pyroxenite host rocks. The FeO content of the pegmatites is similar to the pyroxenite host rocks.

Figure 5.1 (g-i): Binary variation diagrams of major elements showing SiO_2 vs MgO for pegmatites and their pyroxenite host rocks. There is a compositional overlap in the SiO_2 content of the host rocks and the clinopyroxene and orthopyroxene-rich pegmatites.

Figure 5.1(j-l): Binary variation diagrams of major elements showing Al_2O_3 vs MgO for the pegmatites and their pyroxenite host rocks. In general, the pegmatites have a lower Al_2O_3 than the pyroxenite host rocks.

Figure 5.1(m-r): Binary variation diagrams of major elements showing MnO vs MgO (m-o) and MnO vs FeO (p-r), respectively, for the pegmatites and their pyroxenite host rocks. In general, there is a compositional overlap in the MnO concentration of the pegmatites the pyroxenite host rocks.

Figure 5.1 (s-x): Binary variation diagrams of major elements showing TiO_2 vs MgO (s-u) and TiO_2 vs Al_2O_3 (v-x), respectively, for the pegmatites and their pyroxenite host rocks. In general, the pegmatites have a lower TiO_2 concentration than their pyroxenite host rocks.

Figure 5.1 (y-z): Binary variation diagrams of Na_2O vs MgO for the pegmatites and their pyroxenite host rocks. There is a compositional overlap in some samples of the clinopyroxene and orthopyroxene-rich pegmatites and the pyroxenite host rocks.

Figure 5.2: Binary variation diagrams of (a) Sr vs Al_2O_3 and (b) Sr vs CaO for the pegmatites and their pyroxenite host rocks. The Sr content of the pegmatites overlaps with the pyroxenite host rocks. The clinopyroxene-rich pegmatites have a higher Sr/CaO than the host rocks, as shown in Figure 5.2b.

Figure 5.2 (c-d): Binary variation diagrams of (a) K_2O vs Rb and (b) Sr vs Rb for the pegmatites and their pyroxenite host rocks. The Rb and Sr content of the pegmatites overlaps with the pyroxenite host rocks

Figure 5.2(e-g): Binary variation diagrams of (a) Cu vs Ni (b) Co vs Cu, and (c) Co vs Ni for the pegmatites and their pyroxenite host rocks. The concentration of Cu in the pegmatites is controlled by sulphides, whereas Co and Ni are closely associated with the silicate minerals.

Figure 5.2h: Binary variation diagram of FeO and Zn for the pegmatites and their pyroxenite host rocks. The Zn concentration of the pegmatites overlaps with the pyroxenite host rocks.

Figure 5.2i: Binary variation diagram of V and Cr for the pegmatites and their pyroxenite host rocks. The V concentration of the pyroxenite host rocks is higher than the pegmatites, and its concentration in the former is associated with the presence of chromite.

Figure 5.2j: Binary variation diagram of Zr and Y for the pegmatites and their pyroxenite host rocks. There is a compositional overlap in the Zr and Y concentrations of the pegmatites and the pyroxenite host rocks.

Figure 5.2(k-m): Selected ratios of the pegmatites and their pyroxenite host rocks. There is generally a compositional overlap in the Zr/Y, Rb/Zr and Mg# of the pegmatites and the pyroxenite host rocks

Figure 5.3 (a-e): Selected trace elements variation plotted against stratigraphic height (a) Cu, (b) Co, (c) Ni, as well as trace element ratios (d) Cu/Ni, and (e) Ni/Co. There is generally a sympathetic relationship for the elements Cu, Co, and Ni. The elements Cu, Co, and Ni are compatible into sulphides. The concentration of these elements in this pegmatite is controlled by the presence of sulphides. This is also supported by the trace element ratios Cu/Ni and Ni/Co.

Figure 5.3 (f-h): Trace elements variation plotted against stratigraphic height (f) Cr and (g) V, and Cr/V ratio. There is generally a poor correlation between Cr and V, implying that V is mostly not controlled by Cr in this pegmatite.

Figure 5.3 (j-l): Trace elements and trace element ratios plotted against stratigraphic height (i) Zr, (j) Y, (k) Zr/Y and (l) Ba. There is a sympathetic relationship for Zr vs Y. The elements Zr and Y are

incompatible to silicate melts, and will be concentrated in the residual liquid. The pegmatite also show variation in Zr/Y, implying different melts.

Figure 5.4: Binary variation plots of major elements (a) CaO, (b) FeO, (c) SiO2, (d) Al_2O_3, (e) MnO and (f) TiO_2 plotted against MgO (wt. %), for the pegmatites at Dwarsrivier Mine and at Winterveld Mine (Bristow, 1989). The pegmatites at Dwarsrivier mine are compositionally distinctly from the pegmatites at Winterveld mine with regards to CaO and SiO_2, although there is compositional overlap with regards to the elements MnO, Al_2O_3 and TiO_2. The two pegmatites are not genetically related. Cpx= Clinopyroxene, Opx= Orthopyroxene, Ol= olivine, Peg= pegmatite. Wintevld= Winterveld mine.

Figure 5.4 (Continued): Binary variation plots of major elements (g)TiO_2 vs Zr, (h) CaO vs Sr,(i) V vs Cr_2O_3 and Rb/Zr vs Mg# for the pegmatites at Dwarsrivier mine and at Winterveld mine. There is minimal compositional overlap between the pegmatites at Dwarsrivier Mine and Winterveld Mine (Bristow, 1989). The two pegmatites are not genetically related, although the pegmatites at Winterveld are enriched in Cr_2O_3 than the pegmatites at Dwarsrivier mine. Cpx=Clinopyroxene, Opx= Orthopyroxene, Ol= olivine, Peg= pegmatite. Wintevld= Winterveld mine.

Figure 5.5: A FeO-(Na_2O+K_2O+CaO)-MgO ternary diagram for the comparison of the pegmatites at Dwarsrivier Mine and those at Winterveld Mine (Bristow, 1989). Also plotted are the pyroxenite-host rocks at Dwarsrivier. The pegmatites at Winterveld are different from the pegmatites at Dwarsrivier mine, suggesting no genetic link between the pegmatites at both locations. Also plotted are the pyroxenite host rocks (Pxt) at Dwarsrivier Mine. Cpx= Clinopyroxene, Opx= Orthopyroxene, Ol= olivine, Peg= pegmatite. Wintevld= Winterveld mine.

Figure 5.6: A FeO-(Na_2O+K_2O+CaO)-MgO ternary diagram for the comparison of the pegmatites at Dwarsrivier Mine and Winterveld Mine (Bristow, 1989) and the iron-rich ultramafic pegmatites (IRUPs) (Reid & Basson, 2002). Also plotted are the pyroxenite-host rocks at Dwarsrivier. Pxt=Pyroxenite, Cpx= Clinopyroxene, Opx= Orthopyroxene, Ol= olivine, Peg= pegmatite. Wintevld= Winterveld mine

Figure 5.7: Binary variation plots of (a) CaO, (b) FeO, (c) SiO_2, (d) Al_2O_3, (e) MnO, (f) TiO_2 plotted against MgO (wt. %) for the pegmatites at Dwarsrivier mine and the IRUPs. The geochemistry of the IRUPs (Reid & Basson, 2002) is different from the pegmatites at Dwarsrivier mine. There is no genetic link between these two types of pegmatites. Cpx= Clinopyroxene, Opx= Orthopyroxene, Ol= olivine, Peg= pegmatite. Wintevld= Winterveld mine.

Figure 5.7 (Continued): Binary variation plots of (g) TiO_2 vs Zr, (h) V vs Cr_2O_3, (i) RB/Zr vs Mg#, (j) Cr/V vs Mg# and (k) Zr/Y vs Mg# for the pegmatites at Dwarsrivier mine and the IRUPs. The

geochemistry of the IRUPs (Reid & Basson, 2002) is different from the pegmatites at Dwarsrivier mine. There is no genetic link between the pegmatites.

Figure 6.1: A Fo-Di-Qtz ternary phase diagram showing the effects of H_2O and CO_2 on the olivine-liquidus boundary (Fraser, 2005). Olivine crystalizes first from the liquid, and clinopyroxene crystalizes due to the shift of the olivine-orthopyroxene liquidus boundary towards the diopside field.

LIST OF TABLES

LIST OF ABBREVIATIONS

CZ Critical Zone

g Gram

LZ Lower Zone

LG Lower Group chromitite layers

MG Middle Group chromitite layers

MZ Main Zone

RLS Rustenburg Layered Suite

UG Upper Group chromitite layers

UZ Upper Zone

wt. % weight percentage

XRF X-Ray Fluorescence

APPENDICES

Appendix 1: Sample preparation, analytical procedure, analytical conditions.

Appendix 1a: Sample collection.

Appendix 1b: Sample preparation.

Appendix 1c: XRF analysis

Appendix 1d: XRF calibration

Appendix 2: Dimensions of some of the pegmatitic mafic/ultramafic rocks at Dwarsrivier mine.

Appendix 3: Major element geochemistry of the unaltered pegmatites.

Appendix 4: Trace element geochemistry of unaltered pegmatites.

Appendix 5: Major element geochemistry of the altered pegmatites.

Appendix 6: Trace element geochemistry of the altered pegmatites.

Appendix 7: Major element geochemistry of the host rocks at Dwarsrivier mine.

Appendix 8: Trace element geochemistry of the host rocks at Dwarsrivier mine.

CHAPTER 1

INTRODUCTION.

1.1. Locality of study area.

Dwarsrivier Mine is located on the farm Dwarsrivier 372KT in the north-western part of the southern compartment of the Lower Critical Zone of the eastern Bushveld Complex (Figure 1.1). The towns of Lydenburg and Steelpoort are located 60 and 30 km, respectively, away from the mine. The world renowned Dwarsrivier National Monument with excellent UG-1 exposures (Voordouw *et al.*, 2009b) is also located on the farm Dwarsrivier 372KT. Dwarsrivier mine is an underground, mechanized bord and pillar chrome mine that currently exploits the Lower Group chromitite layer number 6 (LG-6). The mine uses a twin decline system, wherein one decline is used for machinery and material transport, and the other decline is for personnel transport. The declines divide the mine into a south and a north section. The western portion of the farm is occupied by Two Rivers platinum mine, which mines the Upper Group chromitite layer number 2 (UG-2) and the Merensky Reef.

1.2. Purpose of the study.

The rock succession at Dwarsrivier Mine contains concordant ultramafic pegmatites at various stratigraphic intervals. These rocks are hosted by, and are disruptive to both, the silicate and the chromitite rocks at Dwarsrivier Mine. Numerous pegmatite outcrops within the LG-6 chromitite layer have been exposed during mining. The pegmatites are a major concern with regards to grade control at the mine. The occurrences of the pegmatites at Dwarsrivier Mine has not been documented previously. This study is undertaken to investigate the occurrence of the pegmatites. The investigation presents the following aspects:

1. To document the occurrence of the pegmatites with regards to their spatial distribution, in relation to the LG-6 chromitite layer.
2. To document their lithological and mineralogical characteristics.
3. To investigate the geochemical (major and trace elements) characteristics.
4. To document their relationship(s) to the host rocks at Dwarsrivier Mine.
5. To investigate their similarity to, and /or difference from other pegmatites in the Bushveld Complex.

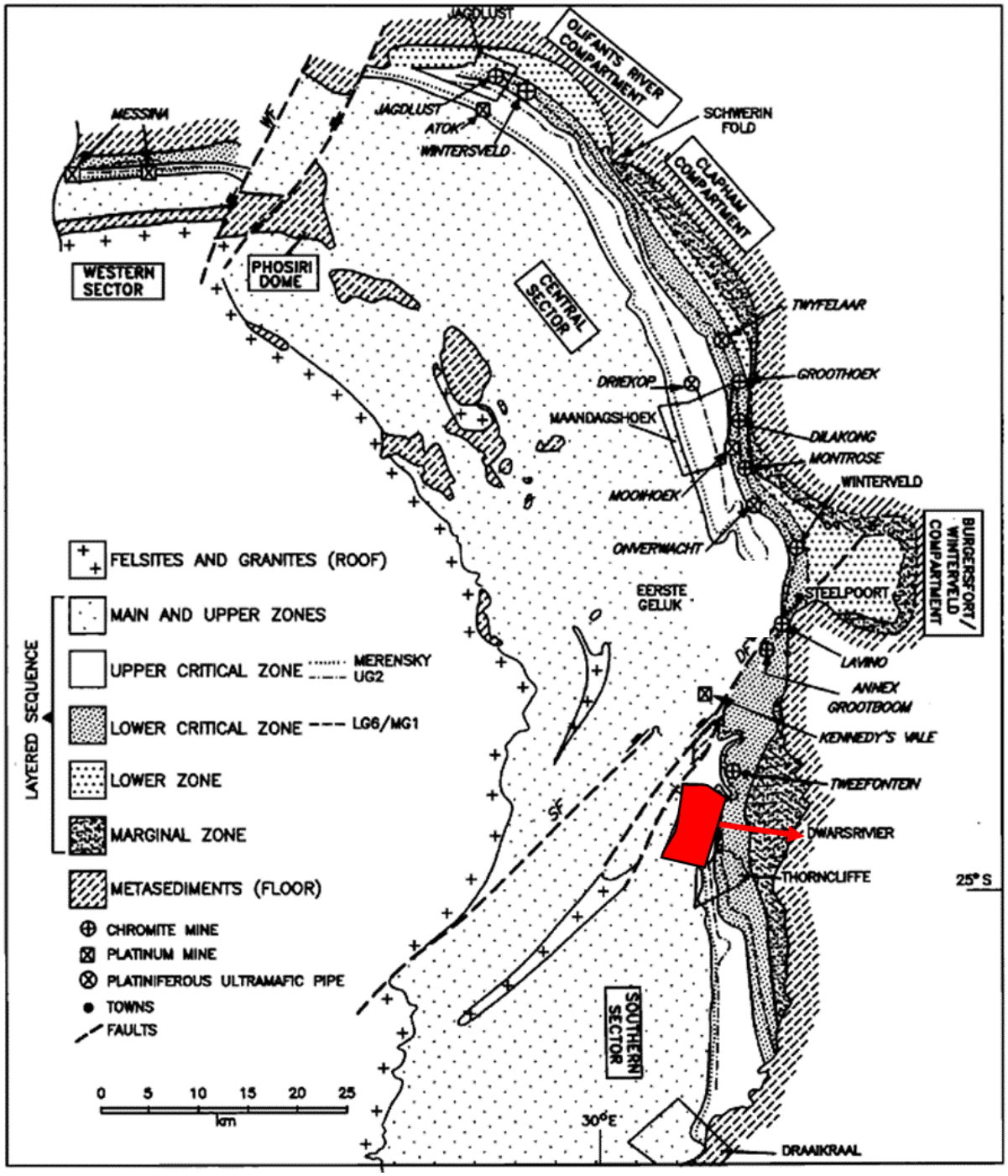

Figure 1.1: The geology of the eastern Bushveld Complex, and the locality of the study area (shaded in red), (Modified after Scoon & Teigler, 1995).

1.3. Scope of study.

A lithological, geochemical, and petrographic investigation of the pegmatites presented in this thesis. The lithological investigation focuses on the occurrences of the pegmatites and their lithological variations. The geochemical investigation reports on the whole rock geochemistry with regards to major and trace elements only. Finally, the petrographic description focuses on the major rock forming minerals, their occurrences and petrographic characteristics.

1.4. Methodology.

Detailed underground mapping and sampling were carried out on the underground exposure of pegmatites at Dwarsrivier Mine. Samples were collected manually from different underground outcrops for analysis of whole rock geochemistry and for thin sections. Sample collection and analytical procedures are listed in Appendix 1.

1.5. Previous work.

Pegmatites were first recorded in the eastern Bushveld Complex as far back as 1929 by Wagner when he discovered an Mg-rich dunite pipe that contained platinum group elements (PGE) of economic levels (Cawthorn, 1999; Wagner, 1929). Since then, numerous pegmatites (though un-economic) have been discovered in various location across the eastern Bushveld Complex by several researchers (Scoon and Mitchell, 1994; Viljoen & Scoon, 1985; Viring & Cowell, 1999). Research into the pegmatites mainly focused on the discordant and intrusive pegmatites, collectively known as iron-rich ultramafic pegmatites (IRUP). However, it has since been discovered that there exist other pegmatite types which are concordant to the rocks of the Bushveld Complex. These pegmatites are associated with the UG2 chromitite layer and the Merensky Reef (Cawthorn & Barry, 1992; Cawthorn & Boerst, 2006; Mathez & Mey, 2005; Nicholson & Mathez, 1991; Viljoen, 1999; Voordouw & Beukes, 2009). Pegmatites are also associated with the chromitite and silicate rocks of the Lower Critical Zone, one example of which are the pegmatites at the Winterveld Mine documented by Bristow *et al.* (1983) and Bristow (1989). The Winterveld mine occurs on the farm Winterveld 293KT, about 35 km south of the study area (Figure 1.1).

The pegmatites described by Bristow *et al. (*1983) and Bristow (1989) at the Winterveld Mine occur in both the chromitite and silicate rocks of the Lower Critical Zone. They are described as being disruptive to mining, and vary in size and shape. The pegmatites are coarse-grained and display similar mineralogy as the host pyroxenite. Bristow (1989) grouped the pegmatites on the basis of dominant mineralogy into: clinopyroxene-, orthopyroxene-, olivine-, and amphibole-rich pegmatites. He concluded on the basis of their relationship with the host rocks, as well as their geochemistry, that there is a genetic

relationship between the pegmatites and their host rocks. He proposed that the pegmatites postdate the formation of the host rocks, and they were crystallized as a result of the migration of intercumulus liquid(s) that prevailed during the late stage consolidation of the host rocks. In this model, the pegmatites formed as a result of either the recrystallization of pyroxenite cumulates in the presence of a volatile-rich liquid, or by the crystallization and growth of pyroxenes from a volatile enriched liquid. This occurred contemporaneously with the formation of the pyroxenite host rocks, hence the disruptive nature of the pegmatites.

As far as the author is aware, a documentation of the occurrences of serpentinised pegmatites in the eastern Bushveld Complex has not been carried out. This may possibly be due to the lack of outcrops or difficulty in accessing mine sites that contain these rocks. In the literature, there is a study on the occurrences of fresh pegmatites at the Winterveld Mine, eastern Bushveld Complex, as described above (Bristow, 1989; Bristow *et al.*, 1983). In the study by Bristow (1989), the pegmatites were referred to as ‘pegmatoids’. However, according to the American Glossary of Geology, the term ‘pegmatoid’ is no longer preferred, and its use has been discontinued. The term ‘pegmatite’ is recommended to describe coarse-grained igneous rocks, and will be used throughout this thesis.

CHAPTER 2: GEOLOGICAL OVERVIEW

2.1. Introduction.

The unique geology of the Bushveld Complex has over the past decades attracted researchers from all over the world, resulting in the accumulation of a large body of knowledge. Aspects that have received attention, amongst others include the parental magmas of the Bushveld Complex (Davies *et al*., 1981; Eales, 2000; Harmer & Sharpe, 1985; Sharpe, 1981, Sharpe,1986), the formation of the chromitite layers (Cameron 1978, 1980; Kinnaird *et al*., 2002; Naldrett *et al*., 2002; Schürmann, 1998;), and the fractionation processes that took place in the magma chamber (Barnes, 1986; Billhaus & Stumpfl, 1986; Eales *et al*., 1988; Eales *et al*., 1990; Eales, 2000; Teigler & Eales, 1996). In addition, there are other enigmatic features that are associated with the normal magmatic rocks of the Bushveld Complex. These features usually disrupt the rocks of the Bushveld Complex, and are useful in providing invaluable insight into the magmatic evolution of the Bushveld Complex. Features such as the discordant, disruptive, and pipe-like pegmatites called the Iron Rich Ultramafic Pegmatites (IRUP) (Reid & Basson, 2002; Scoon & Mitchel, 1994; Viljoen & Scoon, 1985) as well as the concordant ultramafic pegmatites (Bristow *et al.*, 1983; Bristow, 1989), have received a considerable amount of attention in the past. The existence of pegmatites within the Bushveld Complex is an integral part of the evolution of the Bushveld Complex, as it gives insight into the processes that occurred during the formation of the layered sequence (Scoon & Viljoen, 1985).

A short overview of the stratigraphy of the Bushveld Complex is presented below, followed by the regional geology of the eastern Bushveld Complex, and lastly the local geology of the local study area.

2.2. Geological setting of the Bushveld Complex.

The Bushveld Complex was emplaced onto the Kaapvaal Craton and was intruded into the metasedimentary rocks of the Transvaal Supergroup in the Paleoproterozoic ~2.06 Ma (Scoates & Friedman, 2008). It is endowed with an enormous mineral wealth, which includes platinum group elements (PGE) (Cawthorn, 1999; Lee & Tredoux, 1986; Viljoen & Schürmann, 1998; von Gruenewaldt *et al*., 1986); chromite (Cameron, 1977; Cameron & Emerson 1959; Schürmann *et al*., 1988), titanium and vanadium (Cawthorn & Molyneux, 1986; Klemm *et al.*, 1985; Reynolds, 1986a,b; Van der Merwe, 1978; Viljoen *et al.*, 1986). The rocks of the Bushveld Complex cover an area of about 65000 km^2 (Tankard *et al.*, 1982) and are subdivided into: the mafic/ultramafic rocks of the Rustenburg Layered Suite (RLS), the felsic rocks of the Rashoop Granophyre suite, and the Lebowa Granite Suite (Hall, 1932; SACS, 1980; Tankard *et al.*, 1982). Only the Rustenburg Layered Suite will be discussed

in this thesis as the pegmatites are contained within it. The rocks of the RLS outcrop in four major lobes or limbs, namely, the eastern, western, far western and the northern lobe (also known as the Potgietersrus Limb). A fifth lobe, known as the Bethal lobe, is concealed under younger sedimentary cover (Cawthorn & Webb, 2001). These lobes are postulated to have shared a common feeder and may have been connected at depth (Cawthorn & Webb, 2001). Furthermore, these lobes are made up of well-defined cyclic sequences of layered ultramafic/mafic rocks, which are geochemically and lithologically variable, reflecting the unique mixing and differentiation processes that occurred in the basic magma (Cawthorn *et al.*, 2006; Kruger & Marsh, 1982; Maier & Barnes, 1998).

Early workers on the Bushveld Complex initially suggested that the Bushveld Complex intruded as a single lopolith (Daly & Molengraaf, 1924; Hall, 1932). This model was subsequently questioned, largely based on geophysical evidence. Cousins (1959) recognised that based on regional gravity data, the centre of the Bushveld Complex lacks a positive anomaly, and concluded that the ultramafic/mafic rocks are not continuous at depth, but rather consist of two steep-dipping troughs with a dyke-like feeder system. This interpretation was later refined by other workers who suggested that the Bushveld Complex was emplaced as separate intrusions (Cousins, 1959; Meyer & de Beer, 1987; Sharpe *et al.*, 1981), and consists of inward dipping lithologies (Du Plessis & Kleywegt, 1987; Meyer & de Beer, 1987). These observations led Du Plessis (1985) to propose the dipping sheet model for the Bushveld Complex. Subsequent work, on the basis of geophysical data by Cawthorn & Webb, (2001) and Webb *et al.* (2004), proposed that the lobes of the Bushveld Complex are connected at depth. Another model that was proposed for the emplacement of the Bushveld Complex is that of an intrusion triggered by a rising mantle diapirism (Sharpe, 1981). This model was not highly favoured by researchers of the Bushveld Complex.

2.3. The Rustenburg Layered Suite.

Hall (1932) and later the SACS (1980) grouped the cyclic units of the Rustenburg Layered Suite into five zones, namely, the Marginal Zone (MZ); Lower Zone (LZ); Critical Zone (CZ), Main Zone (MZ) and the Upper Zone (UZ). The development and succession of rocks is distinctly different across all five zones.

The **Marginal Zone**, ranging in thickness from 0 to 250 m (Teigler, 1990), is the lowest of the five zones (in terms of stratigraphic position) and is made up of fine-grained, quench-textured rocks such as norites, olivine-rich cumulates, and pyroxenites (Sharpe, 1981). The Marginal Zone has been interpreted as probably representing the relatively rapid crystallization of magmas, which are variably contaminated and differentiated relative to subsequent magmas of the RLS (Cawthorn *et al.*, 2006)

The rocks of the **Lower Zone** are dominated largely by rocks that are constituted of olivine and orthopyroxene, with subordinate chromite, clinopyroxene, plagioclase, and biotite (Eales & Cawthorn, 1996). The main rock types are dunite, pyroxenite, and harzburgite, with intermittent occurrences of norites (Cameron, 1978; Viljoen & Schürmann, 1998). The thickness of the Lower Zone rocks sequence varies markedly and is largely influenced by topography and structure of the underlying sedimentary floor rocks (Cawthorn *et al*., 2006), as the structural complexities in the sedimentary floor have caused localized attenuation of the Lower Zone in certain areas.

The **Critical Zone** has been extensively discussed in the literature (Cameron, 1980; Cameron & Desborough, 1969; Cawthorn *et al.,* 2006; Eales *at al.,* 1988; Kruger, 2005). The Critical Zone is made up mainly of cyclic units (Cameron, 1982; Eales & Reynolds, 1986), and is divided into a pyroxenite-dominated Lower Critical Zone, and a norite-anorthosite-dominated Upper Critical Zone, whose rocks have plagioclase as a cumulus phase (Cawthorn & Walraven, 1998). Nearly all the deposits of economic interest in the Bushveld Complex are restricted to the Critical Zone (Cameron, 1980), except for the magnetite-rich layers which occur in the Upper Zone (Klemm *et al.,* 1985) and the PGE's in the Platreef of the Northern Limb of the Bushveld Complex (Manyeruke *et al.,* 2005; Viljoen & Schürmann, 1998). The Critical Zone is host to some of the world's largest deposits of Platinum Group Elements (PGEs) (Cawthorn, 1999; Kinloch, 1982), as well as vast chromite deposits (Vermaak, 1986, 1997). There are three groups of chromitite layers (Cousins & Ferringa, 1964) in the Critical Zone, namely, the Lower Group (LG), the Middle Group (MG), and the Upper Group (UG), containing up to fifteen individual chromitite layers (Cousins & Ferringa, 1964). The Lower Group has up to seven chromitite layers (LG-1 to LG-7), the Middle Group has up to five chromitite layers (MG-0 to MG-4), and the Upper Group has up to three chromitite layers (UG-1 to UG-3). The development and characteristics of the chromitite layers differ in both the eastern and western lobes of the Bushveld Complex (Hatton & Von Gruenewaldt, 1985; Lee & Parry, 1988). The Platinum Group Elements are hosted mainly by the UG-2 chromitite layer and the Merensky Reef.

The **Main Zone** can be subdivided into five well-layered, mineralogically, and texturally different subzones denoted A to E (Nex, 1998). The stratigraphic sequence of the Main Zone is geochemically distinct from the underlying Critical Zone, with cumulates of the Main Zone having REE contents that are similar to the B3 marginal rocks (Maier & Barnes, 1998; Sharpe, 1981). The Main Zone sequence is dominated mainly by norites, pyroxenites, and gabbronorites with some anorthosites (Eales & Cawthorn, 1996; Mitchel, 1996; Von Gruenewaldt, 1973). Major rock forming minerals are plagioclase and calcium-poor clinopyroxene (Von Gruenewaldt & Weber-Diefenbach, 1977) and minor amounts of quartz, alkali- feldspar and apatite (Maier & Barnes, 1998). The thickness of the Main Zone varies in both the eastern and western limbs and can reach a thickness of up to 4400 m, which makes it the thickest of the other four zones of the Rustenburg Layered Suite. The Main Zone in both the eastern

and western limbs of the Bushveld Complex is considered to be barren of economically exploitable deposits (Barnes & Maier, 2002), while in the northern limb of the Rustenburg Layered Suite, the presence of economic Cu-PGE has been reported by McDonald *et al.* (2017).

The **Upper Zone** has a cumulative thickness of up to 2000 m and hosts between 25-30 magnetite layers (Tegner *et al.*, 2006). The magnetite layers are associated with anorthosite, troctolite and ferrogabbros layers (Klemm *et al.*, 1985). Three subzones (named subzone A-C) have been broadly identified in the Upper Zone (Klemm *et al.*, 1985; Molyneaux, 1970; Reynolds, 1985; Von Gruenewaldt, 1973). The three subzones identified are:

- The apatite-poor, high Ti-magnetite Subzone A
- The apatite-rich, high Ti magnetite Subzone B
- The apatite-poor low Ti magnetite Subzone C.

Scoon & Mitchell (2011) subsequently refined and expanded the subdivision to five subzones (A-E) on the basis of cumulus mineralogy and whole rock geochemistry, subsequently. The magnetite layers are interpreted to have formed as a result of an episodic increase in the oxygen fugacity at the solid-liquid boundary of the magma chamber (Klemm *et al.*, 1982; Reynolds, 1985).

2.4. The eastern Bushveld Complex.

A comprehensive account of the geology of the eastern Bushveld Complex is given by Cameron (1980), Cameron & Emerson (1959), Scoon & Mitchell (2004), Scoon & Mitchell 2011) and Scoon & Teigler (1995). The eastern Bushveld Complex presents the most complete vertical profile of the Bushveld complex, where the different zones can be seen at outcrop scale (Cameron, 1978). The eastern Bushveld Complex is subdivided into three sectors (Figure1.1): the western, the central, and the southern sectors. Two major faults, the Wonderkop and the Steelpoort faults occur between the western and central sector, and between the central and southern sector, respectively. The central sector shows a large lithological variation and is divided into Clapham, Winterveld and the Jagdlust sections (Cameron, 1977; Figure 1.1). The development and succession of rocks, especially the chromitite layers, differs significantly in each sector (Hatton & von Gruenewaldt, 1987), making it difficult to correlate the chromitite layers because not all the chromitite layers are equally well-developed in each sector (Hatton & Von Gruenewaldt, 1987; Schürmann *et al.*, 1998). For example, in the central sector, the Steelpoort chromitite layer (or the LG-6) is the horizon or “reef” that is generally being mined (Cameron, 1977; Von Gruenewaldt *et al.*, 1986). South of the Steelpoort Fault, in the southern sector, the LG-6 is generally reported as absent and there is a debate in the scientific community whether the mines south

of the Steelpoort fault are mining the LG-6 or the MG-1. However, Lee & Perry (1988) have reported the existence of the LG-6 on the farm Thorncliffe 372KT, which is located about 9 km south of the Steelpoort Fault. This chromitite layer is the same layer that is currently being mined at Dwarsrivier Mine. The MG-1 (Von Gruenewaldt *et al.*, 1986) and sometimes locally the MG-0, are the chromitite layers being mined by various mining companies south of the Steelpoort Fault. At Tweefontein, the chromitite layers belonging to the MG-2 to MG-5 (locally) are currently being mined through open cast mining.

2.5. The geology of the study area.

The farm Dwarsrivier 372KT is located in the southern sector of the eastern Bushveld Complex, south of the Steelpoort fault (Figure 1.1). The rock succession that makes up local stratigraphy consists of pyroxenite, norite and anorthosite together with the intervening chromitite layers (Figure 2.1 and Figure 2.2). There are three groups of chromitite layers in the local stratigraphy. Following the nomenclature of Cousins (1964), they are the Lower Group chromitite layers (LG-5 to LG-6A), the Middle Group chromitite layers (MG-1 to MG-5), as well as parts of the Upper Group (UG) chromitite layers (UG-1). The stratigraphic sequence that include the UG-2 up to the Merensky Reef is exposed in the down dip, western portion of the farm, which is an area currently occupied by Two Rivers Platinum Mine (Mabuza, 2006; Voordouw & Beukes, 2009; Rose, 2010).

Dwarsrivier Mine currently exploits the LG-6 as a chromite ore. On the farm Dwarsrivier 372KT, the LG-6 chromitite layer generally has a north-south strike trend, with a gentle dip of 9-10^{o} towards the west. It ranges in thickness from 0.5 to 2.0 m, and is made up of chromite averaging approximately 40 wt. % Cr_2O_3, with pyroxene and plagioclase forming the silicate matrix. The silicate minerals in the LG-6 chromitite layer typically form spherical nodules, with a general diameter of 5 to 20 mm (Bristow, 1989), thereby giving the LG-6 a distinctive spotted /poikilitic texture, locally referred to as “tarentaal” or “guinea fowl” texture (Kinnaird *et al*., 2002). The spotted nature of the LG-6 chromitite layer is also common to all the chromitite layers found at Dwarsrivier Mine. The LG-6 is fairly homogenous with occasional pyroxenite and pegmatite inclusions. It is bounded above and below by a medium-grained pyroxenite. The pyroxenite inclusions are thin (a few centimetres thick), laterally extensive and have sharp contacts with the host chromitite layer. In contrast, the pegmatite inclusions tend to be larger in size (up to 4 m thick), extensive in length (up to 100 m long) and lensoidal in shape. Furthermore, the pegmatites have irregular contacts with the host chromitite layer.

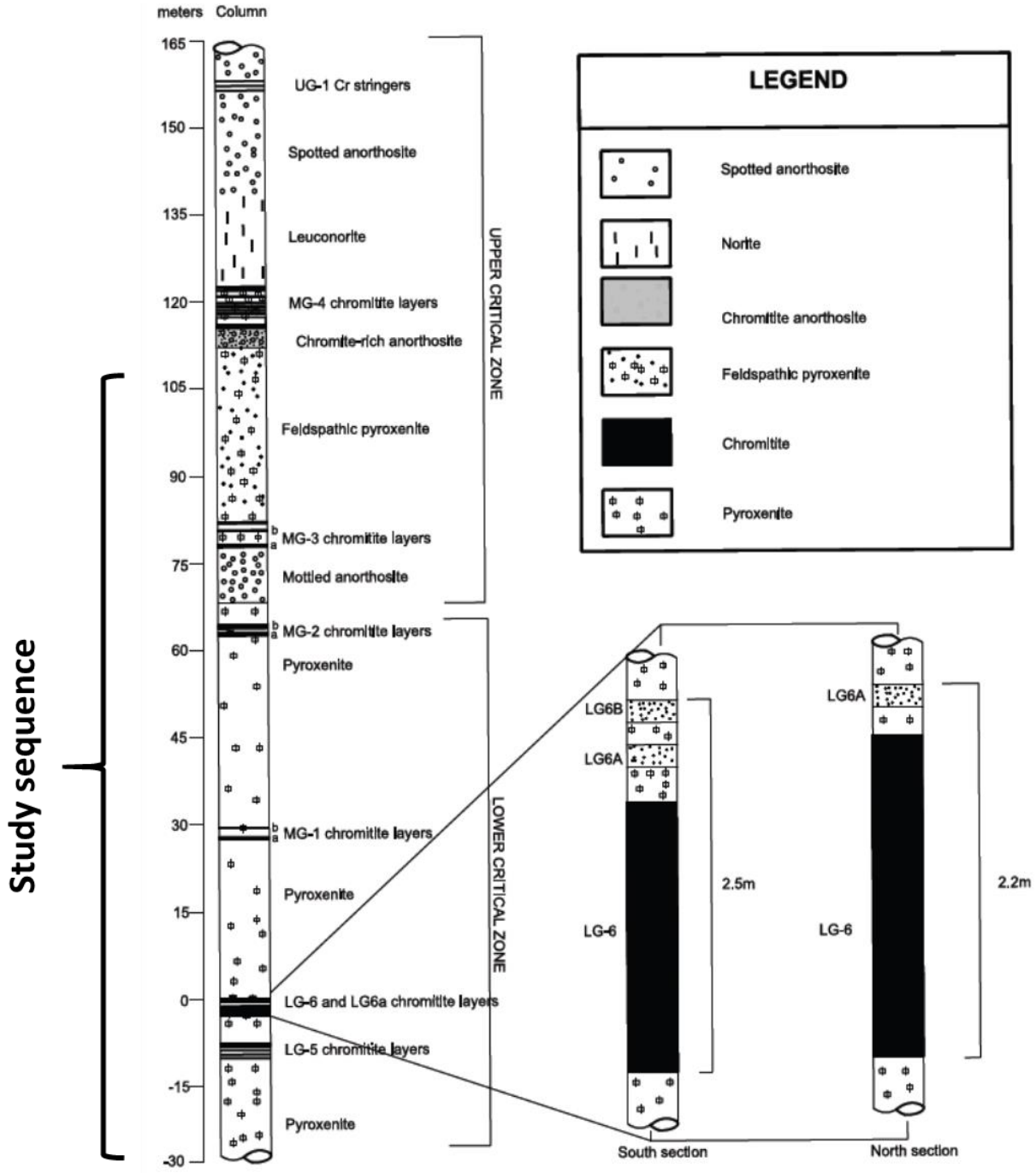

Figure 2.1: Simplified stratigraphic column of Dwarsrivier Mine (adapted from internal company reports). The pegmatites investigated in this thesis are contained within the LG-6 layer.

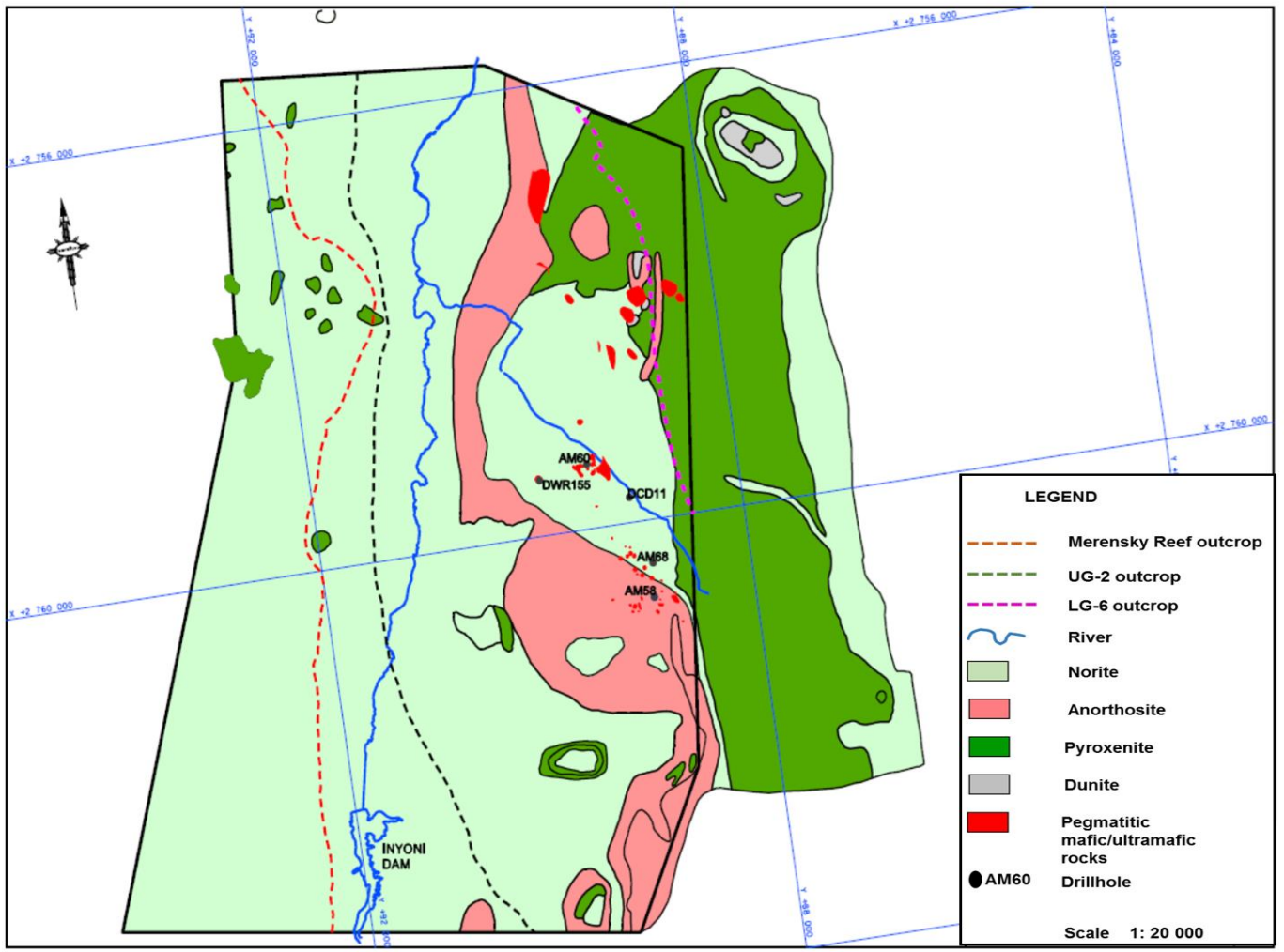

Figure 2.2: A Geological map of the farm Dwarsrivier 372KT. Also shown on the map is the distribution of the pegmatites (shown in red colour) throughout the farm.

CHAPTER 3: THE OCCURRENCES OF PEGMATITES AT DWARSRIVIER MINE.

3.1. Introduction.

The rock succession at Dwarsrivier Mine contains coarse-grained pegmatites of variable sizes and mineralogy. They exhibit a similar mineralogical assemblage as the surrounding pyroxenite host rocks, although texturally, the pegmatites are distinct from the pyroxenite host rocks in that they are coarse-grained. They occur in three stratigraphic horizons relative to the position of the LG-6 chromitite layer: within the LG-6 chromitite layer, within the pyroxenite (silicate) rocks above the LG-6 chromitite layer, and within the silicate rocks below the LG-6 chromite layer. The majority of the pegmatites investigated in this study occur within the LG-6 chromitite layer where they were exposed during mining. Due to their size and abundance, these pegmatites are a major concern with regards to mining and grade control. When large (more than 10 m wide) pegmatites are encountered in the underground areas, these areas are usually abandoned because the pegmatites negatively affect the chrome grade.

3.2. Field relations.

The pegmatites at Dwarsrivier Mine can be divided into two groups on the basis of alteration: Mode 1 and Mode 2. Mode 1 pegmatites are fresh, unaltered pegmatites, whereas Mode 2 pegmatites are altered and usually serpentinised. Mode 1 pegmatites are distributed throughout the mine, whereas Mode 2 pegmatites restricted to the south section of the mine, where they occur in geologically complex areas, characterised by faulting and jointing. Both groups of pegmatites exhibit similar and mineralogical textural characteristics. The pegmatites contain variable amounts of clinopyroxene, orthopyroxene, olivine, interstitial plagioclase and amphiboles such as phlogopite. In hand specimen, the phlogopite occurs as large crystals (Figure 3.1 & Figure 3.2), and is associated with plagioclase.

3.3. The Occurrence of Mode 1 pegmatites.

Mode 1 pegmatites are more common than Mode 2 pegmatites, and occur throughout the stratigraphy that is exposed at the mine. Intersections of Mode 1 pegmatites in the underground sections have indicated that the larger bodies (measuring more than 1 x 1x 1 m) are coarse-grained and exhibit mineralogical and textural layering. The layers are characterised by the prominence of one mineral over the other. The layers could either be clinopyroxene-, orthopyroxene-, or olivine-rich, but they do not

occur in any consistent order (Figure 3.3 and Figure 3.4). Mineralogical layering is more pronounced in the larger (more than 1 m thick) pegmatites. The clinopyroxene-rich pegmatites are more pervasive, followed by the orthopyroxene-rich pegmatites. Orthopyroxene in the clinopyroxene-rich pegmatites occurs as large crystals (Figure 3.5).

The olivine-rich pegmatites are scant. In any layered pegmatite, the olivine-rich layers usually occur as thin layers (a few centimetres) or as patches of medium-grained dunite. Whenever a clinopyroxene-rich layer is in contact with an olivine-rich layer, a reaction rim, not exceeding 2 cm, develops. The reaction rim is made of orthopyroxene (Figure 3.6).

The smaller (less than 1 m thick) fresh pegmatite bodies also show well defined layering (Figure 3.7 to 3.9). Commonly, the smaller pegmatites may be zoned with a clinopyroxene-rich core and an outer orthopyroxene-rich layer (Figure 3.10). During the period of the study no pegmatite was found with an orthopyroxene-rich pegmatite and an outer clinopyroxene-rich layer.

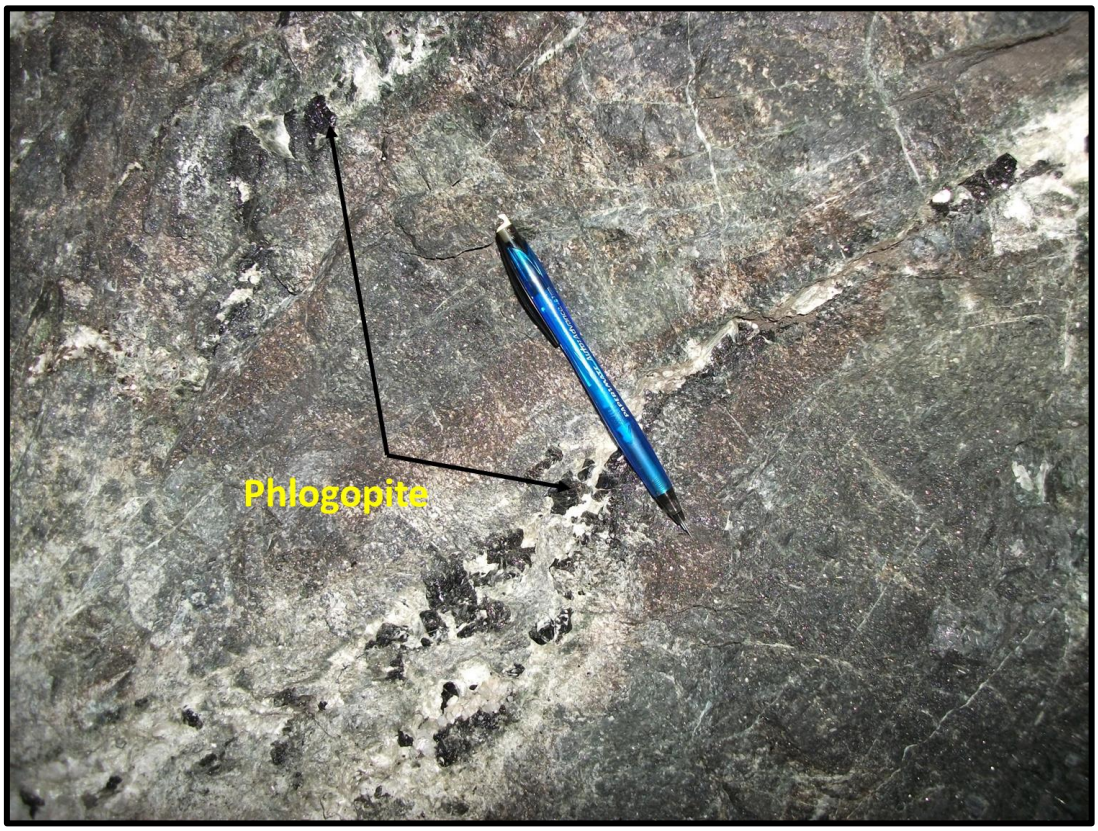

Figure 3.1: A photograph of a pegmatite showing phlogopite flakes. The phlogopite occurs in association with plagioclase.

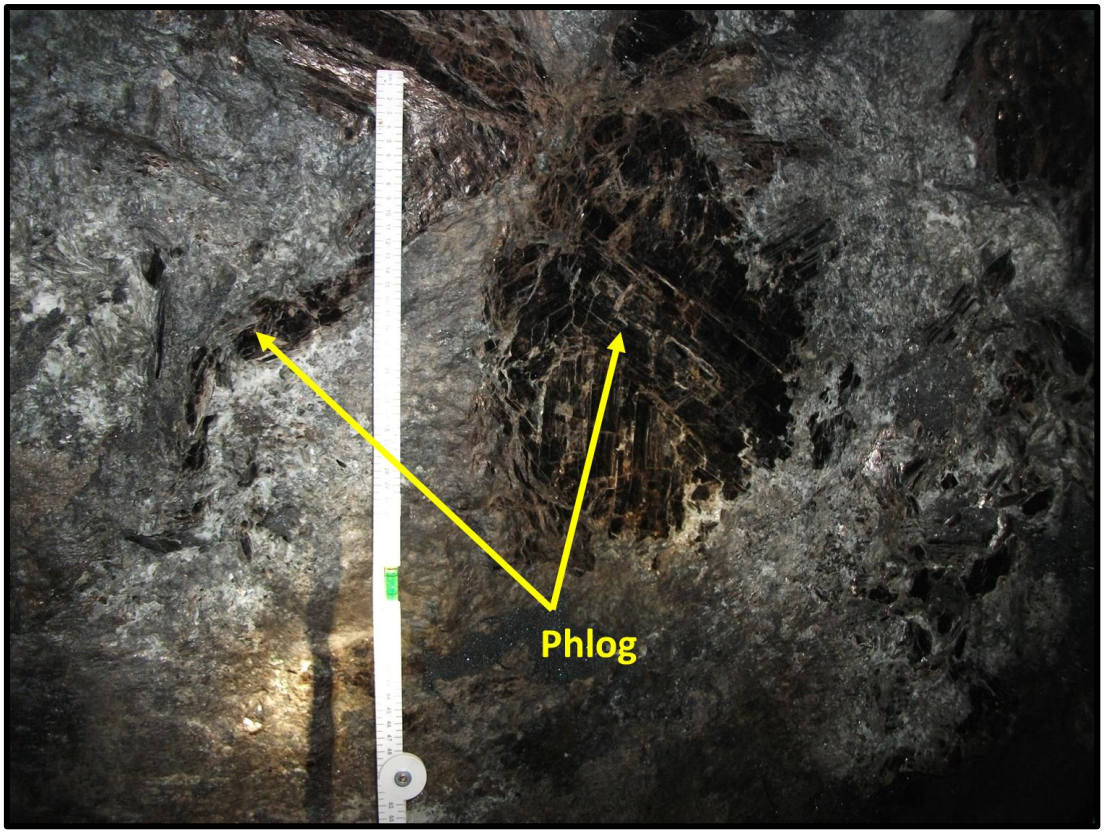

Figure 3.2: a photograph of a pegmatite in which phlogopite occurs as large crystals. This is a rare occurrence of phlogopite in the pegmatites.

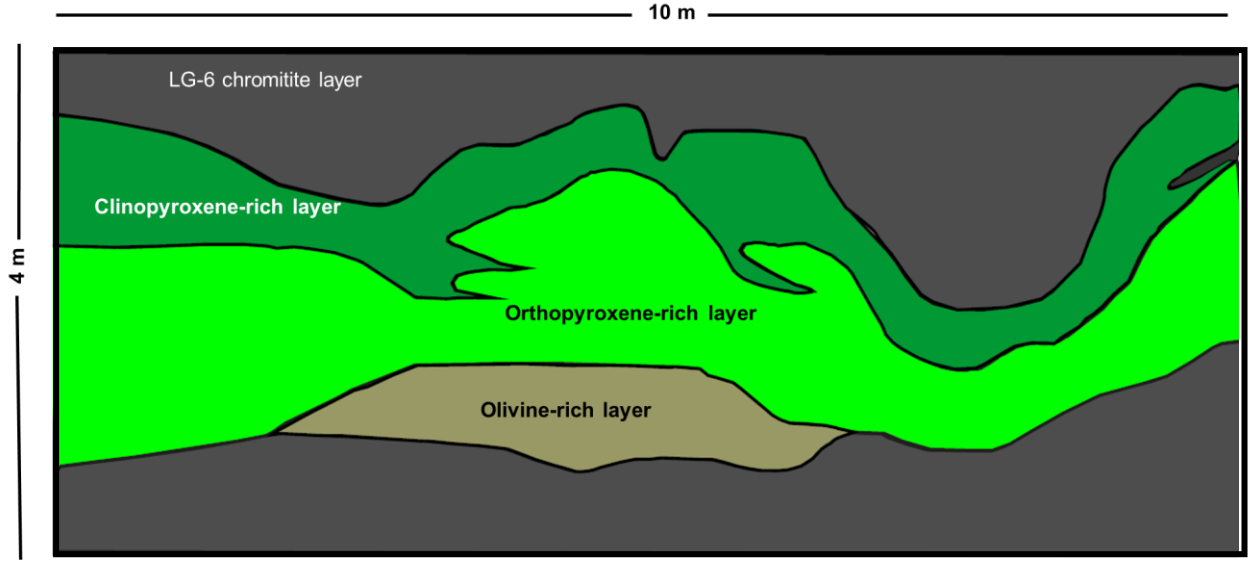

Figure 3.3: A cross sectional sketch of representing a pegmatite that shows mineralogical layering. This layering is very common in larger (more than 1m thick) pegmatites.

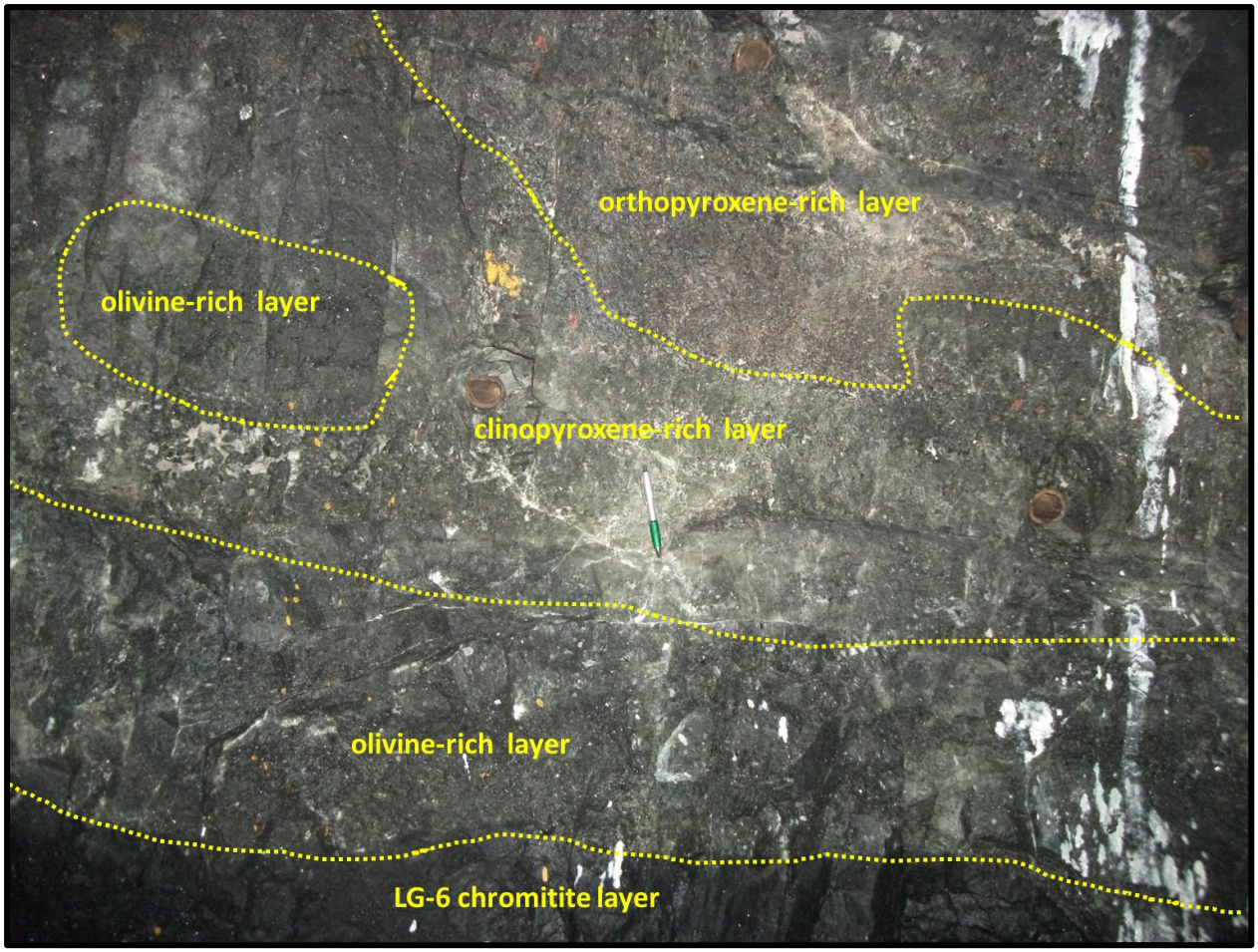

Figure 3.4: A photograph of Mode 1 pegmatite which shows mineralogical layering, where orthopyroxene-, clinopyroxene-and olivine-rich layers are visible. This is one clear example of mineralogical layering in the large pegmatites.

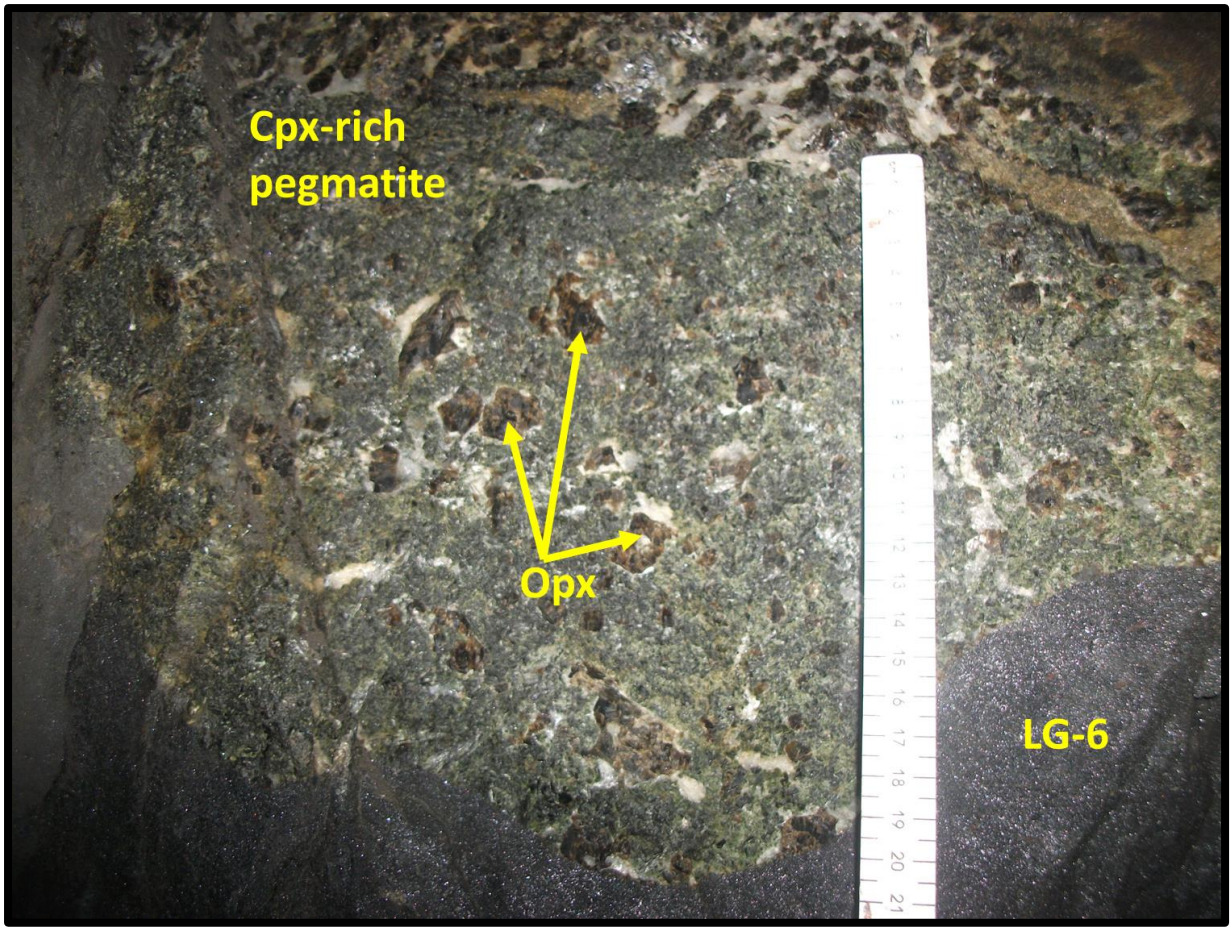

Figure 3.5: A photograph of a clinopyroxene-rich pegmatite showing large orthopyroxene crystals. This texture is very common and characteristic for clinopyroxene-rich pegmatites.

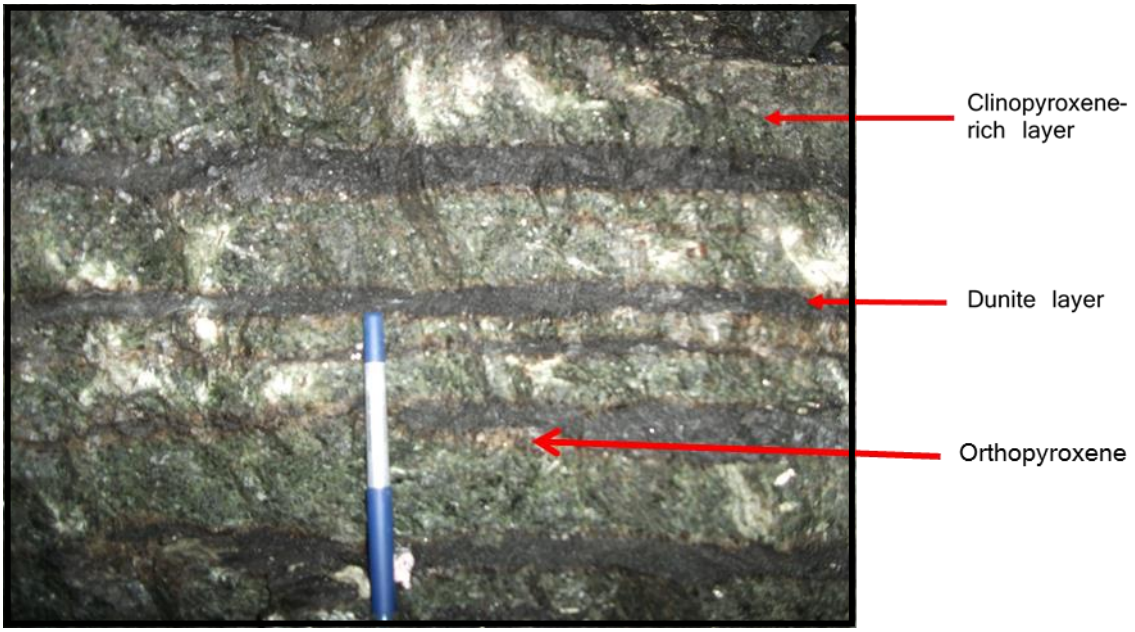

Figure 3.6: A layered pegmatite in which clinopyroxene-rich layers (green) alternate with olivine-rich layers (dark green). These layers are parallel to one another, as well as parallel to the igneous layering of the host rocks. The dunite layers are separated from the clinopyroxene-rich layers by a thin (not more than 2cm thick) layer of orthopyroxene.

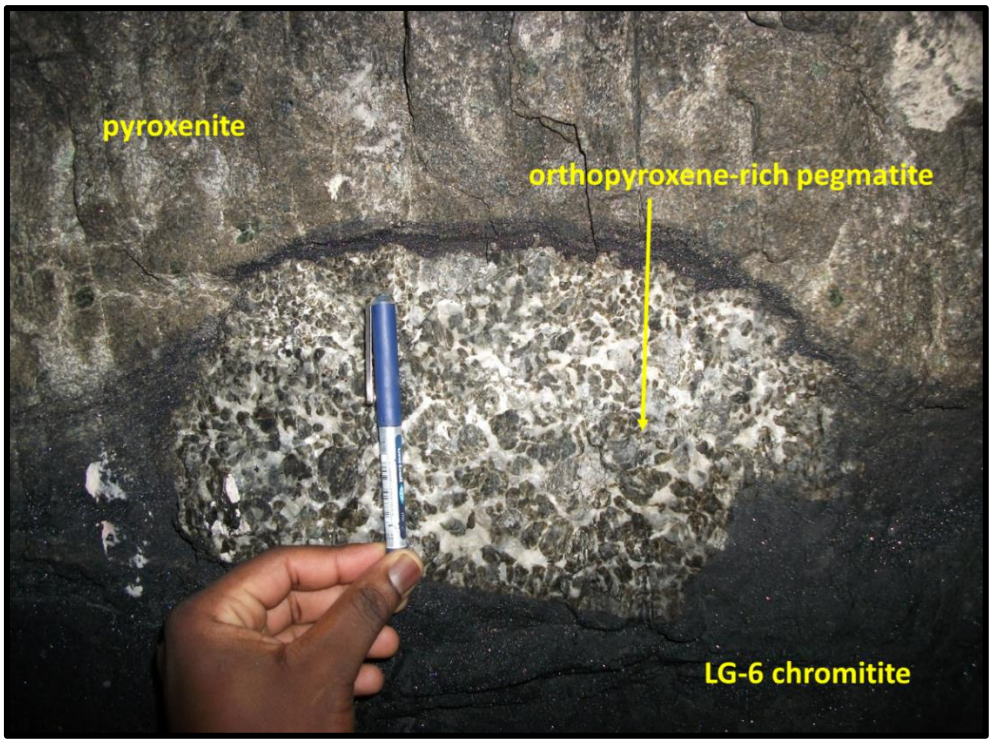

Figure 3.7: A rounded orthopyroxene-rich pegmatite which occurs within the LG-6 chromitite. In this pegmatite, layering is not perceivable. The contact between the LG-6 chromitite layer and the pegmatite is irregular and deformed.

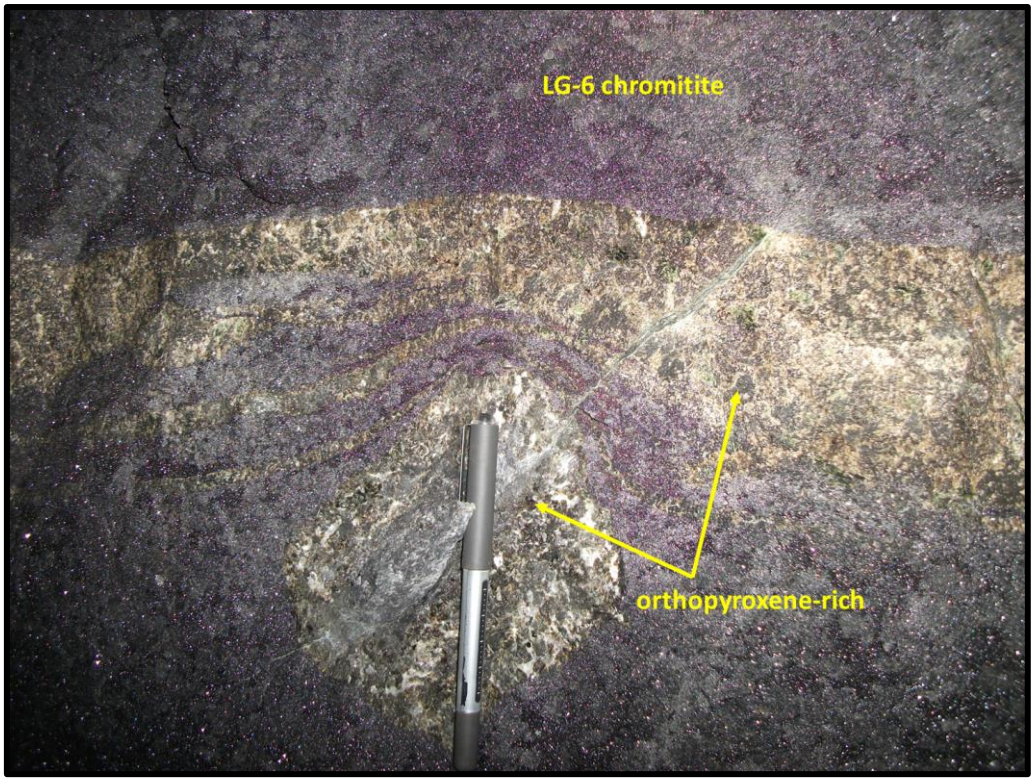

Figure 3.8: Two orthopyroxene-rich pegmatites in which layering is not perceivable. It is very common in the smaller pegmatite bodies not to have perceivable layering.

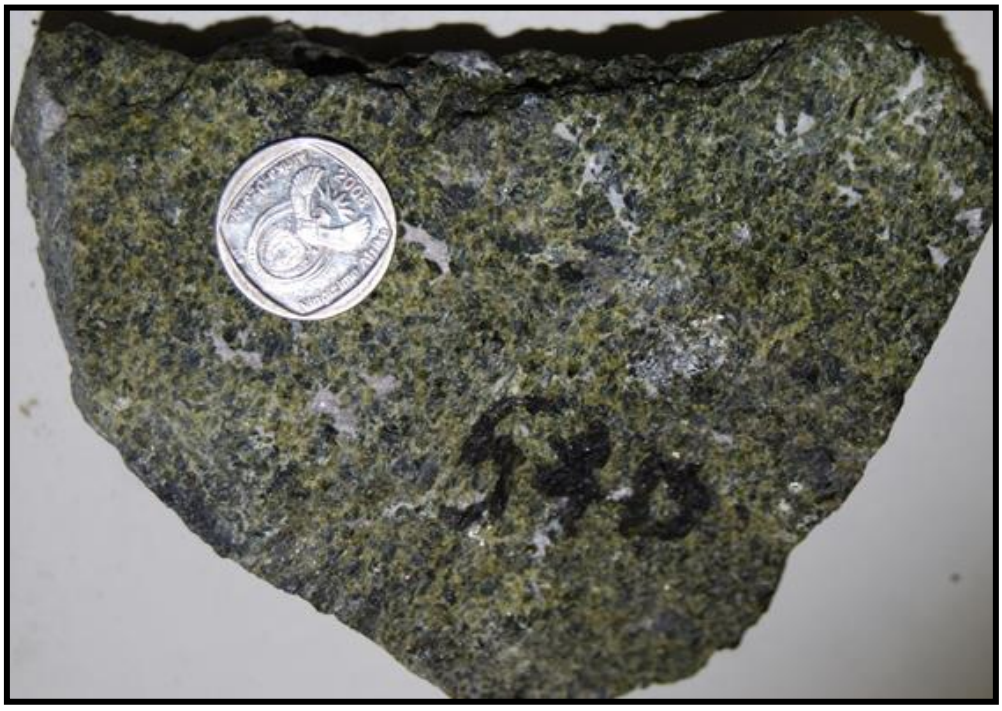

Figure 3.9: A hand specimen of a fresh olivine-rich pegmatite showing a characteristic sugary grain texture.

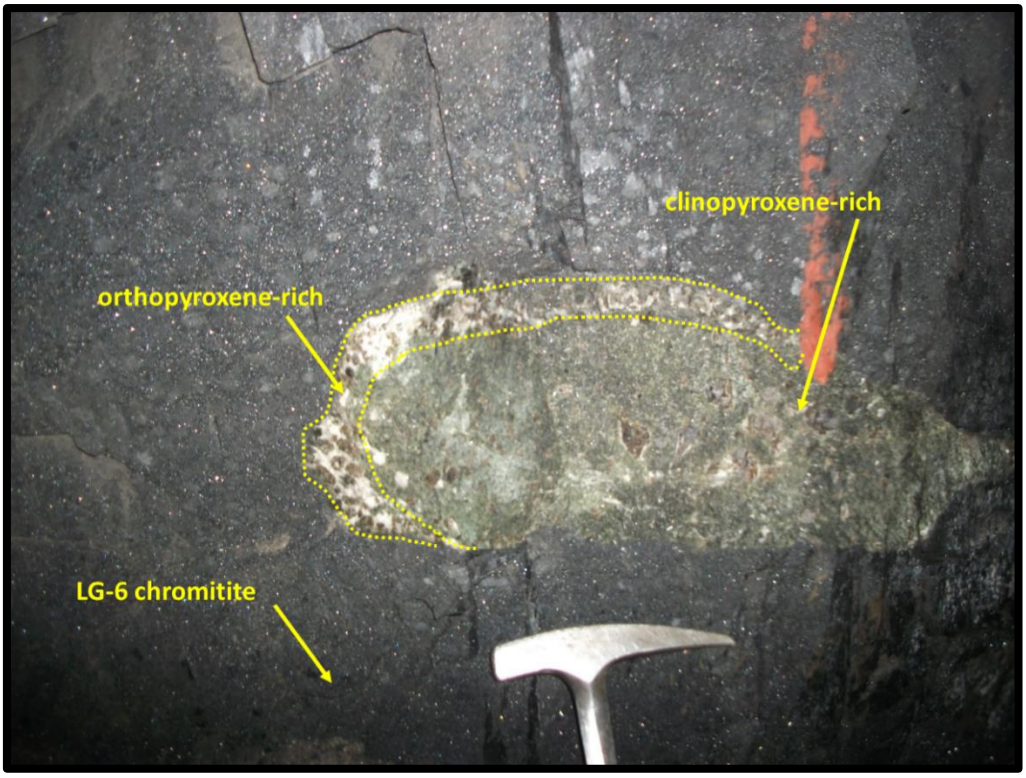

Figure 3.10: A photograph of a clinopyroxene-rich pegmatite that occurs within the LG-6 chromitite layer. The pegmatite is layered.

Several features are worth noting in the Mode 1 pegmatites contained within the LG-6 chromitite layer. The contact between the LG-6 and the pegmatites is usually irregular. In contrast, the contact between the LG-6 chromitite layer and the pyroxenite host rocks is sharp and planar. Furthermore, the contact between the LG-6 chromitite layer and the pegmatites is usually undulating, with the chromitite forming depression structures into the pegmatite.

Moreover, several smaller (typically less than 5 cm thick) chromitite stringers from the host chromitite layer transgress into the pegmatite (Figure 3.11). These chromitite stringers do not continue for more than 50 cm into the pegmatite - they taper off. A thin (about 2 mm) rim of clinopyroxene usually develops around these chromitite stringers. Some of the chromitite stringers may be dismembered from the host chromitite layer, and be completely enclosed by the pegmatite. Moreover, there are cases where large slabs of chromitite occur as xenoliths within the pegmatite, completely separated from the host chromitite. Lastly, the LG-6 chromitite layer may form collapse/depression structures into the pegmatite, in which case the chromitite forms tooth-like structures, protuberant into the enveloping pegmatite.

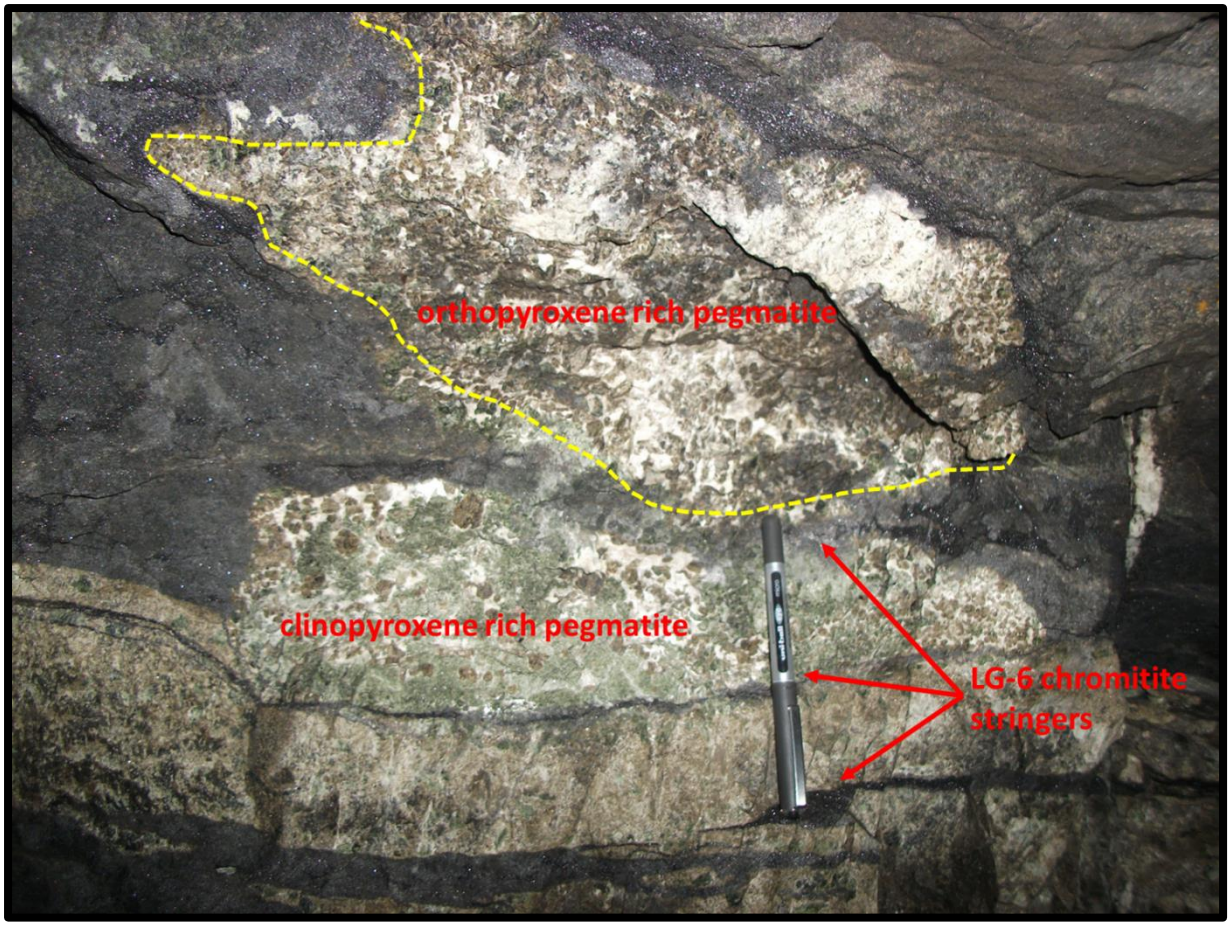

Figure 3.11: A photograph of a layered pegmatite where thin chromitite stringers from the host LG-6 chromitite layer are transgressing into it. The chromitite stringers are not continuous, they taper off.

3.4. Occurrences of Mode 2 pegmatites- the altered (serpentinised) pegmatites.

Mode 2 pegmatites are commonly found in the south section of the mine, generally in association with areas of structural disturbances, characterised by faults and joints. Unlike their Mode 1 counterparts, Mode 2 pegmatites are highly altered, making it difficult to estimate mineralogy in hand specimen. Characteristically, they are made up of two lithological units: a thick (typically 1 m or more) well layered, highly serpentinised unit which forms the core (Figure 3.12 & Figure 3.13A-B), and a partially altered pegmatitic pyroxenite which forms an envelope. The enveloping pegmatitic pyroxenite is coarse-grained, and has a similar mineralogical assemblage as Mode 1 pegmatites, i.e. constituted by variable amounts of clinopyroxene, orthopyroxene, and olivine.

The development of layers (about 1 mm thick) within the serpentinised portion of Mode 2 pegmatites is common (Figure 3.13B), more commonly in the larger pegmatite bodies. This micro layering can

occasionally be deformed and contorted. Variation in the proportion, repetition, and development of individual layers within the serpentinised pegmatites is very common. However, smaller (less than 1 m thick) serpentinised pegmatite bodies tend to show no perceivable layering, just like the smaller Mode 1 pegmatites.

Texturally, the layers in the larger serpentinised pegmatite bodies may either be fine-grained (in which case they are highly serpentinised) (Figure 3.13A-B) or coarse grained, mottled and moderately altered (Figure 3.14C-D). The main minerals that constitute the serpentinised pegmatites are, in the order of decreasing abundance, orthopyroxene, olivine (relicts), serpentine, chlorite, talc, calcite, and magnetite. Some serpentinised pegmatites may display a porphyritic texture, where elongate pyroxene crystals are surrounded by a fine-grained serpentinised matrix. The pyroxene crystals can either be dark brown (altered) (Figure 3.15A) or green (fresh) (Figure 3.15B).

For the purposes of description, Mode 2 pegmatites are grouped in accordance to their association with the LG-6 chromitite layer. They occur:

1. Within the LG-6 chromitite layer.
2. In the silicate rocks above the LG-6.
3. In the silicate rocks below the LG-6.

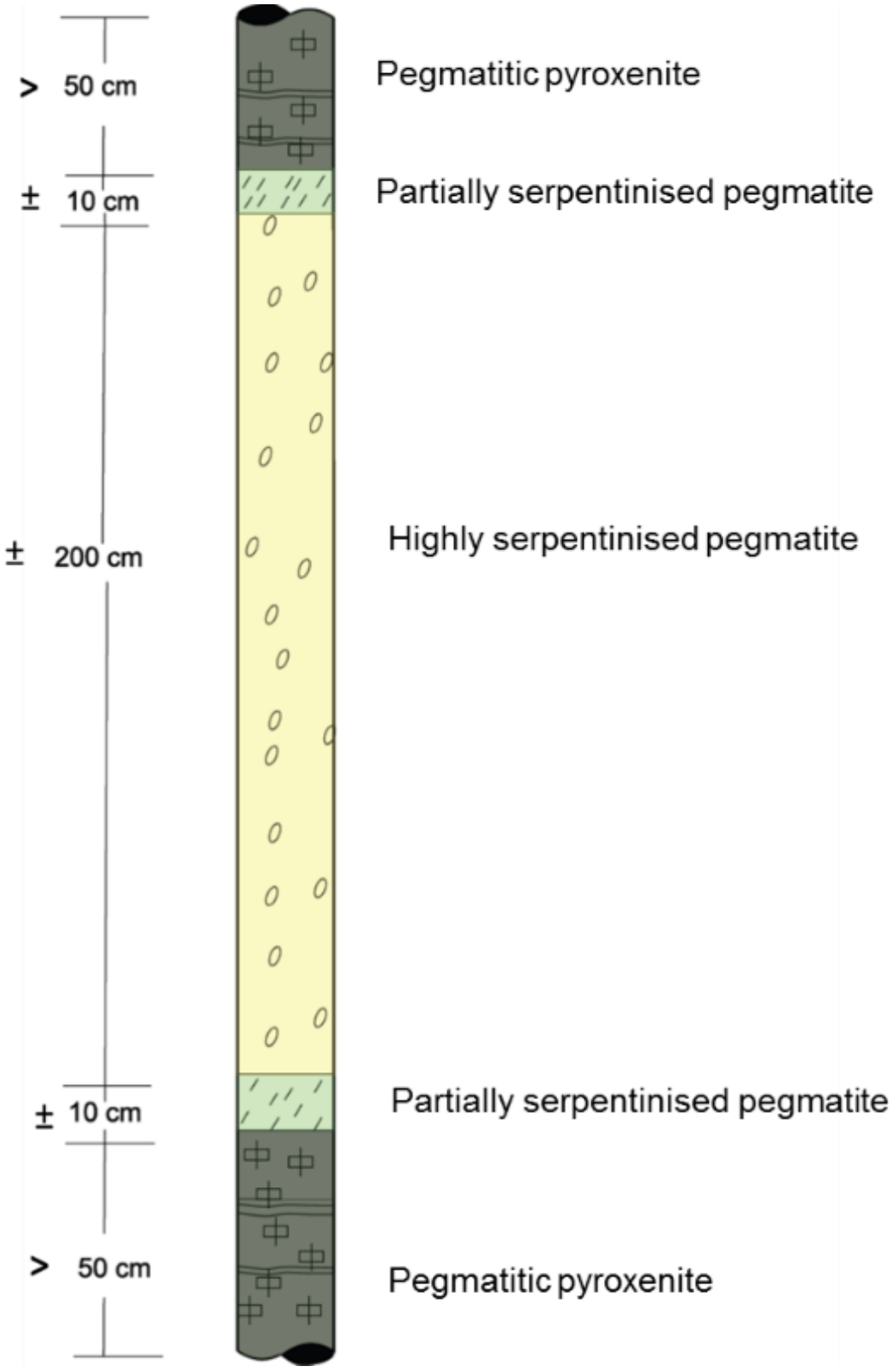

Figure 3.12: Representative section of Mode 2 pegmatites showing the principal lithological units. This pegmatite could be contained within the LG-6 chromitite layer, or it could be in the silicate rocks above or below the LG-6 chromitite layer.

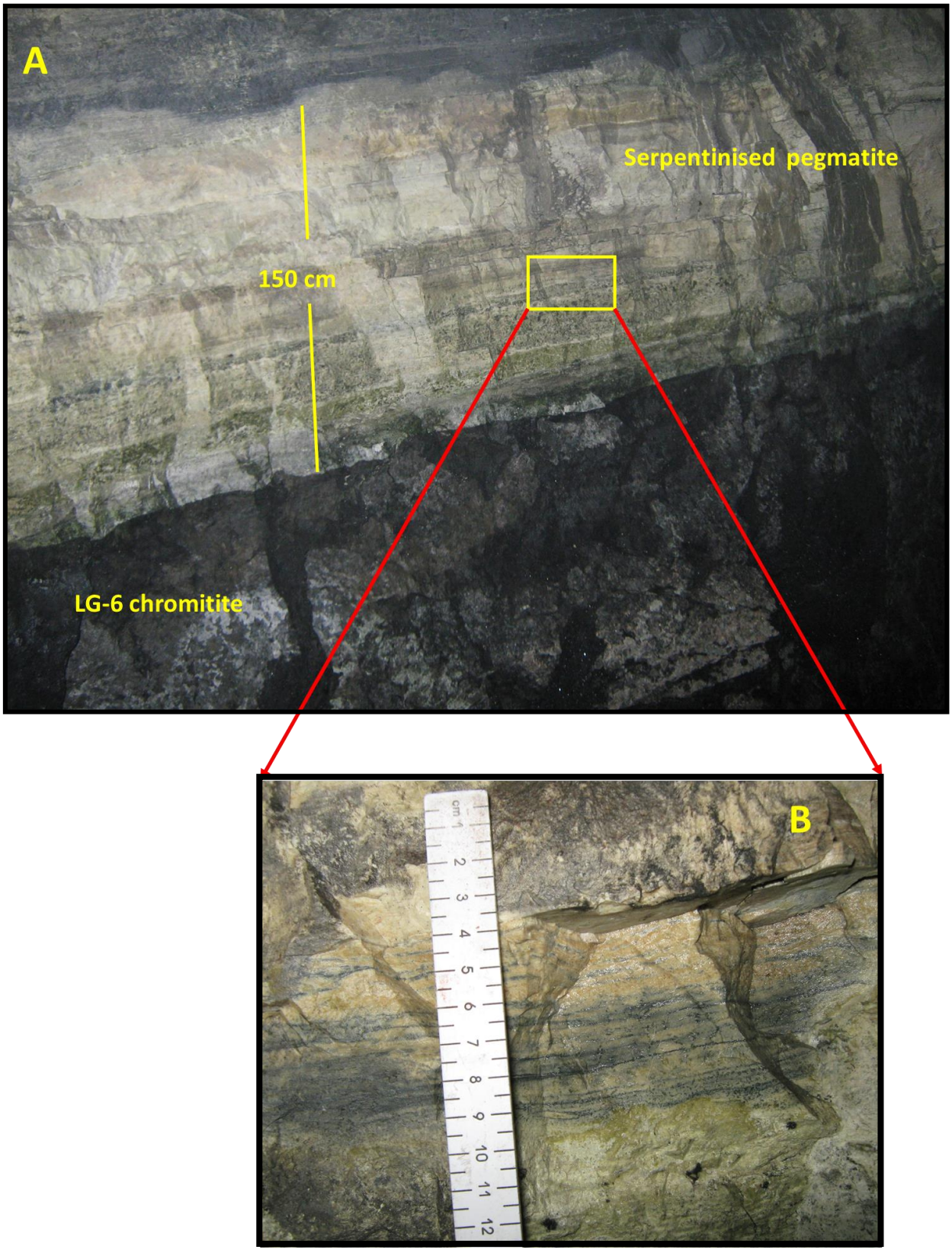

Figure 3.13: Photographs showing underground exposures of a serpentinised pegmatite. (A) A 150 cm thick pegmatite which occurs within the LG-6 chromitite layer. (B) A close-up of the serpentinised pegmatite showing micro-layering.

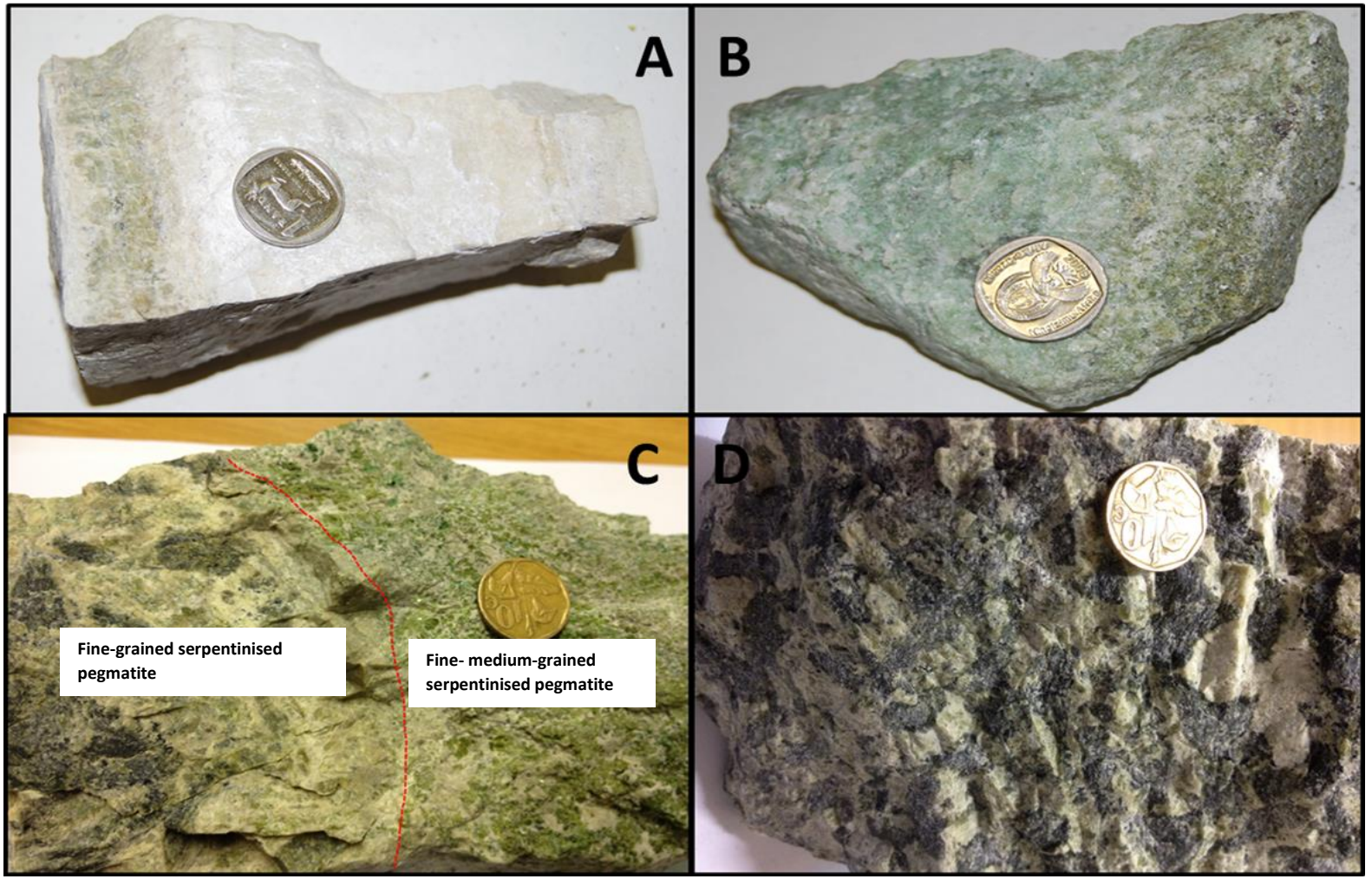

Figure 3.14: Photographs showing the grain size variation in the serpentinised pegmatite. (A) A fine- grained serpentine-rich layer. (B) A clinopyroxene-rich layer, (C) A fine to medium grained serpentinised layer in contact with a fine-grained layer. (D) A mottled serpentinised pegmatite layer.

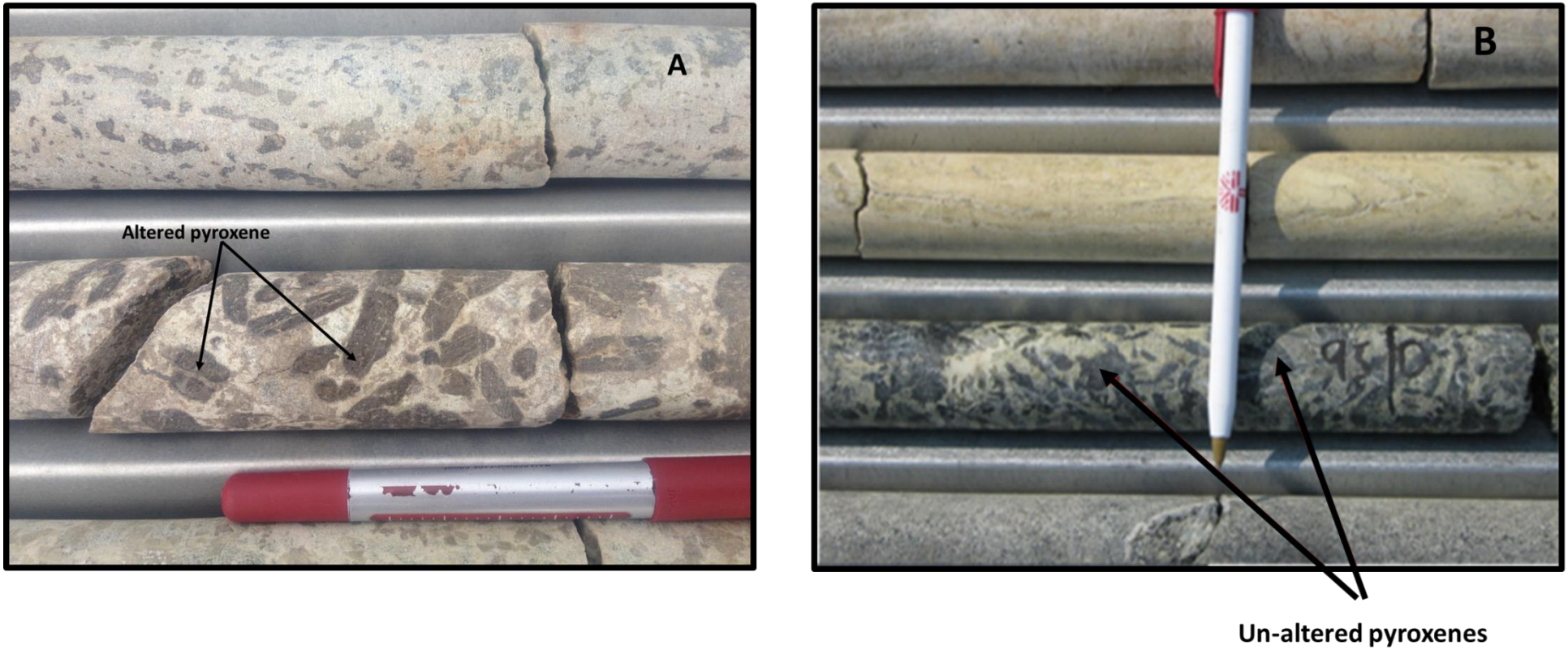

Figure 3.15: Photographs of porphyritic serpentinised pegmatites intersected in borehole core, showing differently coloured phenocrysts of pyroxene. (A) The pyroxenes are altered and brown in colour and (B) the pyroxenes are un-altered and green in colour. In both examples, the pyroxenes are surrounded by a fine grained serpentinised matrix.

3.5. Serpentinised pegmatites contained within the LG-6 chromitite layer.

The serpentinised pegmatites contained within the LG-6 chromitite layer are the most common pegmatites. They are generally lenticular in shape, laterally extensive (up to 100 m in length), and rarely exceeding 2 m in thickness. Commonly, they are enveloped by a coarse-grained pyroxenite. The thickness of the enveloping coarse-grained pyroxenite varies from 10 cm to 50 cm. At one location, at S3B section (Figure 3.16B), the enveloping coarse-grained pyroxenite protruded into the serpentinised pegmatite. With regards to layering, the layering of the serpentinised pegmatite may be deformed, wavy, and contorted.

A reaction rim, generally not more than 10 cm thick, occurs at the contact between the serpentinised pegmatite and its enveloping pyroxenite. The reaction rim is dominated by chlorite. The enveloping coarse-grained pyroxenite can be partially serpentinised (Figure 3.17), is usually green in colour, and is dominated by clinopyroxene with minor plagioclase and quartz. The plagioclase can be occasionally stained, displaying a distinct reddish colour. In rare cases, where the enveloping pegmatite is absent and the serpentinised pegmatite is in direct contact with the LG-6 chromitite layer, a ± 10 cm reaction zone dominated by chlorite is also present, giving the chromitite a distinct greenish-black appearance.

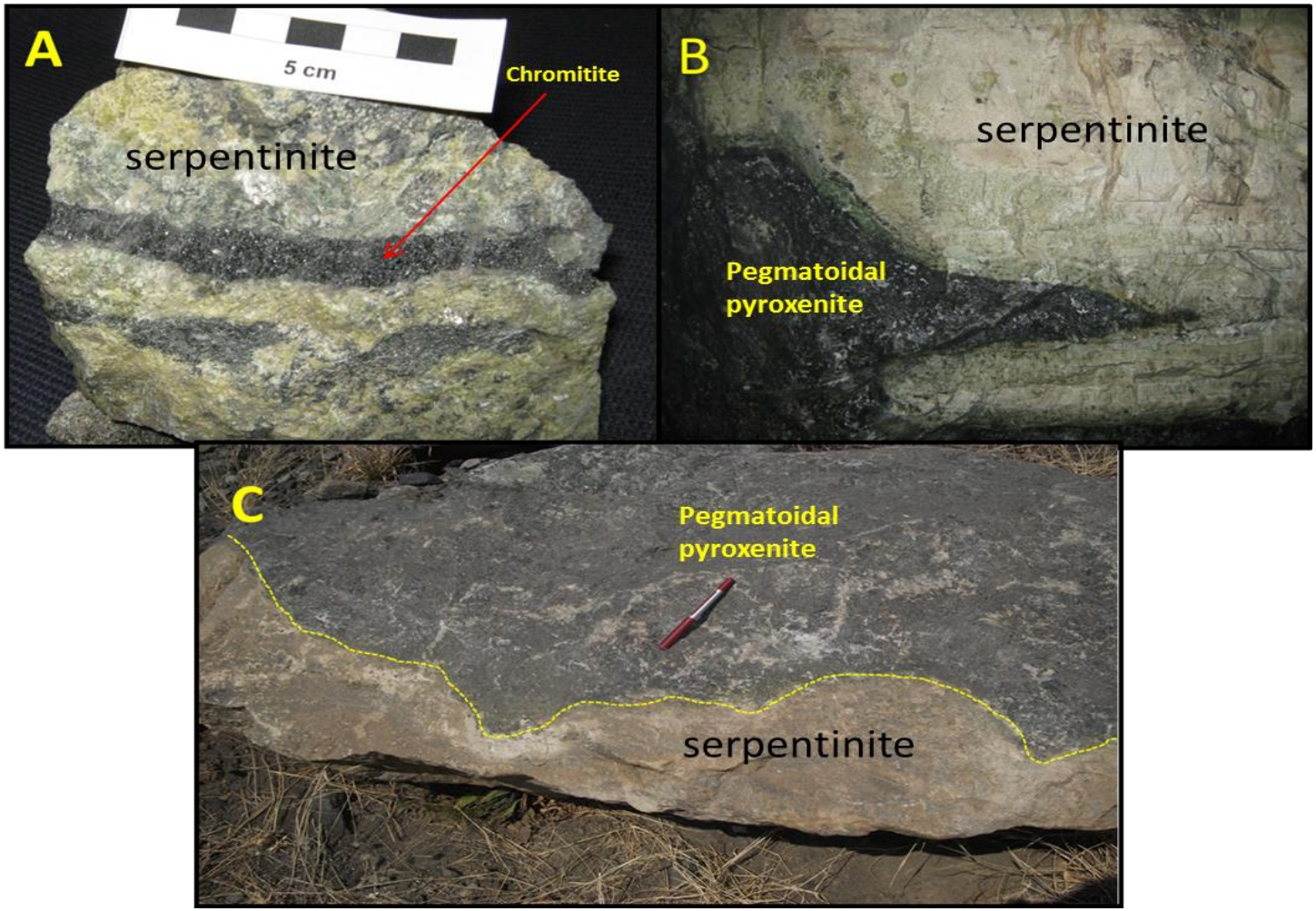

Figure 3.16: Some features seen in the pegmatitic mafic/ultramafic rocks. (A) A chromitite stringer interlayered with a serpentinised pegmatite. (B) A serpentinised pegmatite layer transgressing into an un-serpentinised pegmatite layer. (C) Wavy/undulating contact between a coarse-grained pegmatite and a serpentinised pegmatite.

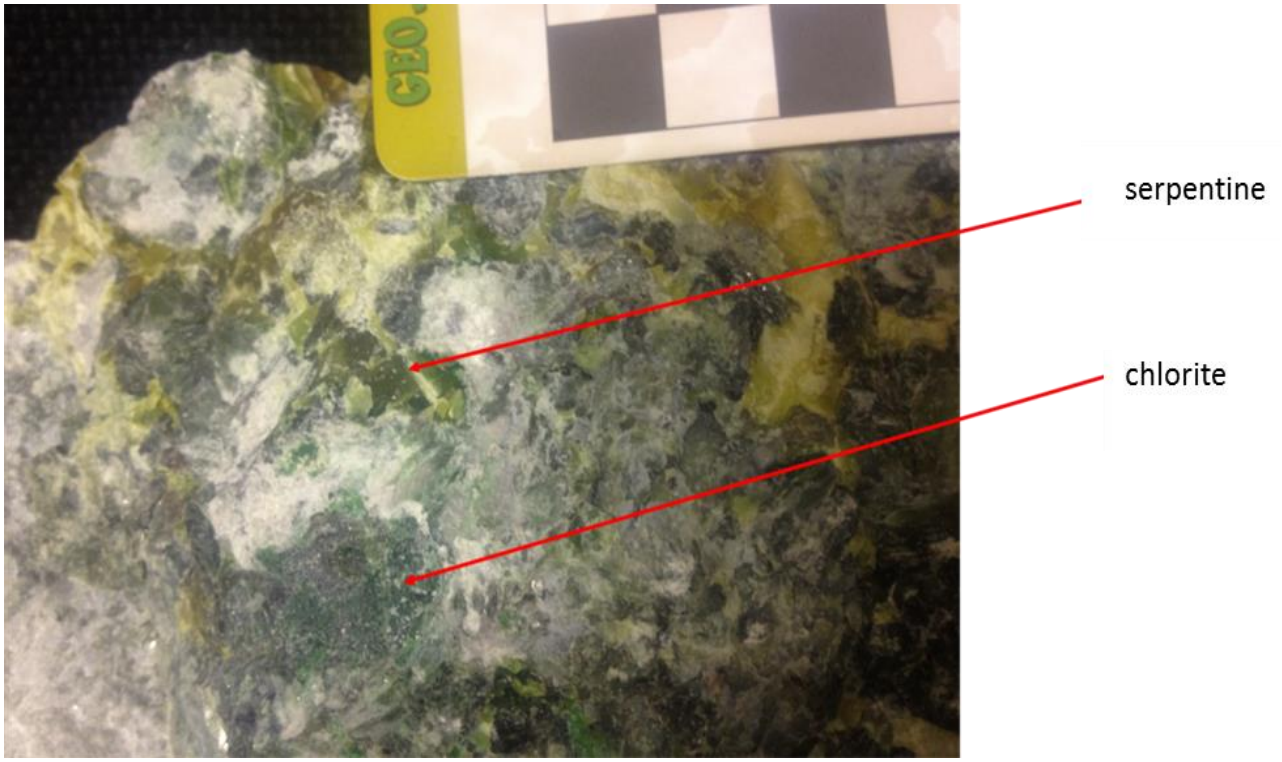

Figure 3.17: A photograph showing a partially altered pegmatite that occurs at the contact between a serpentinised and an un-serpentinised pegmatite. The green mineral is chlorite, whereas the yellow mineral is serpentine.

3.6. Serpentinised pegmatites hosted in the hanging wall the LG-6 chromitite layer.

During the period of the study, no underground exposures of serpentinised pegmatites in the hanging wall of the LG-6 chromitite layer were observed; probably due to the fact that the mining height (the height of the underground workings) at Dwarsrivier Mine only extends to the top of the LG-6A (mining height is approximately 2 m). The only known occurrences of serpentinised pegmatites in the hanging wall of the LG-6 chromitite layer are from borehole core intersections. Five out of two hundred-and-eighty (280) exploration borehole cores drilled on the farm Dwarsrivier 372KT to date have intersected serpentinised pegmatites (Figure 3.18-20). The pegmatites intersected in the boreholes do not appear to be spatially connected to each other, as the boreholes are more than 450 m apart. From the several underground pegmatite outcrops, no pegmatite that is continuous for more than 100 m has been identified yet. The thickness of the intersected serpentinised pegmatites in the five boreholes ranges from 0.77 to 4 m. The thickness of the serpentinised pegmatites in the borehole cores, and the manner in which they occur is consistent with the underground observations of other pegmatites. This suggests that these pegmatitic rocks, irrespective of where they occur in relation to the LG-6 chromitite layer, rarely exceed 4 m in thickness.

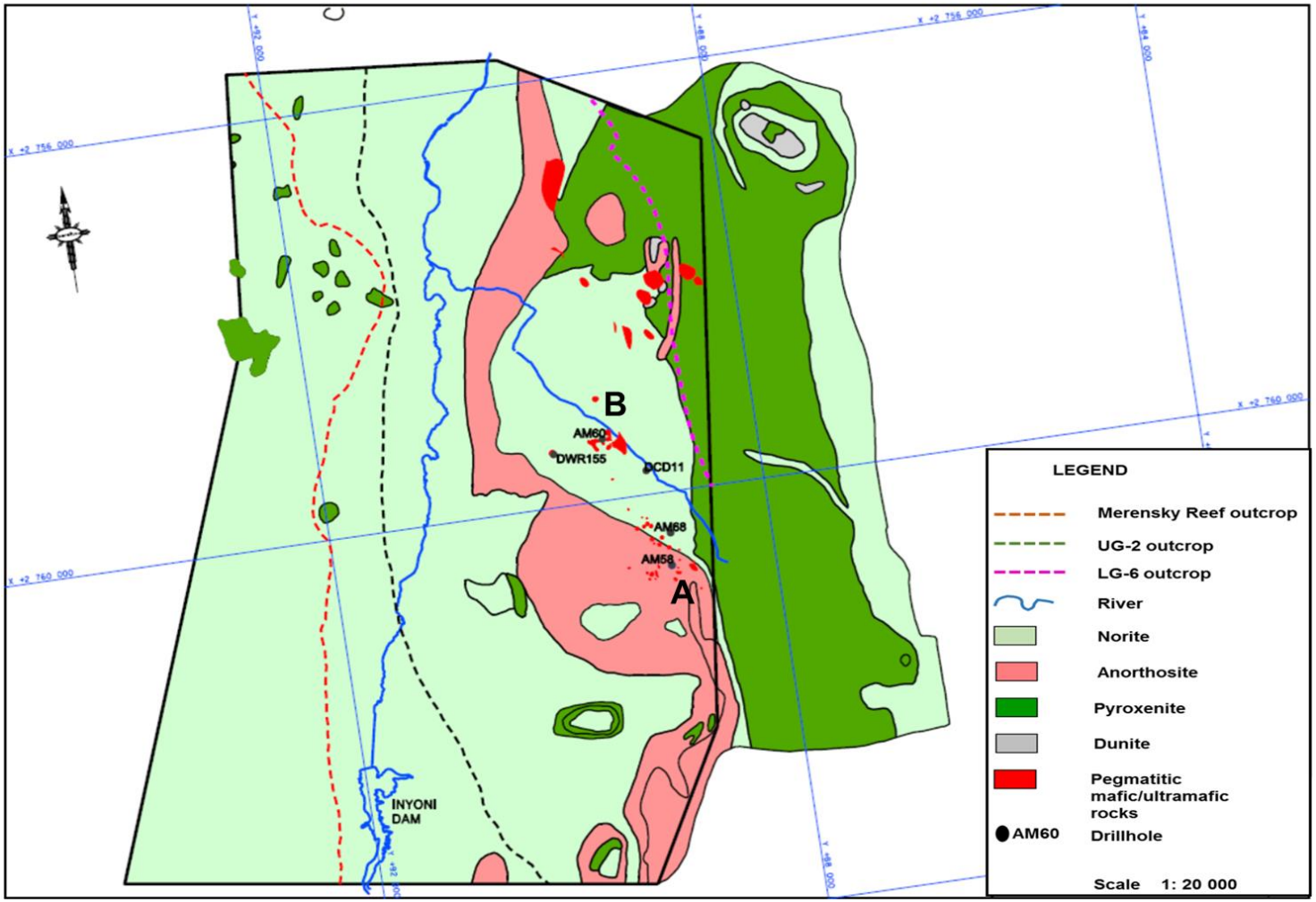

Figure 3.18: A geology map of the farm Dwarsrivier 372KT, where the boreholes that intersected the serpentinised pegmatites above the LG-6 chromitite layer are shown. The boreholes are approximately 450 m apart. The letters A-B represent a section line depicted in Figure 3.20 below.

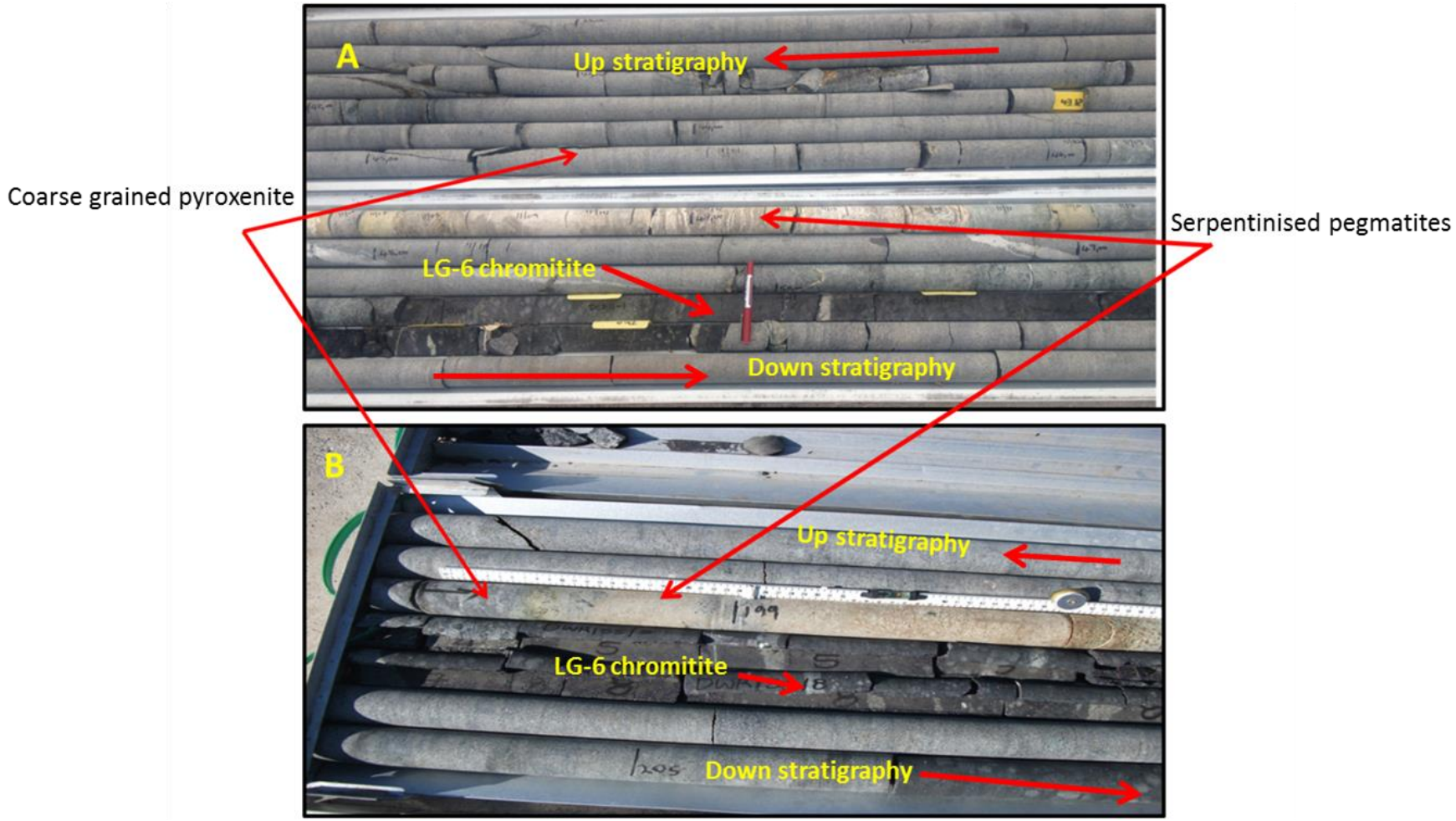

Figure 3.19: Photographs of two separate borehole cores. (A) Borehole DCD 11 and (B) borehole DWR155 showing the intersection of pegmatitic mafic/ultramafic rocks. Note the similarities with regards to the layering, the veins and the colour of the serpentinised pegmatite. A graphical representation of the borehole cores is presented in Figure 3.20 below.

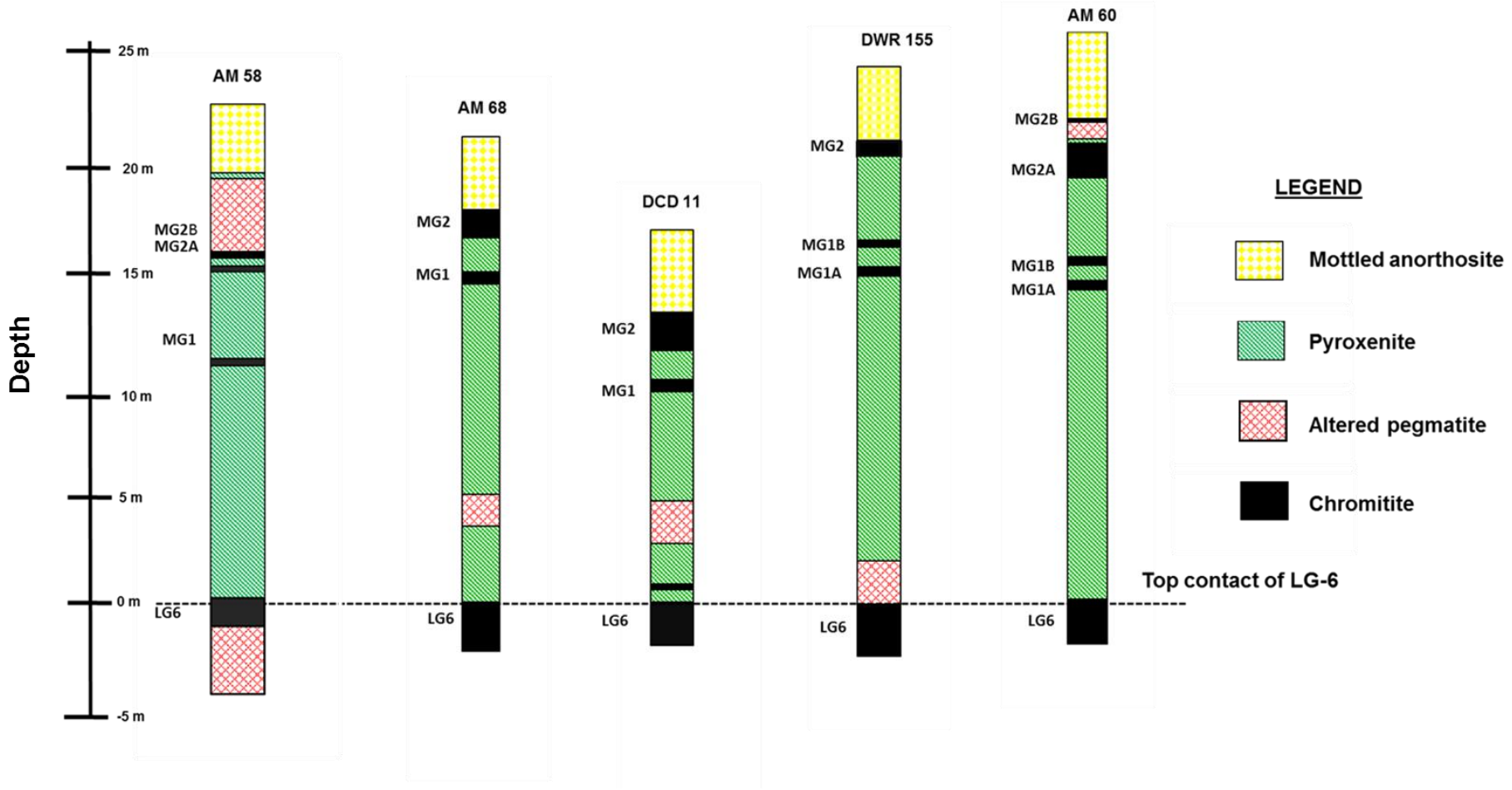

Figure 3.20: A section along A-B showing the boreholes that have intersected the serpentinised pegmatites. The serpentinised pegmatites are intersected at various stratigraphic levels.

3.7. Serpentinised pegmatites found in the footwall to the LG-6 chromitite layer.

The normal footwall of the LG-6 is made up mainly of a medium-grained pyroxenite which may occasionally grade to a coarse-grained pyroxenite. In addition to the normal footwall, there exist serpentinised pegmatites in the footwall of the LG-6. The serpentinised pegmatites found in the footwall of the LG-6 display lithological and mineralogical similarities with the serpentinised pegmatites that occur within and above the LG-6 chromitite layer. However, due to their limited exposure in the underground workings, it was difficult to determine the exact thickness of the individual bodies. They are laterally extensive, and are traceable for tens of meters (Figure 3.21). Large serpentinised pegmatites severely affect the mining process, resulting in the abandonment of such areas.

The contact of the serpentinised portion of the pegmatite with the enveloping coarse-grained pyroxenite is wavy and rugged (Figure 3.22e). Furthermore, the LG-6 chromitite layer changes its thickness across the underlying pegmatite (Figure 3.22f), although the composite thickness does not change. It is worth mentioning that at the south section, the footwall of the LG-6 occasionally undulates and rolls, forming peaks of about 0.5-1.5 m high. There is localised association between the existence of the pegmatites and the footwall undulations. Contrastingly, in areas where the LG-6 rolls, both the footwall and the hanging wall roll synchronously, with no perceivable change in the thickness of the LG-6 chromitite layer (Figure 3.23).

All the serpentinised pegmatites found within the LG-6 chromitite layer, in the footwall and hanging wall of the LG-6, are similar in the manner in which they occur. Their thickness and lateral extent are similar.

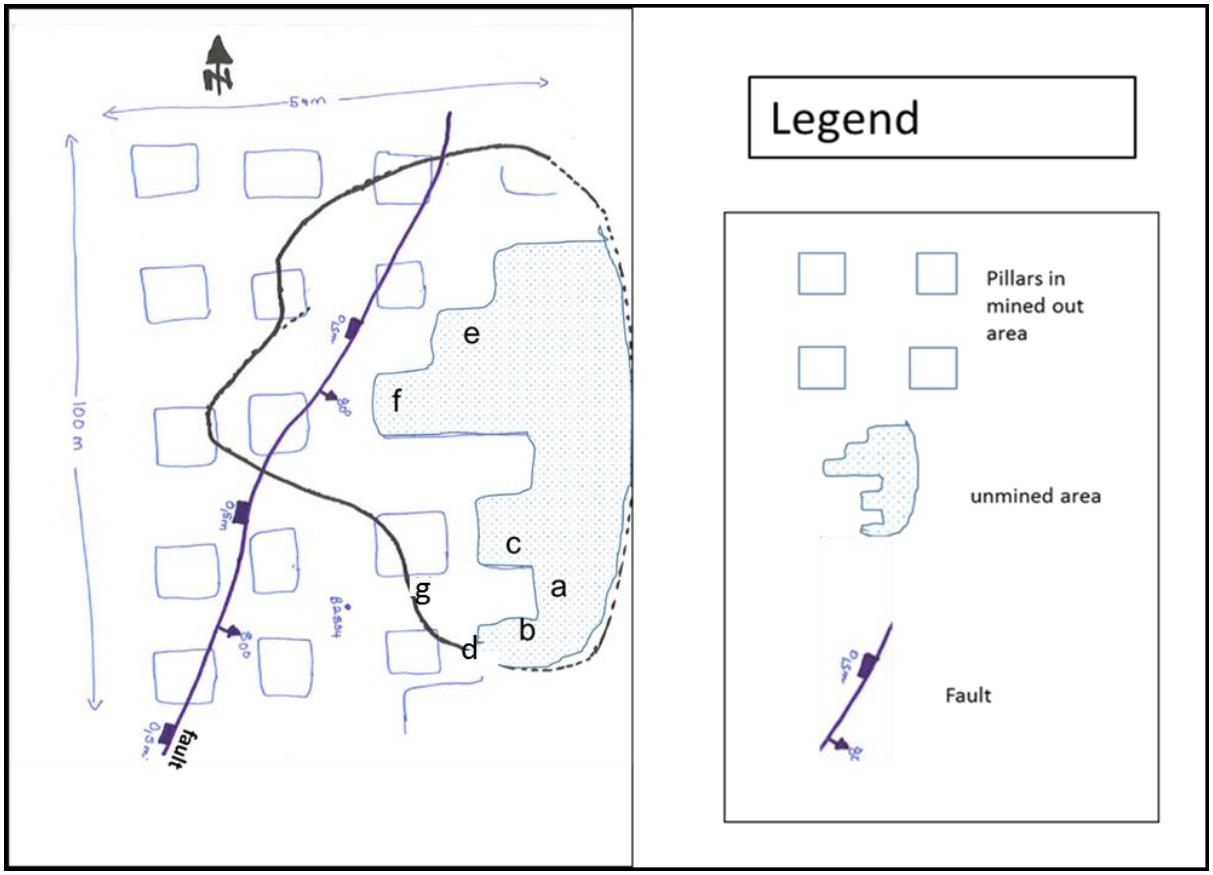

Figure 3.21: A sketch depicting an underground section, where a large pegmatite (approximately 100 m) was encountered. The serpentinised pegmatite occurs within the LG-6 chromitite layer, and such a pegmatite will affect mining, resulting in the abandonment of the area. The letters on the plan indicate the position of the cross sections presented in Figure 3.22.

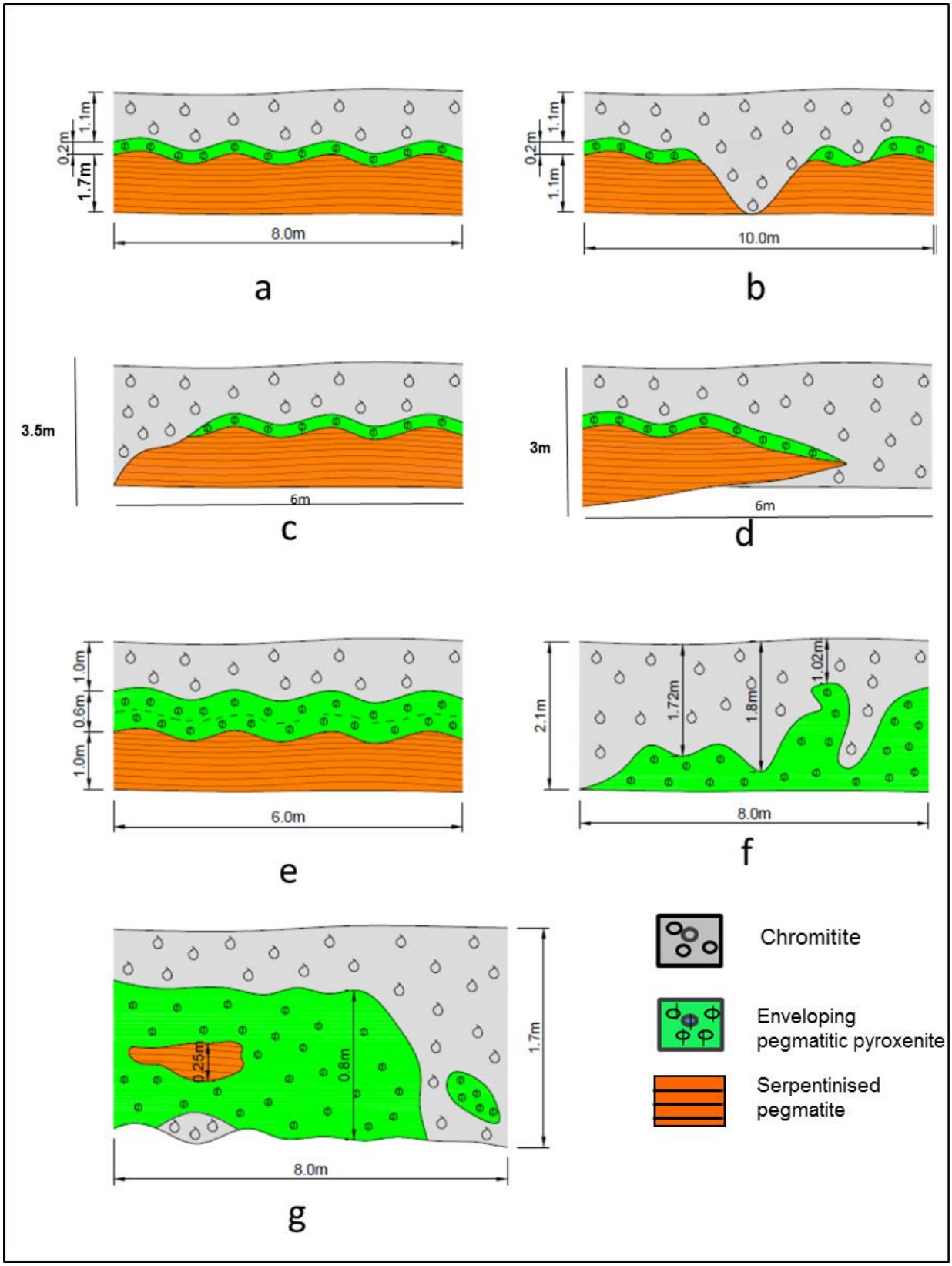

Figure 3.22: Cross sections of various parts of the serpentinised pegmatite shown in Figure 3.16. The LG-6 chromitite layer is deformed by the serpentinised pegmatite. In some instances, the chromitite forms depression structures into the underlying pegmatite (b and f).

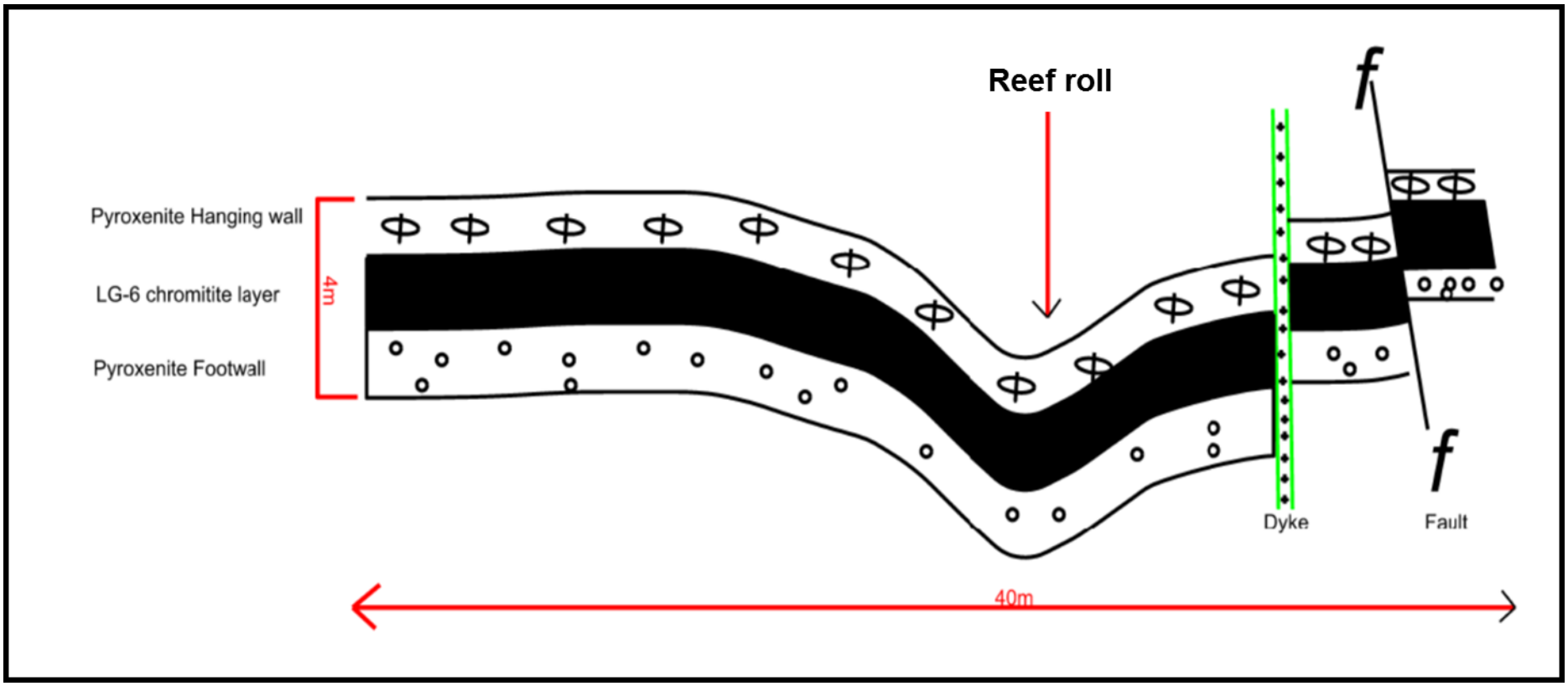

Figure 3.23: A schematic cross section showing a reef roll structure. Note the synchronous rolling of the hanging and footwall pyroxenite.

CHAPTER 4: PETROGRAPHY

4.1. Introduction.

The petrography of the pegmatites is subdivided into two sections: the first section discusses the fresh pegmatites, and the second section focuses on the altered (serpentinised) pegmatites. The aim of the petrographic investigation was to document the occurrences of major rock forming minerals with regards to their petrographic characteristics.

4.2. Petrographic description of the un-altered (fresh) pegmatites.

The mineralogy of the pegmatites is similar to the surrounding pyroxenite host rocks, although they differ in the modal abundance of clinopyroxene, orthopyroxene, olivine, and plagioclase. The abundance of clinopyroxene, orthopyroxene, and olivine in the pegmatites makes it possible to subdivide them into clinopyroxene-rich pegmatites, orthopyroxene-rich pegmatites, and olivine-rich pegmatites. Phlogopite and biotite occur in association with plagioclase in all the pegmatites. Clinopyroxene in the clinopyroxene-rich pegmatites usually occurs subhedral crystals (Figure 4.1) and exhibits blebby type orthopyroxene exsolution lamellae (Figure 4.2). Plagioclase is less than 5% in modal abundance, and occurs along crystal boundaries of clinopyroxene in association with rounded olivine (Figure 4.1). The contact between the plagioclase and the olivine is characterised by clinopyroxene reaction rim (Figure 4.1). Amphibole alteration in the form of hornblende is also common in the clinopyroxene-rich pegmatites.

Orthopyroxene crystals in the orthopyroxene-rich pegmatites display a variety of textures. They occur as subhedral to euhedral crystals (Figure 4.3 and Figure 4.4). Plagioclase occurs either as laths within the orthopyroxene crystals or along orthopyroxene crystal margins in association with biotite (Figure 4.5). In one sample phlogopite was observed adjacent to an orthopyroxene crystal (Figure 4.6). Clinopyroxene, in the orthopyroxene-rich pegmatites, is poikilitically enclosed by the orthopyroxene, or occurs as a reaction product when olivine is in contact with plagioclase (Figure 4.7).

In the olivine-rich pegmatites, olivine occurs primarily as small, rounded crystals poikilitically enclosed by large pyroxene crystals (Figure 4.8). The olivine appears moderately altered to serpentine along crystal fractures. Scattered, euhedral chromite is present in minute amounts (Figure 4.9). Noticeably, chromite is far less abundant in all the pegmatites than in the surrounding silicate host rocks.

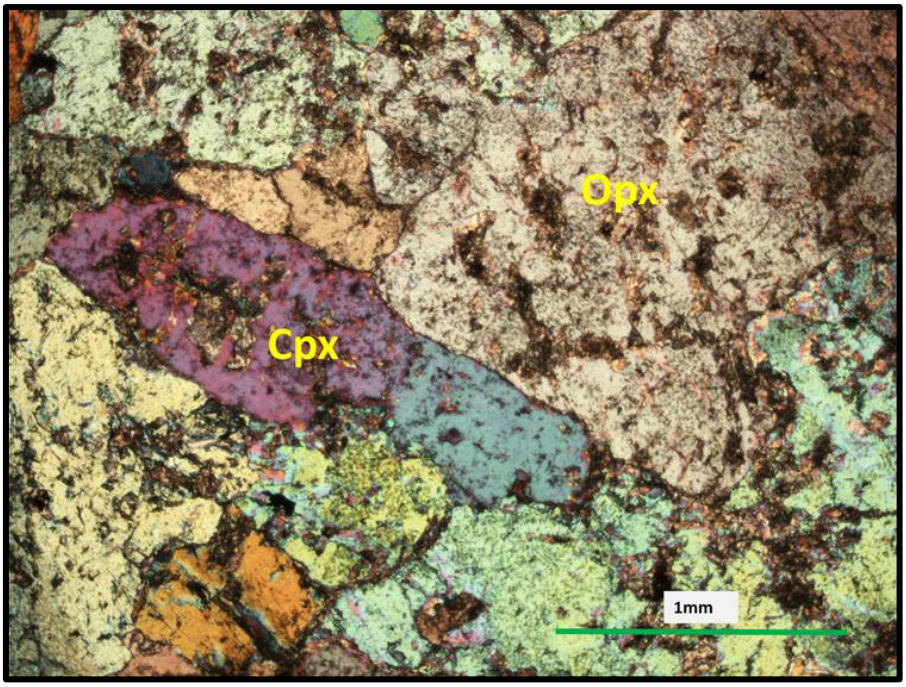

Figure 4.1: Photomicrograph of a fresh, coarse-grained clinopyroxene-rich pegmatite showing euhedral to subhedral clinopyroxene (Cpx) with orthopyroxene (Opx) crystal. Photomicrograph taken in cross-polarised light (XPL). Alteration in the fresh pegmatites is minimal, as can be seen in this photograph.

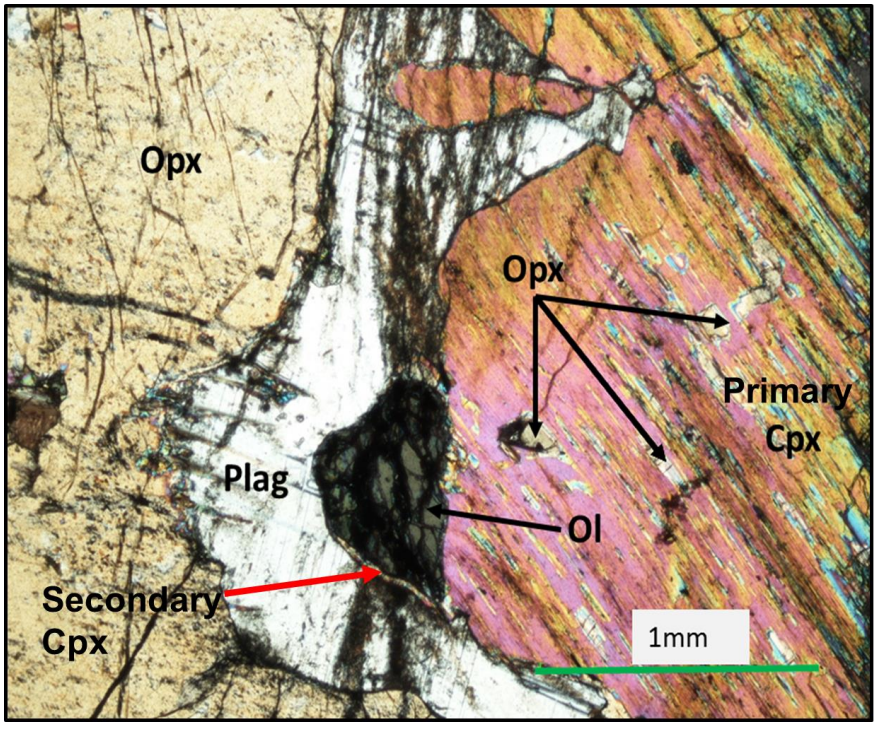

Figure 4.2: Photomicrograph of the clinopyroxene-rich pegmatite showing orthopyroxene exsolution in primary clinopyroxene. Secondary clinopyroxene develops when olivine is in contact with plagioclase. Photomicrograph taken in cross-polarised light (XPL).

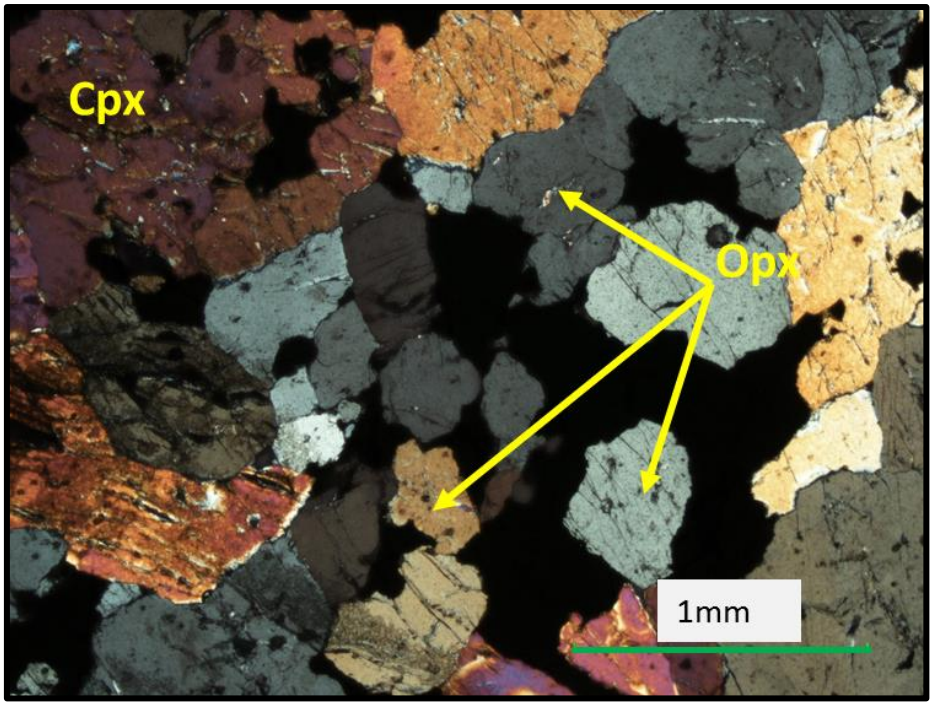

Figure 4.3: Photomicrograph of an orthopyroxene-rich pegmatite showing euhedral to subhedral orthopyroxene in textural equilibrium with clinopyroxene. The orthopyroxene crystals are slightly smaller than the clinopyroxene crystals. Photomicrograph taken in cross-polarised light (XPL).

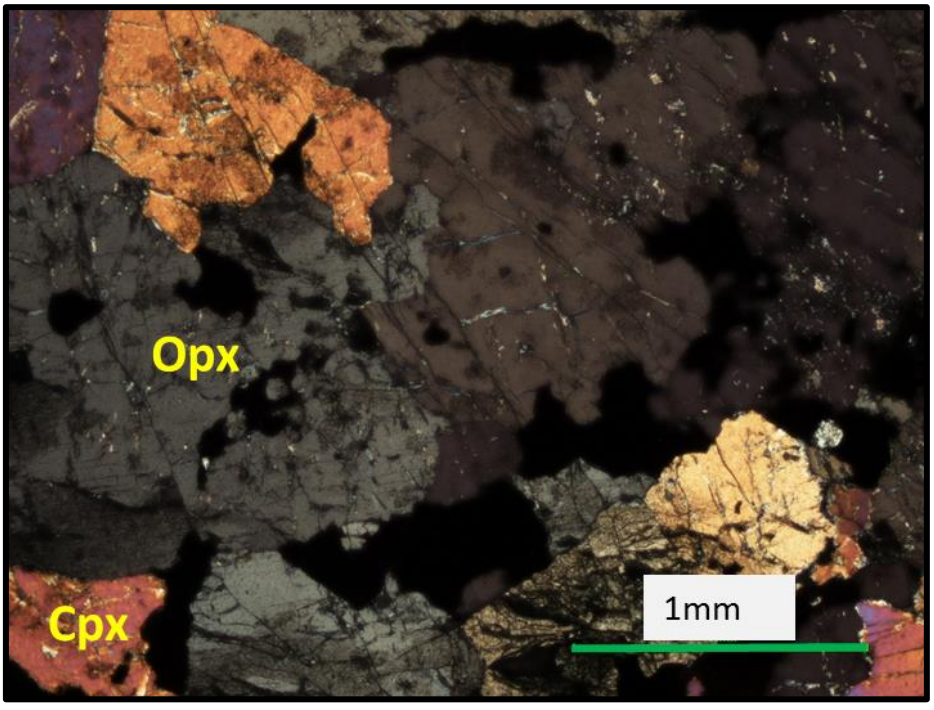

Figure 4.4: Photomicrograph of an orthopyroxene-rich pegmatite showing orthopyroxene crystals in textural equilibrium with the clinopyroxene. No alteration of either minerals is visible. Photomicrograph taken in cross-polarised light (XPL).

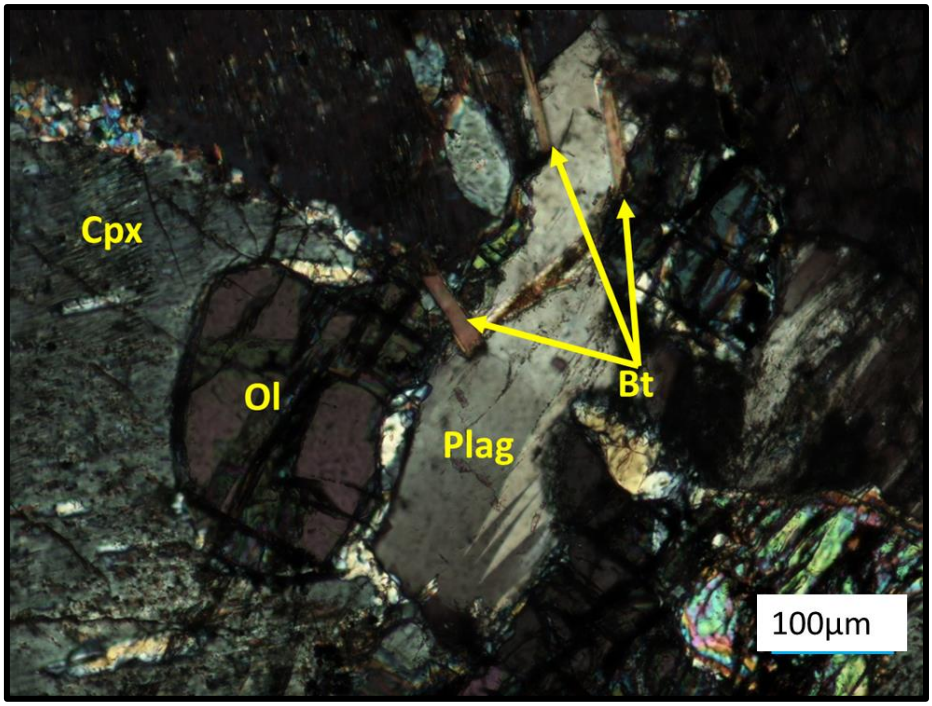

Figure 4.5: An orthopyroxene-rich pegmatite, where orthopyroxene (Opx) coexists with intercumulus plagioclase (Plag) and olivine (Ol). Biotite (Bt) occurs in association with plagioclase. The photomicrograph was taken under crossed polarised light (XPL).

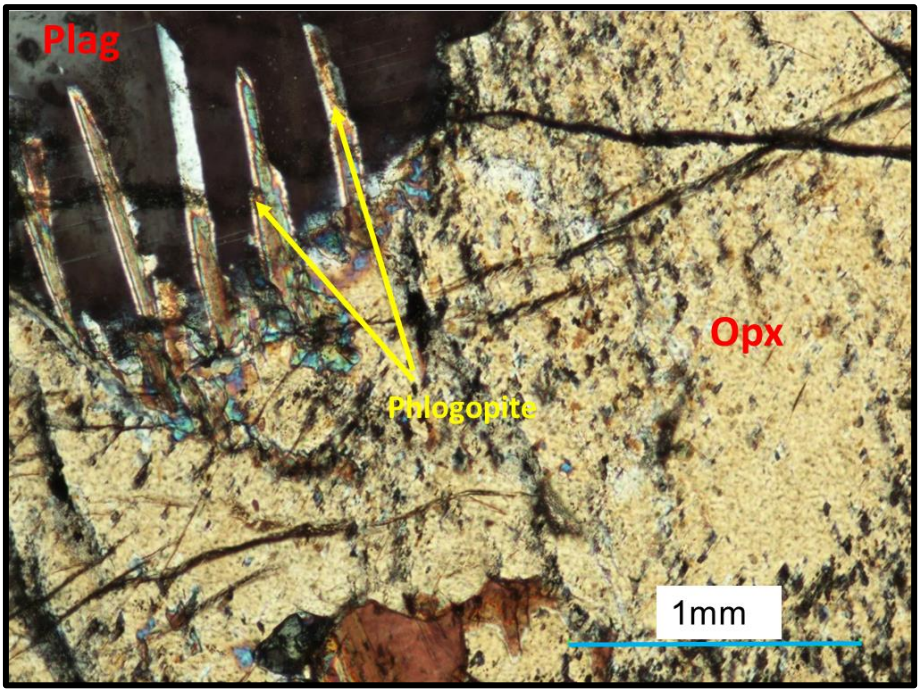

Figure 4.6: Photomicrograph of an orthopyroxene-rich pegmatite showing phlogopite which occurs in association with plagioclase. Photomicrograph taken under XPL.

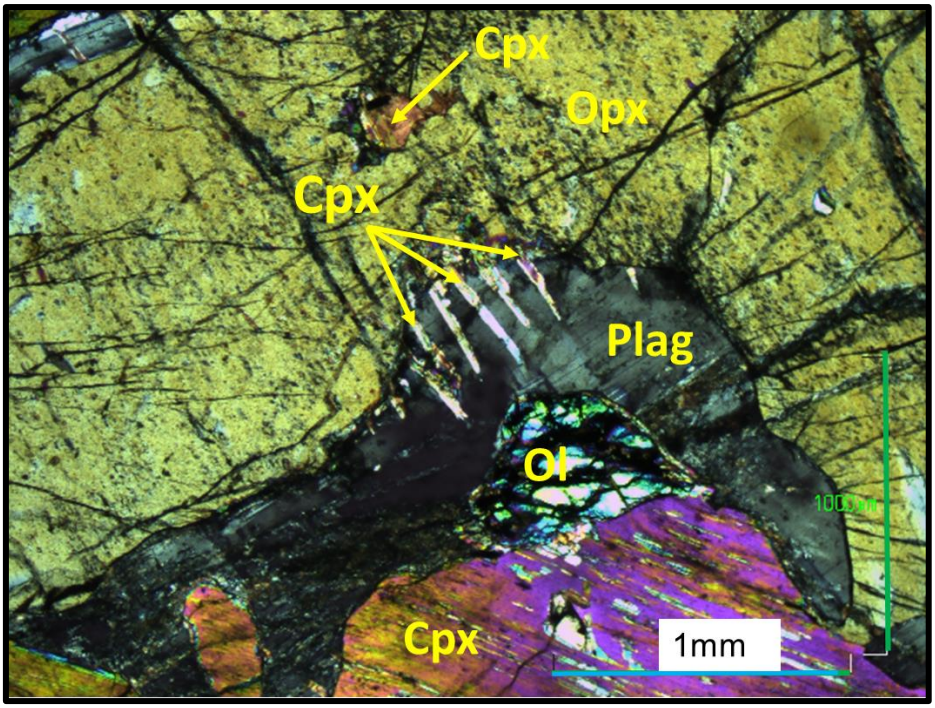

Figure 4.7: Photomicrograph of an orthopyroxene-rich pegmatite, where orthopyroxene coexists with plagioclase (Plag), olivine (Ol) and clinopyroxene (Cpx). Photomicrograph taken in cross-polarised light (XPL).

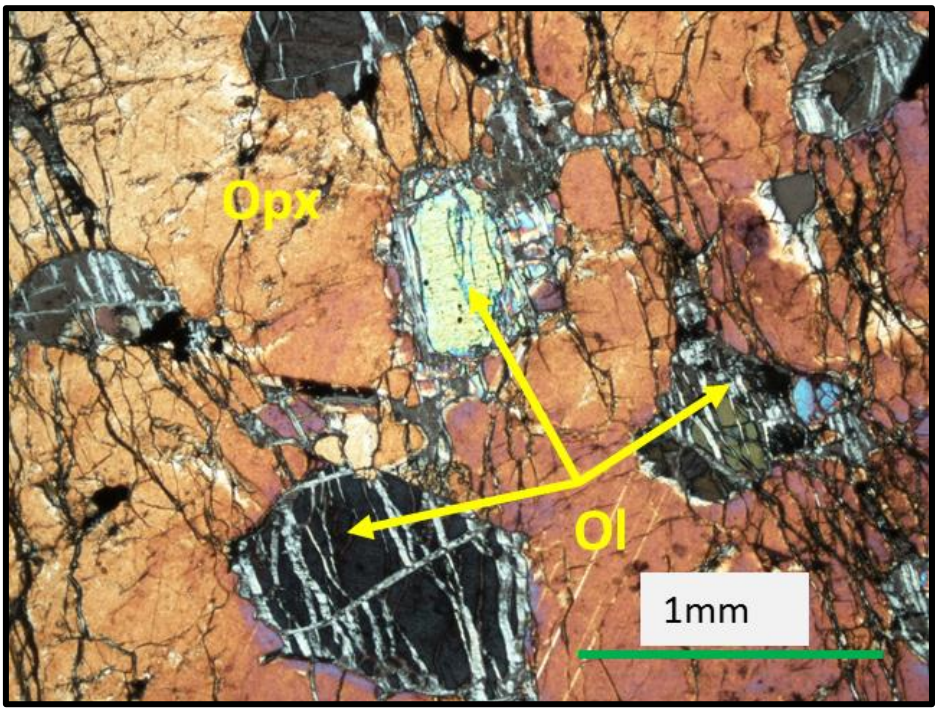

Figure 4.8: Photomicrograph of an olivine-rich pegmatite, in which subhedral olivine crystals are poikilitically enclosed by a clinopyroxene crystal. The olivine crystals are well rounded and show evidence of moderate alteration to serpentine, whereas the orthopyroxene crystal does not show alteration. This is common in olivine-rich pegmatites. Photomicrograph taken in cross-polarised light (XPL).

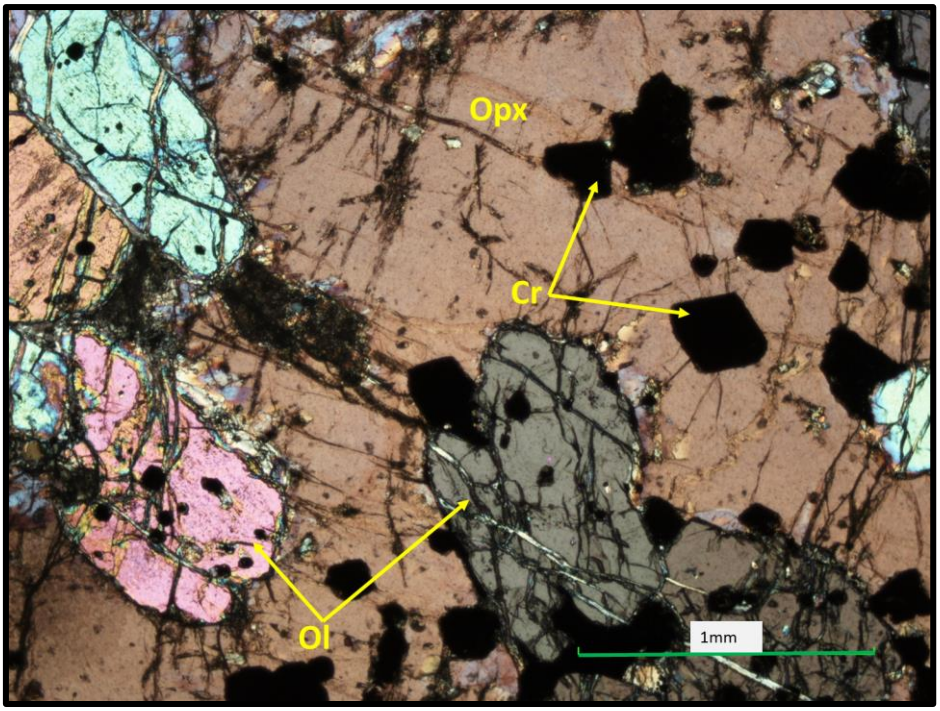

Figure 4.9: A photomicrograph of an olivine-rich pegmatite, where olivine (Ol) crystals occur within a large orthopyroxene crystal. Also in the thin section, there is chromite (Cr) occurring in association with orthopyroxene (Opx). Chromite crystals were observed in the olivine-rich pegmatites only. The olivine shows moderate alteration. Photomicrograph was taken under crossed polarised light (XPL).

4.3. Petrographic description of the altered (serpentinised) pegmatites.

The mineralogy of the altered pegmatites is similar to that of the fresh pegmatites. The major difference between the two types of pegmatites is in their alteration and the degree of alteration. The alteration process in the pegmatites produced a mineral assemblage that is dominated by, in the order of decreasing abundance, serpentine, magnetite, epidote, and calcite. The severity of alteration in the altered pegmatites differs, with the olivine-rich pegmatites showing the most severe alteration. In the severely altered olivine-rich pegmatites, there is the development of serpentine pseudomorphs after olivine. In the olivine-rich pegmatites, where the pyroxenes enclose olivine, the olivine is completely replaced by serpentine (Figure 4.10 & Figure 4.11). Olivine crystals in the moderately altered olivine-rich pegmatites are altered primarily along crystal fractures. Magnetite occurs along these fractures in association with serpentine in the olivine-rich pegmatites (Figure 4.12).

The clinopyroxene and orthopyroxene-rich pegmatites show moderate alteration, with a mineral assemblage that is still dominated by the original mineralogy. Carbonate minerals such as calcite and dolomite occur in close association with orthopyroxene (Figure 4.13 & Figure 4.14). Epidote group minerals such as epidote and clinozoisite occur in association with the pyroxene and olivine in the pegmatites (Figure 4.15 & Figure 4.16).

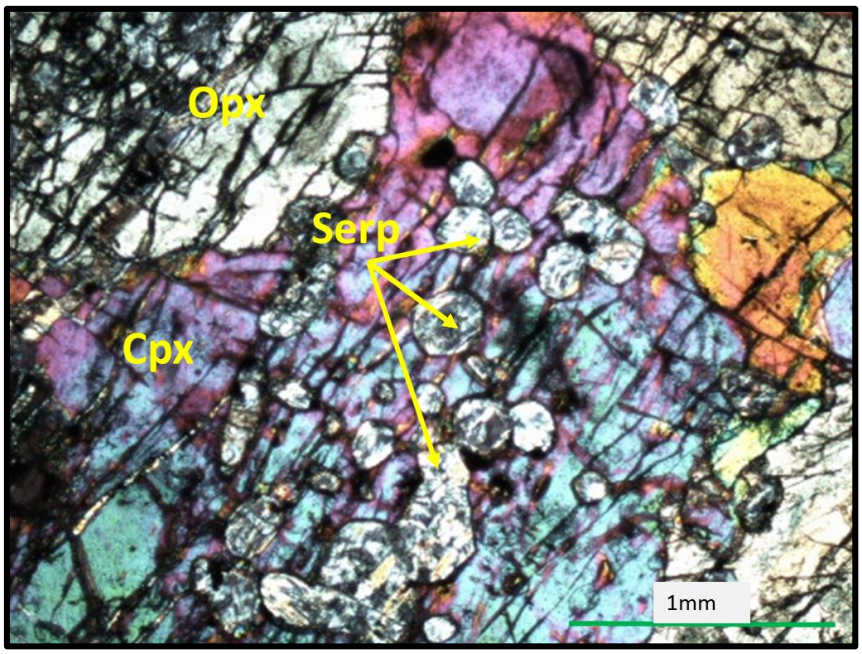

Figure 4.10: A photomicrograph of an olivine-rich pegmatite in which serpentine (Serp) replaces olivine. The olivine poikilitically enclosed by clinopyroxene (Cpx) and orthopyroxene (Opx), is almost completely altered to serpentine. Both the clinopyroxene and the orthopyroxene are moderately altered. This is common in olivine-rich pegmatites, where the olivine is almost completely replaced by serpentine. Photomicrograph was taken under crossed polarised light (XPL).

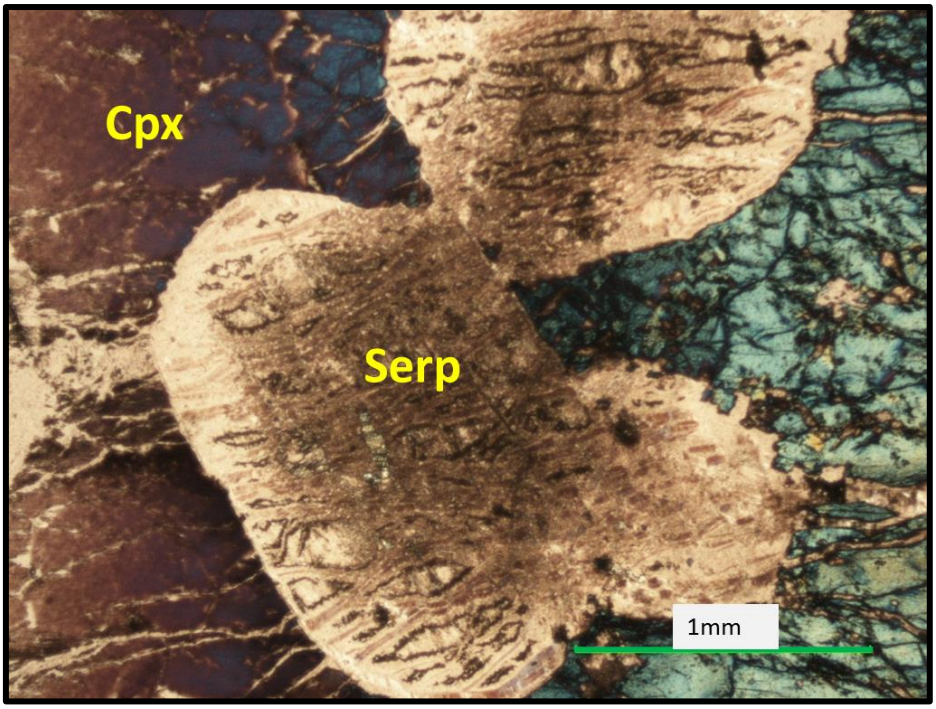

Figure 4.11: A photomicrograph of an olivine-rich pegmatite showing serpentine (Serp) pseudomorphs after olivine. The olivine in this sample is completely replaced by serpentine. Olivine-rich pegmatites show the most severe alteration. Photomicrograph was taken under crossed polarised light (XPL).

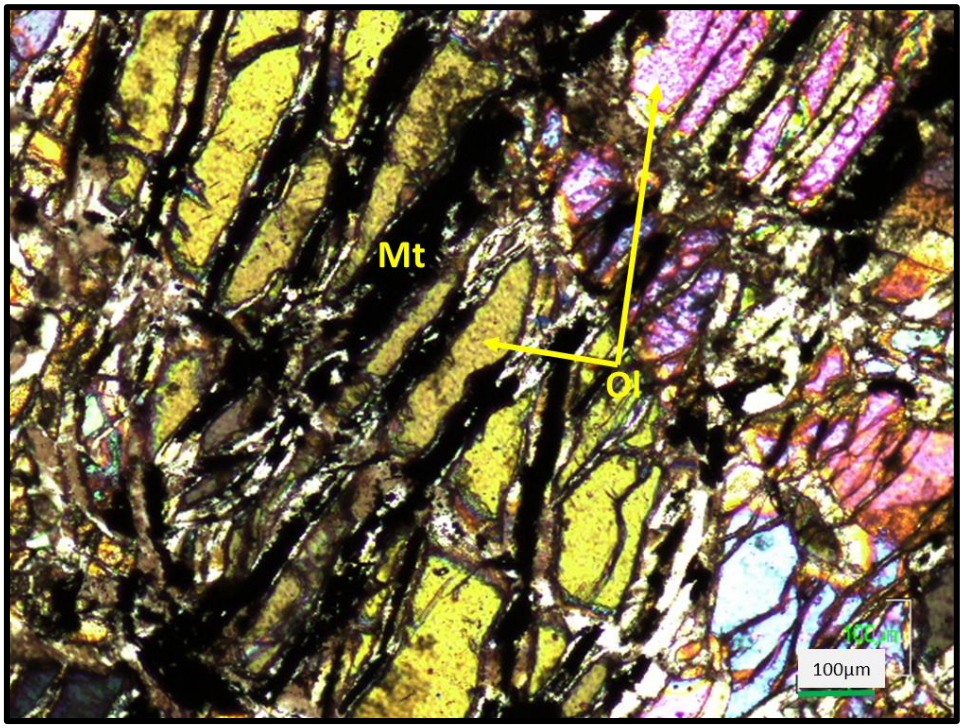

Figure 4.12: A photomicrograph of an olivine-rich pegmatite showing that olivine is preferentially altered along crystals fractures to produce magnetite. This is typical of olivine-rich pegmatites. Photomicrograph was taken under crossed polarised light (XPL).

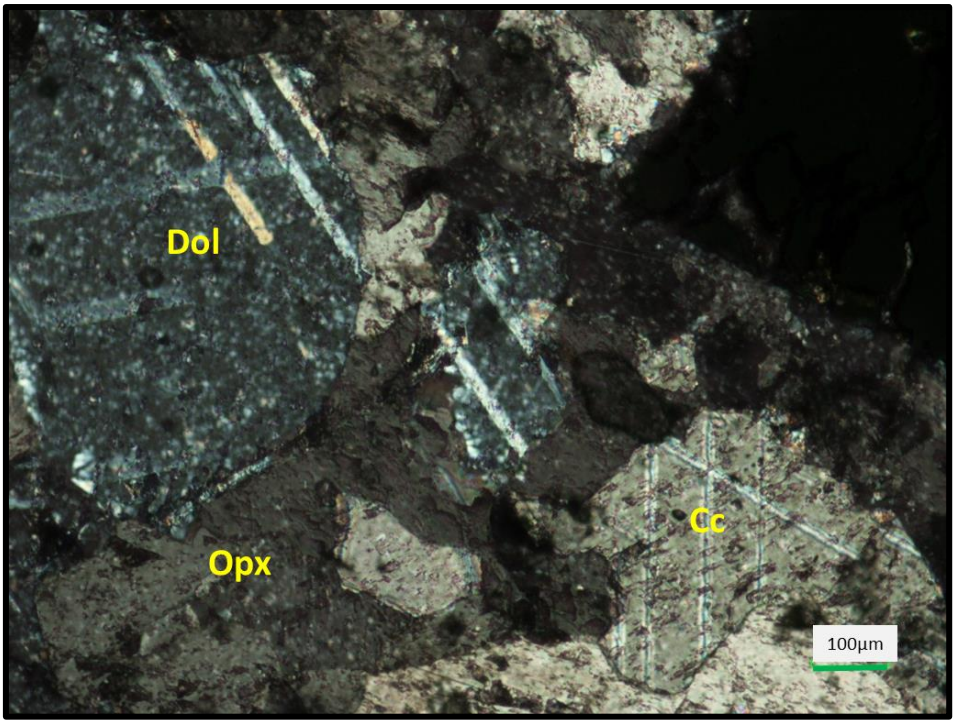

Figure 4.13: A photomicrograph of a moderately altered orthopyroxene-rich pegmatite showing calcite (Cc) and dolomite (Dol) in association with orthopyroxene (Opx). Photomicrograph was taken under crossed polarised light (XPL).

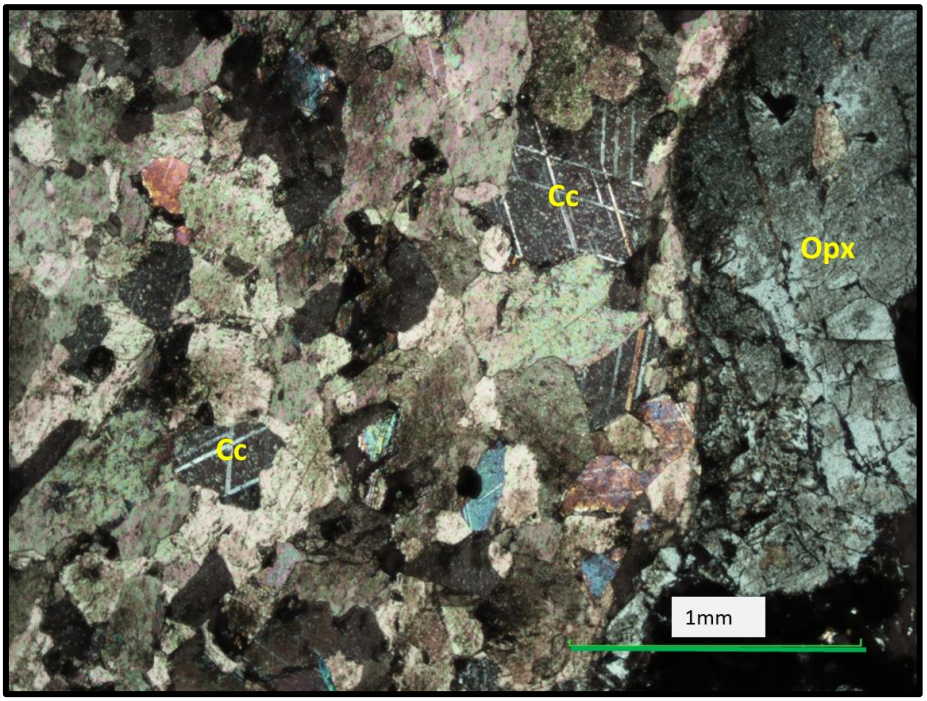

Figure 4.14: A photomicrograph of an altered orthopyroxene-rich pegmatite showing calcite (Cc) in association with orthopyroxene (Opx). The carbonates are a post magmatic replacement feature. Photomicrograph was taken under crossed polarised light (XPL).

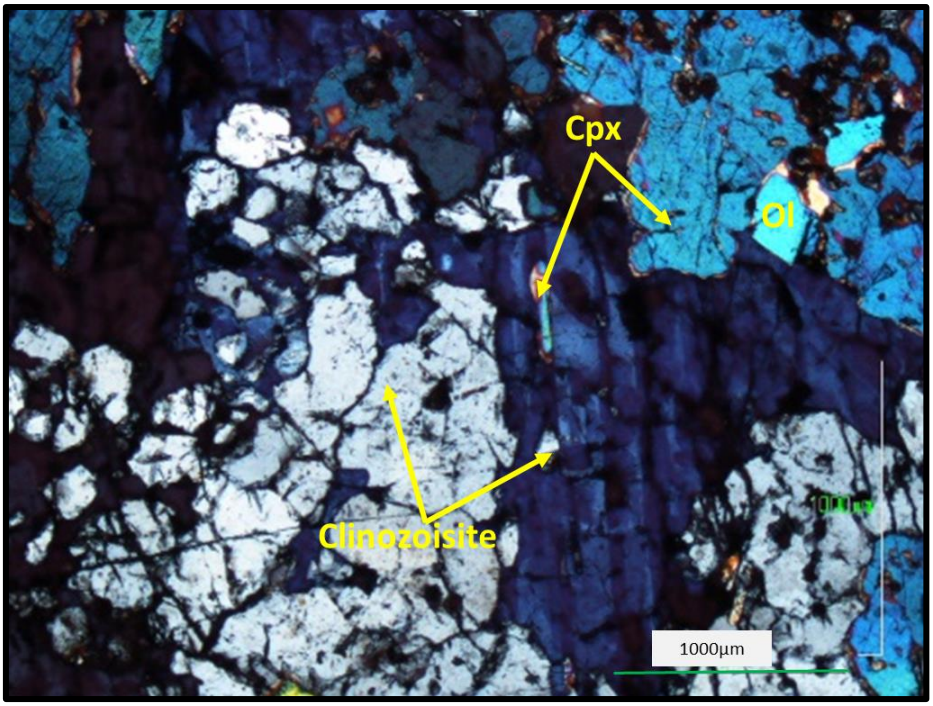

Figure 4.15: A photomicrograph of an altered clinopyroxene-rich pegmatite showing prismatic clinozoisite in association with clinopyroxene (Cpx). When the clinopyroxene alters, it produces clinozoisite. Photomicrograph was taken under crossed polarised light (XPL).

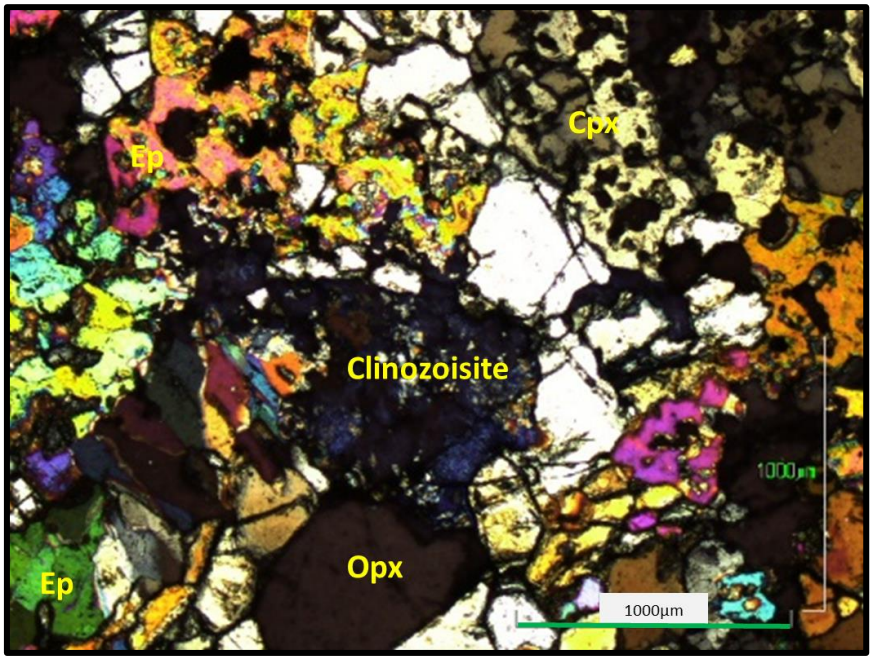

Figure 4.16: A photomicrograph of an altered clinopyroxene-rich pegmatite, showing clinozoisite and epidote (Ep) in association with clinopyroxene (Cpx) and orthopyroxene (Opx). The clinozoisite and epidote are common alteration mineral assemblages in the clinopyroxene-rich pegmatites. Photomicrograph was taken under crossed polarised light (XPL).

CHAPTER 5: WHOLE ROCK GEOCHEMISTRY

5.1. Introduction.

In this chapter the geochemical data (determined by XRF) of the pegmatites and their host rocks are presented. The full results are listed in appendices 3-8. XRF analyses were carried out on underground samples as well as borehole cores. The samples were taken as follows: sixteen (16) samples of the pyroxenite host rocks; twenty-eight (28) samples of fresh, un-altered pegmatites and thirty-three (33) samples of altered pegmatites. The analytical method and conditions are given in Appendix 1. The analytical results for the pegmatites and the pyroxenite host rocks are listed in Table 1-2 and Table 3-4, respectively.

5.2. Major elements geochemistry.

In this section, the geochemistry of the pegmatites is presented together with the geochemical data for the pyroxenite host rocks. The pegmatites will also be compared to pegmatites from elsewhere in the Bushveld Complex, in order to investigate any similarities / differences.

The following major elements were analysed for (wt. %): SiO_2, TiO_2, Al_2O_3, FeO, MnO, MgO, CaO, Na_2O, K_2O, P_2O_5. Loss on Ignition (LOI) was determined for all samples.

The concentration of major elements in the pegmatites is controlled by the modal abundances of clinopyroxene, orthopyroxene, and olivine. Interrelationships of the different elements are best demonstrated by plotting MgO (wt. %) against the other major elements on binary variation diagrams, as MgO is a major constituent of the pyroxenes that characterise the pegmatites.

Table 1: **Major element geochemistry of the unaltered pegmatites.**

			Analyses are given in wt %													
SAMPLE NAME	**ALTERATION**	**PEGMATITE TYPE**	**SiO_2**	**TiO_2**	**Al_2O_3**	**FeO**	**MnO**	**MgO**	**CaO**	**Na_2O**	**K_2O**	**P_2O_5**	**Cr_2O_3**	**LOI**	**Total**	**Mg#**
CL6B4	UN-ALTERED	CPX	32.08	0.13	4.43	2.28	0.22	25.69	23.54	0.01	0.01	0.01	0.02	11.02	99.43	95.25
CL6B(1)	UN-ALTERED	CPX	39.36	0.11	4.33	5.50	0.17	23.80	21.62	0.01	0.01	0.01	0.08	4.96	99.94	88.52
CL6B5	UN-ALTERED	CPX	50.39	0.15	2.03	6.46	0.14	21.71	16.67	0.01	0.12	0.01	0.21	2.05	99.94	85.69
CL6B8	UN-ALTERED	CPX	53.04	0.16	1.80	6.33	0.15	20.02	15.39	0.01	0.16	0.01	0.60	2.28	99.95	84.93
13	UN-ALTERED	CPX	49.95	0.21	4.98	3.45	0.16	15.86	26.12	0.01	0.01	0.04	0.10	0.90	101.79	89.12
11	UN-ALTERED	CPX	49.97	0.17	4.21	3.42	0.17	18.59	23.91	0.01	0.00	0.00	0.23	0.50	101.18	90.64
12	UN-ALTERED	CPX	48.40	0.20	7.47	5.08	0.19	15.73	24.75	0.01	0.00	0.01	0.92	0.20	102.95	84.65
CL15	UN-ALTERED	CPX	32.74	0.10	5.11	2.65	0.10	26.45	16.38	0.01	0.01	0.01	0.03	16.38	99.95	94.68
CL55	UN-ALTERED	CPX	41.67	0.06	2.21	4.70	0.48	20.79	25.88	0.01	0.01	0.01	0.04	4.16	100.00	88.74
CL56	UN-ALTERED	CPX	38.84	0.06	3.72	7.53	0.51	23.05	17.42	0.01	0.01	0.01	0.04	8.69	99.87	84.51
CL63	UN-ALTERED	CPX	48.50	0.25	6.10	4.56	0.33	15.57	23.38	0.01	0.09	0.01	0.08	1.11	99.97	85.88
CL37-1B	UN-ALTERED	CPX	43.23	0.26	4.72	5.59	0.06	23.51	17.84	0.01	0.01	0.01	0.10	4.54	99.87	88.23
CL53B	UN-ALTERED	CPX	47.27	0.19	6.56	4.92	0.37	21.26	18.62	0.01	0.12	0.01	0.10	0.54	99.96	88.50
CL37	UN-ALTERED	CPX	44.51	0.35	5.39	5.13	0.11	18.61	21.61	0.01	0.01	0.01	0.09	4.18	99.99	86.60
CL60	UN-ALTERED	CPX	49.03	0.07	12.42	2.98	0.13	11.73	22.87	0.01	0.01	0.01	0.08	0.45	99.77	87.52
CL36	UN-ALTERED	CPX	43.87	0.17	4.58	8.42	0.26	24.12	15.24	0.01	0.08	0.01	0.30	2.90	99.95	83.62
CL08	UN-ALTERED	OL	36.12	0.09	5.83	7.26	0.08	45.06	0.25	0.01	0.01	0.01	0.01	4.00	98.71	91.71
CL6B-0.1	UN-ALTERED	OL	35.68	0.01	6.68	5.71	0.25	35.27	10.22	0.01	0.01	0.01	0.11	6.03	99.98	91.67
8	UN-ALTERED	OL	40.70	0.06	1.60	7.24	0.76	37.20	5.04	0.01	0.00	0.00	0.01	7.80	100.41	90.15
10	UN-ALTERED	OL	43.15	0.12	5.94	6.43	0.24	28.71	11.33	0.01	0.13	0.00	0.01	4.41	100.48	88.83
9	UN-ALTERED	OL	47.70	0.21	2.17	7.46	0.44	22.75	17.72	0.01	0.01	0.07	0.06	3.30	101.90	84.46
CL47B	UN-ALTERED	OL	38.48	0.05	7.58	9.05	0.12	32.58	1.58	0.01	0.01	0.01	0.07	10.37	99.89	86.51
CL59	UN-ALTERED	OL	38.67	0.05	1.76	13.46	0.26	37.73	1.55	0.01	0.05	0.01	0.09	6.25	99.89	83.32
CL19	UN-ALTERED	OL	35.73	0.03	4.19	6.44	0.72	26.47	13.45	0.01	0.01	0.01	0.03	12.85	99.93	87.99
CL61	UN-ALTERED	OL	45.12	0.09	3.15	9.41	0.23	34.25	5.00	0.01	0.05	0.01	0.16	2.44	99.90	86.64
CL49	UN-ALTERED	OL	39.67	0.10	3.49	9.52	0.20	30.41	12.58	0.01	0.01	0.01	0.19	3.75	99.93	85.05
CL08	UN-ALTERED	OL	36.12	0.09	5.83	7.26	0.08	45.06	0.25	0.01	0.01	0.01	0.01	5.16	99.87	91.71
1	UN-ALTERED	OPX	50.27	0.19	5.46	7.83	0.32	23.62	14.19	0.01	0.06	0.01	0.02	0.50	102.48	84.31
CL53A	UN-ALTERED	OPX	49.50	0.15	4.84	8.48	0.22	23.48	9.32	0.10	0.37	0.01	0.31	1.90	98.67	83.15

Note: CPX- Clinopyroxene-rich pegmatites OPX= Orthopyroxene-rich pegmatites OL= Olivine-rich pegmatites

Table 2: Trace element geochemistry of unaltered pegmatites.

			Analyses given in ppm												
SAMPLE NAME	ALTERATION	PEGMATITE TYPE	Nb	Cu	Ni	Rb	Sr	Y	Zn	Zr	Co	Cr	V	Ba	La	Zr/Y
CL6B4	FRESH	CPX	3.69	2.77	13.87	2.29	6.35	9.28	145.59	20.38	12.49	128.36	16.81	29.12	5.27	2.20
CL6B(1)	FRESH	CPX	4.06	10.19	87.21	3.40	17.57	7.69	135.04	12.88	30.10	585.86	20.97	25.59	5.66	1.67
CL6B5	FRESH	CPX	4.99	31.12	343.51	8.78	57.66	10.12	58.43	25.53	56.38	1702.39	79.84	122.99	9.78	2.52
CL6B8	FRESH	CPX	4.82	7.36	304.85	7.27	17.06	18.80	33.11	29.86	48.21	4309.12	116.98	47.07	11.74	1.59
13	FRESH	CPX	4.13	2.00	27.79	5.21	61.81	13.22	58.14	92.17	34.27	798.57	86.10	41.49	38.80	6.97
11	FRESH	CPX	4.18	2.00	55.07	10.20	43.14	11.45	62.50	72.92	33.31	1837.77	74.18	65.18	36.06	6.37
12	FRESH	CPX	5.57	2.00	100.00	4.97	42.45	14.34	152.72	89.04	67.00	7049.25	91.13	24.48	38.27	6.21
CL15	FRESH	CPX	2.00	2.92	18.27	2.00	6.20	6.59	58.26	10.00	14.14	182.00	16.81	29.29	8.85	1.52
CL55	FRESH	CPX	4.43	3.07	3.08	4.86	61.87	6.57	471.23	10.98	18.42	270.09	16.81	35.31	19.06	1.67
CL56	FRESH	CPX	5.02	4.29	20.64	2.56	6.37	18.50	103.75	32.23	30.11	303.00	42.25	20.07	26.63	1.74
CL63	FRESH	CPX	5.99	63.28	21.15	10.40	84.00	15.55	137.64	51.36	17.15	408.20	83.26	143.84	11.12	3.30
CL37-1B	FRESH	CPX	4.45	5.02	108.50	3.50	28.29	14.48	26.39	52.95	26.60	655.08	52.83	31.60	4.26	3.66
CL53B	FRESH	CPX	3.92	32.54	18.98	6.20	75.50	13.50	128.05	54.79	26.53	616.76	66.22	119.34	18.15	4.06
CL37	FRESH	CPX	4.99	7.20	75.96	4.60	55.09	17.74	30.69	66.26	22.14	581.20	60.29	60.35	10.45	3.74
CL60	FRESH	CPX	4.34	8.11	30.64	5.26	187.53	13.83	37.42	37.42	22.60	606.13	158.86	52.75	22.54	2.71
CL36	FRESH	CPX	5.94	57.71	307.58	11.20	84.16	10.81	65.81	32.31	62.90	1896.34	95.19	112.56	4.26	2.99
CL08	FRESH	OL	2.00	33.92	47.47	2.00	3.00	3.00	23.94	10.00	40.27	73.30	25.97	13.82	6.36	3.33
CL6B-0.1	FRESH	OL	2.70	2.95	77.75	2.00	3.00	5.76	129.85	10.00	33.01	635.98	17.95	18.45	4.26	1.74
8	FRESH	OL	2.00	2.00	50.60	2.31	6.32	4.74	139.59	23.60	81.39	45.30	19.20	1298.00	22.68	4.98
10	FRESH	OL	3.10	10.10	118.53	10.90	39.91	7.39	132.23	56.45	60.50	78.97	45.84	75.99	24.71	7.64
9	FRESH	OL	5.31	761.68	235.01	7.59	58.48	15.01	222.73	56.15	127.53	546.28	89.49	68.51	35.70	3.74
CL47B	FRESH	OL	3.13	5.08	20.01	2.53	5.33	16.18	294.19	17.38	45.79	139.97	16.81	24.90	77.15	1.07
CL59	FRESH	OL	4.09	241.54	281.86	2.75	25.30	4.66	132.09	17.48	121.56	535.44	24.15	27.08	4.89	3.75
CL19	FRESH	OL	2.00	48.78	137.50	2.00	19.86	3.00	20.19	10.00	38.10	408.19	54.29	20.33	4.26	3.33
CL61	FRESH	OL	2.99	10.75	588.35	4.13	20.20	5.58	81.02	17.22	89.71	1294.45	39.36	36.12	4.41	3.09
CL49	FRESH	OL	4.30	11.73	548.10	3.35	30.43	8.96	68.23	28.42	83.63	1375.92	63.31	46.56	8.78	3.17
CL08	FRESH	OL	4.30	33.92	47.47	2.00	3.00	3.00	23.94	10.00	40.27	73.30	25.97	13.82	6.36	3.33
1	FRESH	OPX	43.23	22.43	61.72	7.74	99.51	12.79	143.55	45.15	87.60	158.79	84.27	100.87	33.00	3.53
CL53A	FRESH	OPX	5.27	19.07	327.51	12.00	51.39	19.55	61.87	34.64	68.20	2256.25	115.70	145.33	13.20	1.77

Note: CPX- Clinopyroxene-rich pegmatites OPX= Orthopyroxene-rich pegmatites OL= Olivine-rich pegmatites

Table 3: **Major element geochemistry of the pyroxenite host rocks.**

Analyses are given in wt %

SAMPLE NAME	ROCK TYPE	SiO_2	TiO_2	Al_2O_3	FeO	MnO	MgO	CaO	Na_2O	K_2O	P_2O_5	Cr_2O_3	LOI	Total	Mg#
DWR 74/06	Pyroxenite	41.25	0.44	16.11	8.36	0.22	23.21	4.79	0.68	0.12	0.07	5.22	1.20	101.66	83.19
DWR 74/09	Pyroxenite	50.18	0.28	12.48	7.53	0.23	21.75	4.49	0.62	0.14	0.05	3.45	0.20	101.40	83.73
DWR 74/11	Pyroxenite	52.17	0.22	11.68	6.30	0.22	22.84	3.98	0.48	0.16	0.11	3.26	0.20	101.64	86.59
DWR 74/ 13	Pyroxenite	42.50	0.44	17.89	9.02	0.19	19.68	4.69	0.35	0.05	0.03	4.56	1.20	100.58	79.55
DWR 74/21	Pyroxenite	45.29	0.32	13.98	9.68	0.19	19.57	4.56	0.66	0.10	0.03	4.89	1.80	101.06	78.28
DWR 74/27	Pyroxenite	47.60	0.45	15.33	10.75	0.20	18.98	3.13	0.59	0.09	0.03	3.13	0.96	101.24	75.89
DWR 74/33	Pyroxenite	52.52	0.18	13.62	1.82	0.27	28.33	1.93	0.03	0.11	0.02	1.93	0.20	100.98	96.51
DWR 74/34	Pyroxenite	45.74	0.32	14.70	5.78	0.25	24.26	3.01	0.08	0.12	0.02	3.01	2.70	99.98	88.19
DWR172/01	Pyroxenite	35.95	0.51	17.19	10.32	0.20	14.68	2.82	0.61	0.17	0.03	17.43	1.20	101.11	71.72
DWR172/06	Pyroxenite	54.27	0.27	12.75	6.37	0.22	19.06	3.73	0.74	0.35	0.08	2.10	1.30	101.24	84.21
DWR172/07	Pyroxenite	52.46	0.29	13.38	7.00	0.23	18.65	3.91	0.83	0.22	0.06	2.90	0.90	100.83	82.60
DWR172/09	Pyroxenite	55.91	0.18	11.96	5.64	0.23	20.46	4.13	0.53	0.20	0.05	0.65	1.30	101.24	86.60
DWR172/27	Pyroxenite	49.66	0.35	13.65	6.97	0.22	18.75	2.91	0.89	0.25	0.07	6.22	1.50	101.43	82.75
DWR172/28	Pyroxenite	52.93	0.28	12.42	5.93	0.21	19.22	3.97	0.69	0.38	0.06	3.84	1.60	101.54	85.24
DWR172/29	Pyroxenite	45.51	0.43	14.40	7.46	0.21	17.18	4.08	0.78	0.20	0.04	9.65	0.60	100.53	80.40
DWR172/30	Pyroxenite	50.78	0.30	12.98	6.63	0.21	19.00	3.72	0.72	0.25	0.08	5.28	0.50	100.44	83.61

Table 4: **Trace element geochemistry of the pyroxenite host rocks.**

Analyses are given in ppm

SAMPLE NAME	ROCK TYPE	Cu	Ni	Rb	Sr	Y	Zn	Zr	Co	Cr	S	V	Ba	La	Zr/Y
DWR 74/06	Pyroxenite	2	352	1	191	5	57	20	138	103155	61	794	40	15	4.00
DWR 74/09	Pyroxenite	4	767	8	60	5	290	26	88	16980	0	206	15	11	5.20
DWR 74/11	Pyroxenite	3	531	6	66	9	96	32	80	9555	371	162	59	9	3.56
DWR 74/ 13	Pyroxenite	5	514	8	55	11	77	26	150	126382	0	929	23	12	2.36
DWR 74/21	Pyroxenite	4	820	2	51	5	317	27	119	83051	57	622	21	17	5.40
DWR 74/27	Pyroxenite	3	647	5	68	5	210	23	138	117702	61	712	29	23	4.60
DWR 74/33	Pyroxenite	4	796	5	57	5	260	19	91	8702	27	139	50	-2	3.80
DWR 74/34	Pyroxenite	2	632	3	6	3	93	20	114	47495	130	433	61	4	6.67
DWR172/01	Pyroxenite	2	841	11	62	4	367	35	166	134301	80	1037	48	14	8.75
DWR172/06	Pyroxenite	18	547	10	61	8	105	46	95	15363	71	233	124	5	5.75
DWR172/07	Pyroxenite	16	570	9	59	5	112	37	91	20713	67	265	66	1	7.40
DWR172/09	Pyroxenite	10	529	8	49	11	70	44	86	4784	31	122	68	0	4.00
DWR172/27	Pyroxenite	30	585	5	50	7	153	31	95	46380	162	368	66	8	4.43
DWR172/28	Pyroxenite	17	528	16	43	7	108	38	95	28199	76	254	98	4	5.43
DWR172/29	Pyroxenite	23	621	8	53	5	210	29	119	72356	128	527	60	8	5.80
DWR172/30	Pyroxenite	21	553	12	50	7	131	60	101	39134	92	319	72	13	8.57

In general, no discernible relationships are observed for most major and trace elements when plotted against MgO and Mg# (Mg^{2+}/ Mg^{2+}+Fe^{2+}).

MgO and CaO

The clinopyroxene- and orthopyroxene-rich pegmatites in general have a higher CaO content than the olivine-rich pegmatites. The CaO concentration of all the pegmatites at Dwarsrivier mine is higher than their pyroxenite host rocks (Figure 5.1a and Figure 5.1b). In the rocks of the Bushveld Complex, CaO is usually contained in plagioclase, clinopyroxene and amphibole (Eales *et al.*, 1993). Both plagioclase and amphibole occur in modal abundances not exceeding 5% in these pegmatites, whereas clinopyroxene occurs in larger proportion. It is therefore concluded that in the absence of plagioclase and amphiboles, the elevated amounts of CaO in the pegmatites is associated with clinopyroxene. The MgO concentration of the clinopyroxene- and orthopyroxene-rich pegmatites is similar to the pyroxenite host rocks, whereas the MgO content of the olivine-rich pegmatites is higher than the pyroxenite host rocks and also it is the highest for all pegmatites (Figure 5.1c). The MgO and the CaO contents of the pegmatites are useful in discriminating the different pegmatites. Using both the MgO and CaO contents, it is possible to characterise the pegmatites as follows (Table 5):

Table 5: Composite table of average major element concentration for the different pegmatites types.

Rocktype		CaO	MgO
Cpx-rich pegmatite	Avg.	22.36	20.62
	Min.	13.80	11.73
	Max.	36.93	30.60
n=33	Std	5.30	4.61
Opx-rich pegmatite	Avg.	11.82	23.97
	Min.	9.32	23.56
	Max.	14.19	24.78
n=4	Std	2.74	0.56
Ol-rich pegmatite	Avg.	8.91	34.04
	Min.	0.25	22.75
	Max.	19.66	45.06
n=24	Std	6.22	5.77

Note: Cpx= Clinopyroxene-rich pegmatites Opx= Orthopyroxene-rich pegmatites Ol= Olivine-rich pegmatites.

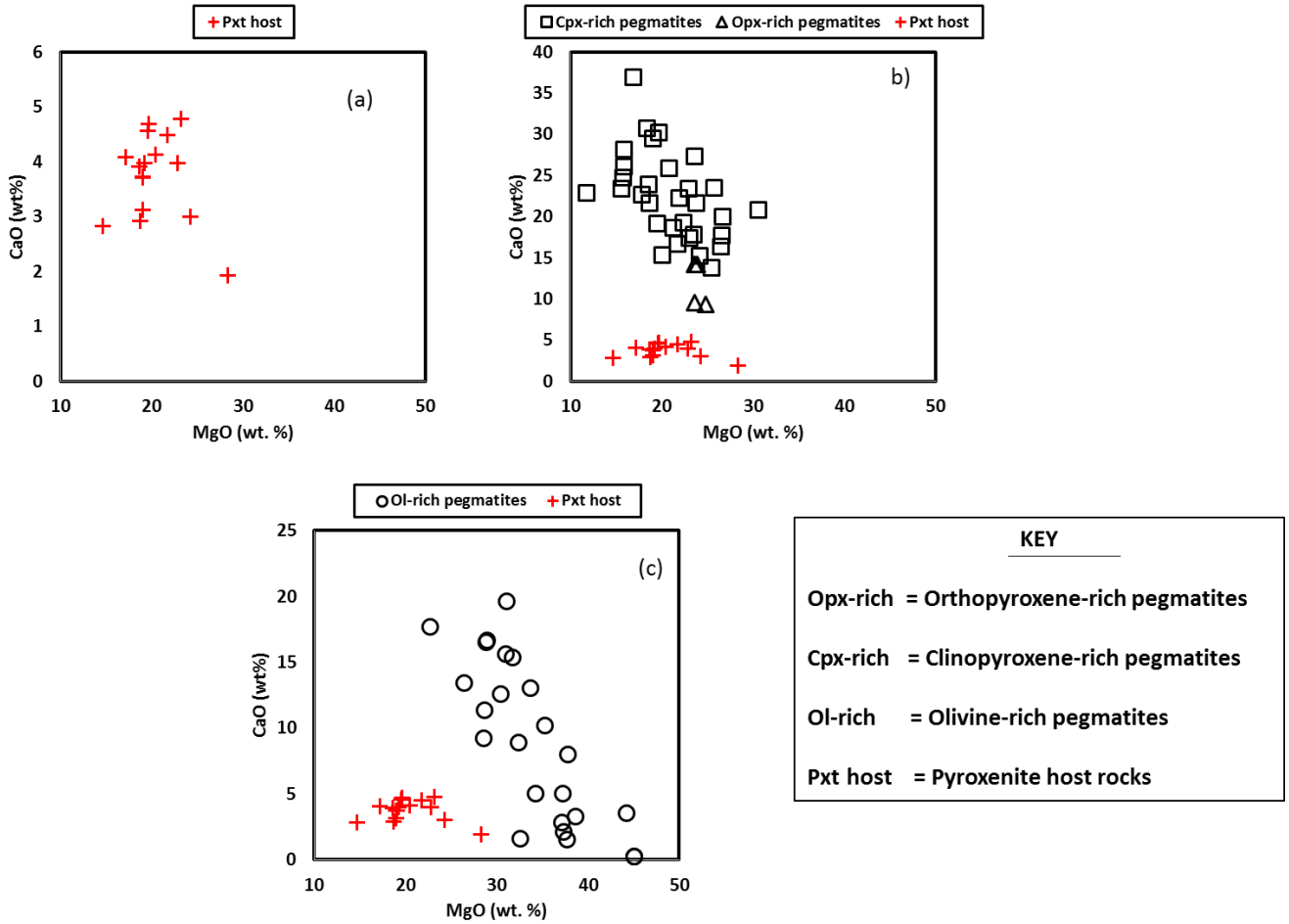

Figure 5.1(a-c): Binary variation diagrams of major elements showing CaO vs MgO for the pegmatites and their pyroxenite host rocks. The data indicate that the pyroxenite host rocks have lower CaO content than the pegmatites due to the modal abundance of clinopyroxene.

FeO

In general, the data indicate a compositional overlap in the FeO content of the pegmatites and their pyroxenite host rocks (Figure 5.1e and Figure 5.1f), although a few olivine-rich pegmatite samples have a slightly higher FeO content than pyroxenite host rocks.

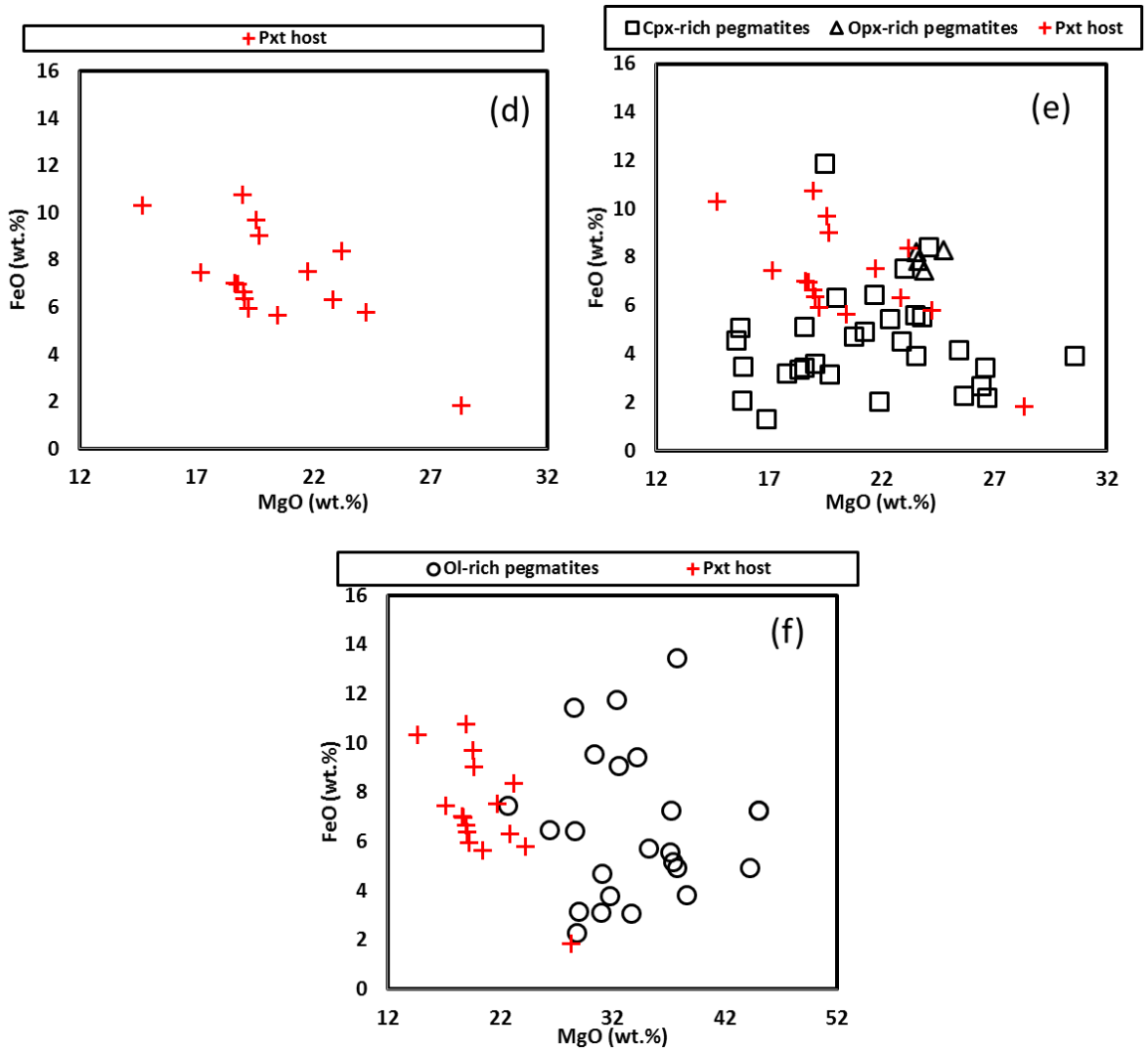

Figure 5.1 (d-f): Binary variation diagrams of major elements showing FeO vs MgO for the pegmatites and their pyroxenite host rocks. The FeO content of the pegmatites is similar to the pyroxenite host rocks.

SiO_2

SiO_2 is accommodated in all mafic minerals and it can be used in this study in combination with other major elements to discriminate the different pegmatites in this study. The data show that the SiO_2 concentration of the clinopyroxene- and orthopyroxene-rich pegmatites is similar to the pyroxenite host rocks, whereas the SiO_2 concentration of the olivine-rich pegmatites is lower than the other two groups of pegmatites, and also lower than the pyroxenite host rocks (Figure 5.1h and Figure 5.1i).

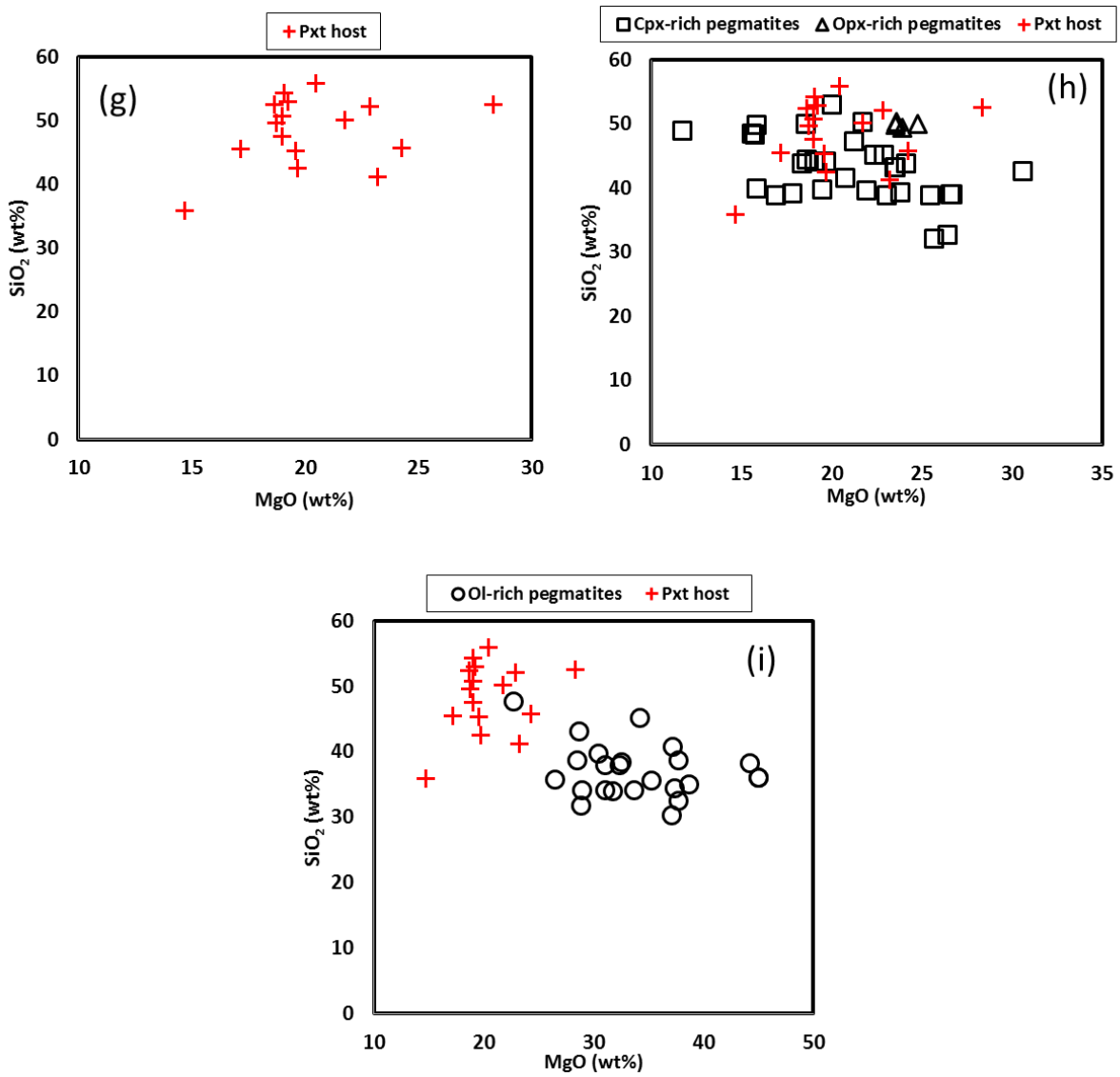

Figure 5.1(g-i): Binary variation diagrams of major elements showing SiO_2 vs MgO for pegmatites and their pyroxenite host rocks. There is a compositional overlap in the SiO_2 content of the host rocks and the clinopyroxene- and orthopyroxene-rich pegmatites.

Al_2O_3

The pegmatites in general, have a lower Al_2O_3 concentration than their pyroxenite host rocks (Figure 5.1k-l). The Al_2O_3 concentration of mafic rocks in the layered sequence of the Bushveld Complex is largely controlled by the presence of plagioclase (Eales *et al.*, 1993). Plagioclase in the pegmatites is less than 5% in modal abundance.

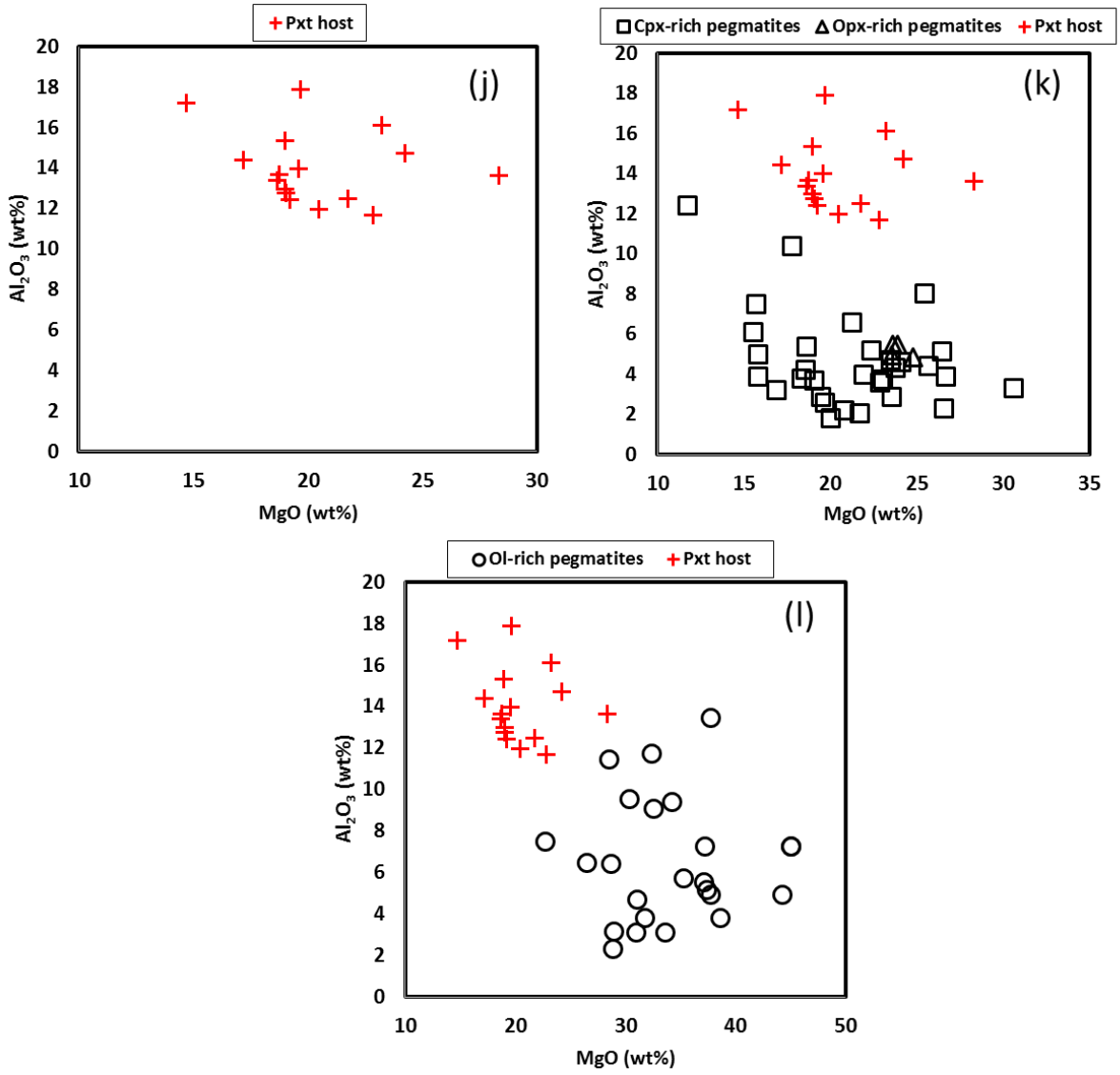

Figure 5.1 (j-l): Binary variation diagrams of major elements showing Al_2O_3 vs MgO for the pegmatites and their pyroxenite host rocks. In general, the pegmatites have a lower Al_2O_3 than the pyroxenite host rocks.

MnO

There is a compositional overlap between in the MnO concentration of the pegmatites and their pyroxenite host rocks (Figure 5.1n and Figure 5.1o). In mafic rocks MnO is usually contained, in decreasing amounts, in the following minerals: ilmenite, magnetite, orthopyroxene, olivine, chromite, clinopyroxene, and plagioclase (Hulbert, 1983). Because of its valence Mn^{2+} usually substitute for Fe^{2+} or Mg^{2+} in mafic minerals (Ford *et al.*, 1983), hence the negative correlation between MnO and FeO in the pyroxenite host rocks (Figure 5.1). In the pegmatites, MnO does not correlate with FeO (Figure 5.1)

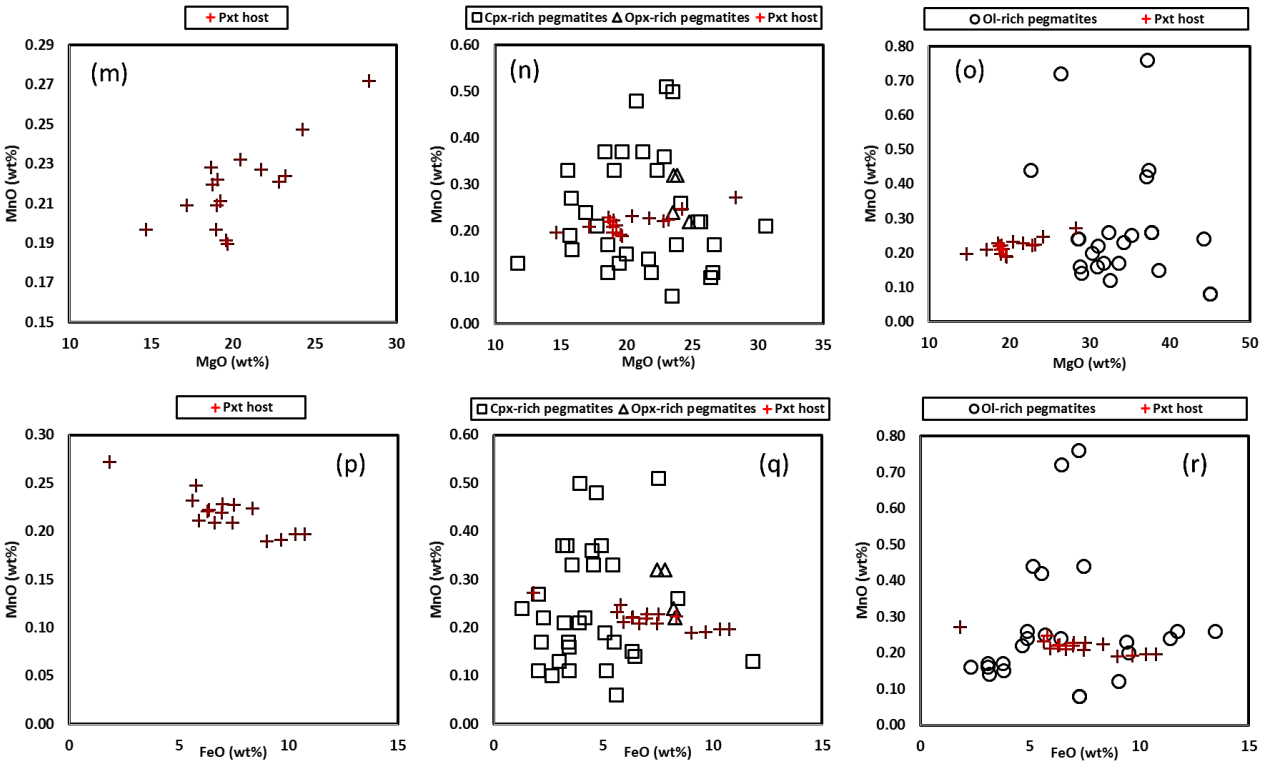

Figure 5.1 (m-r): Binary variation diagrams of major elements showing MnO vs MgO (m-o) and MnO vs FeO (p-r), respectively, for the pegmatites and their pyroxenite host rocks. In general, there is a compositional overlap in the MnO concentration of the pegmatites the pyroxenite host rocks.

TiO_2

The pegmatites are generally lower in TiO_2 than their pyroxenite host rocks, although some compositional overlaps occur with a few samples (Figure 5.1s-u). The element Ti has a low partition coefficient (D) into major cumulus minerals (Rollinson, 1993), and will preferentially partition into the residual melt / accessory phases (Hulbert, 1983; Pearce & Nowry, 1979). Therefore, magmas that are least differentiated would have the lowest TiO_2 content. Eales et al. 1993 have also reported an increase in Ti with the crystallization of plagioclase in the orthopyroxenes of the Lower Critical Zone. In the pegmatites and the pyroxenite host rocks, the concentration of TiO2 increases with increasing Al_2O_3 content (Figure 5.1v-x). This trend can be explained as Ti being incorporated into the accessory phases as plagioclase crystallizes from the pegmatite melt.

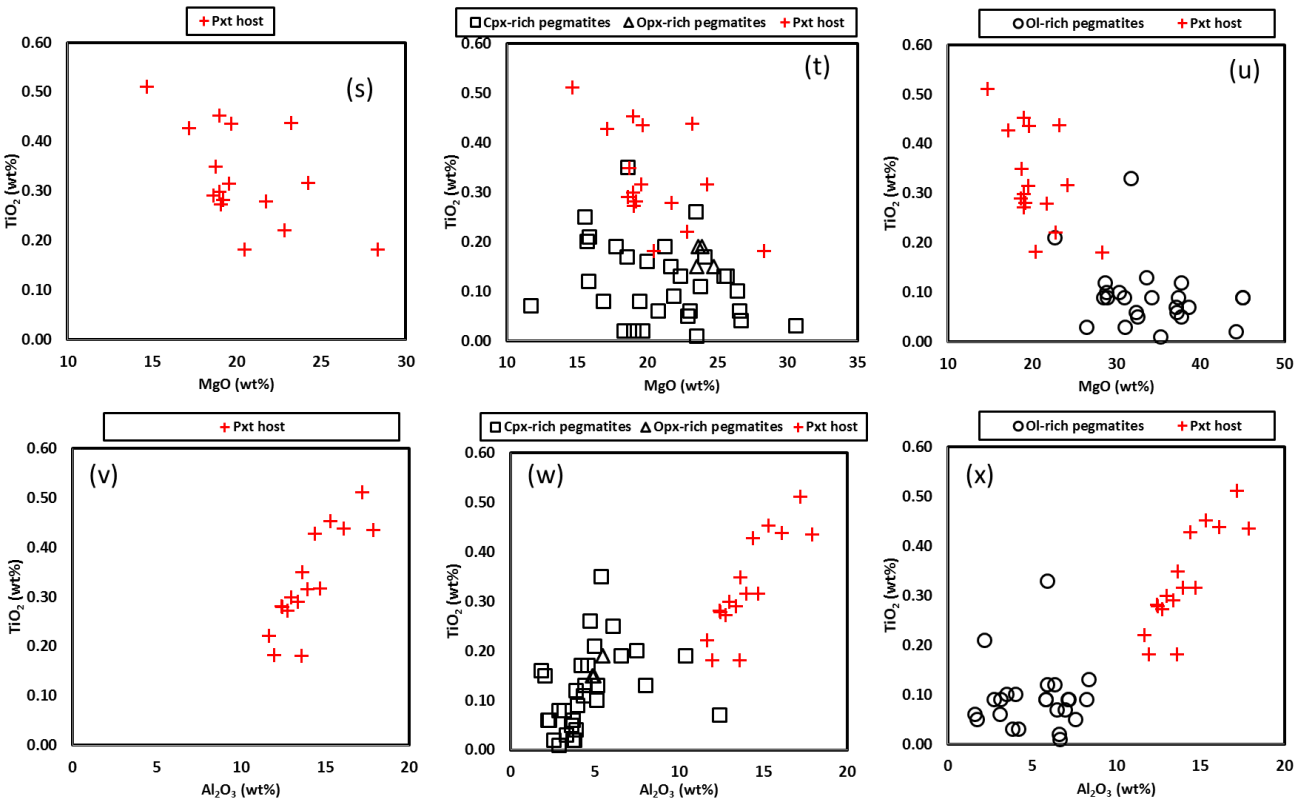

Figure 5.1(s-x): Binary variation diagrams of major elements showing TiO_2 vs MgO (s-u) and TiO_2 vs Al_2O_3 (v-x), respectively, for the pegmatites and their pyroxenite host rocks. In general, the pegmatites have a lower TiO_2 concentration than their pyroxenite host rocks.

K_2O and Na_2O

The concentration of Na_2O and K_2O in the cumulates of the Bushveld Complex is controlled by plagioclase (Eales *et al.*, 1993) and its concentration will largely be controlled by the modal proportion and composition of plagioclase (Seabrook, 2005). The Na_2O+K_2O concentration of the orthopyroxene-rich and clinopyroxene-rich pegmatites overlap with the pyroxenite host rocks (Figure 5.1y). The olivine-rich pegmatites have a lower Na2O+K_2O than the pyroxenite as they lack plagioclase.

Cr_2O_3

Except for a few chromite-rich samples, the pegmatites are generally lower in Cr_2O_3 relative to their pyroxenite host rocks. As has been discussed in Chapter 4, all the pegmatites are poor in Cr_2O_3.

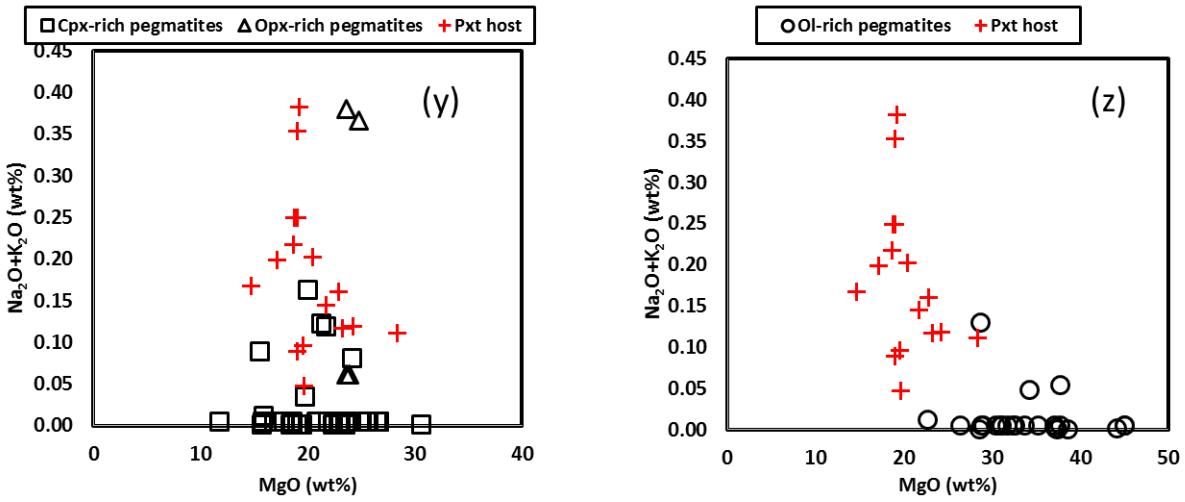

Figure 5.1 (y-z): Binary variation diagrams of Na_2O vs MgO for the pegmatites and their pyroxenite host rocks. There is a compositional overlap in some samples of the clinopyroxene and orthopyroxene-rich pegmatites and the pyroxenite host rocks.

5.3. Trace elements geochemistry.

The partitioning of trace elements into mafic minerals is largely controlled and influenced by several factors such as the nature of the parental magma, its state of differentiation, the modal proportions of the main rock-forming minerals, the composition and proportion of trapped melt and percolation of late magmatic and hydrothermal fluids (Maier *et al*., 2012). Following the complex interplay of the above mentioned factors, some trace elements will either be compatible or incompatible with the mafic minerals. As has been observed with the major elements concentration in the pegmatites, the concentration of trace elements is controlled by the modal abundance of the mafic minerals in the pegmatites. Elements such as Co, Cu, Ni, Zn and V are compatible to orthopyroxene, whereas elements such as Sr are compatible into the crystal lattice of plagioclase and clinopyroxene, and their concentration will be influenced by the modal abundance of orthopyroxene and clinopyroxene in the rocks (Seabrook, 2005). Elements such as Zr and Y are incompatible to the mafic minerals, and will concentrate in the residual liquid and form accessory minerals (Eales *et al*,. 1993).

The following trace elements were analysed for (ppm): Rb, Sr, Y, Zr, Nb, Co, Ni, Cu, Zn, V, Cr and Ba

Strontium (Sr)

The Sr concentration of the pegmatites generally overlaps with the pyroxenite host rocks (Figure 5.2a). The Sr partition coefficients into plagioclase, clinopyroxene and orthopyroxene are 1.4, 0.10, and 0.01, respectively (Philipotts & Schnezler, 1970). From these partition coefficients, it is evident that Sr will

readily partition into plagioclase. The concentration of Sr in mafic rocks is controlled mainly by the modal proportion of plagioclase, where Sr substitutes for calcium in the plagioclase. As plagioclase crystallizes out of the magma, the Sr concentration will decrease. However, the plagioclase modal proportions is less than 5% in the pegmatites, hence there is no discernible relationship between Sr and Al_2O_3 in the pegmatites (Figure 5.2a). The elevated Sr concentration in the pegmatites is therefore mainly controlled by the presence of clinopyroxene, and to a smaller degree, by plagioclase. To further illustrate the relationship of Sr and clinopyroxene in the pegmatites, a plot of Sr and CaO is presented in Figure 5.2b. There is generally a positive correlation between Sr and CaO for all the pegmatites. The clinopyroxene-rich pegmatites have a higher Sr/CaO ratio than all the other pegmatites due to the modal abundance of clinopyroxene.

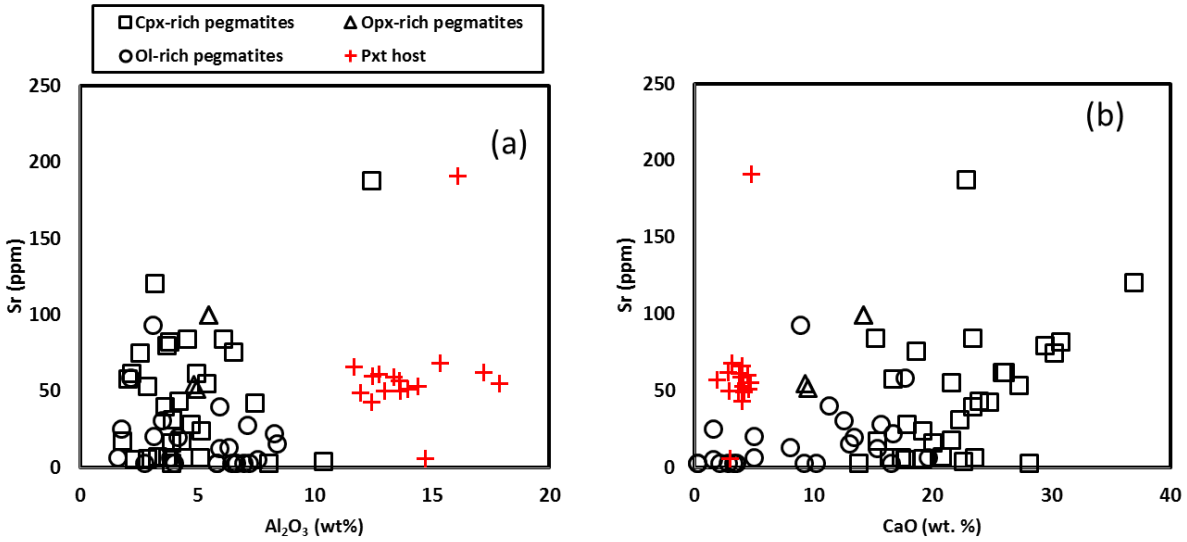

Figure 5.2: Binary variation diagrams of (a) Sr vs Al_2O_3 and (b) Sr vs CaO for the pegmatites and their pyroxenite host rocks. The Sr content of the pegmatites overlaps with the pyroxenite host rocks. The clinopyroxene-rich pegmatites have a higher Sr/CaO than the host rocks, as shown in Figure 5.2b.

Rubidium

The element Rubidium (Rb) has an ionic radius (1.47 Å) similar to that of potassium (K) (1.33 Å) (Maier, 1991). Rb will preferentially partition into K-feldspars and mica. In the absence of K-feldspars and mica, Rb will concentrate in the residual intercumulus liquid. Mica in the form of phlogopite and biotite are present as accessory phases in the pegmatites. The concentration of Rb of the pegmatites generally overlaps with the pyroxenite host rocks (Figure 5.2c). Rb in the pegmatites also shows a

positive trend when plotted against Sr, indicating the control of Rb by the presence of interstitial plagioclase (Figure 5.2d)

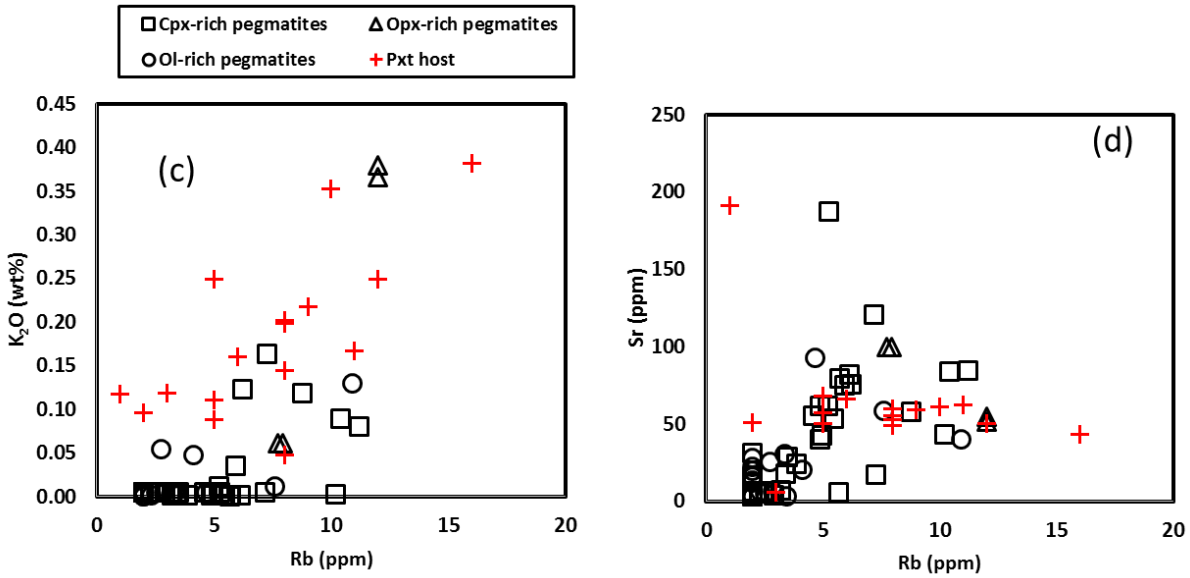

Figure 5.2 (c-d): Binary variation diagrams of (c) K_2O vs Rb and (d) Sr vs Rb for the pegmatites and their pyroxenite host rocks. The Rb and Sr content of the pegmatites overlaps with the pyroxenite host rocks.

Nickel, Copper and Cobalt

The element copper is generally incompatible to the mafic minerals of the Bushveld Complex, and will preferentially partition into sulphides than in silicate minerals (Maier *et al.*, 2012). The presence of Cu in the rocks of the Bushveld Complex is associated with sulphides, and can generally be used as an indicator for localised sulphide enrichment. The Cu concentration of the pegmatites overlaps with the pyroxenite host rocks, although some clinopyroxene-rich pegmatite samples have a Cu content higher than the pyroxenite host rocks (Figure 5.2e). Nickel readily enters the cationic sites of olivine and orthopyroxene (Maier, 1991). Ni also has an affinity to sulphides, and can be used to indicate the presence of sulphides (Lee & Fesq, 1986). Due to this dual compatibility, Ni therefore cannot be used solely as an indicator of the presence of sulphides in mafic rocks. Generally, Ni in the pegmatites is lower than the pyroxenite host rocks (Figure 5.2d). The highest Ni values in the pegmatites correspond to the olivine-rich pegmatite. In early magmatic processes cobalt, with a similar charge and ionic radius as Mg and Fe, readily partitions into minerals such as pyroxene, olivine, magnetite, ilmenite and sulphides (Hulbert, 1983; Rajamani & Naldrett, 1978). From the fact that no significant sulphides were observed in the pegmatites, it is concluded that the cobalt in the pegmatites is contained primarily in

the mafic minerals rather than in sulphides. This observation is consistent with that of Gauert (1998) who reported that Co preferentially substitutes for Mg in olivine and orthopyroxene, and its high concentrations depends on the modal proportion of olivine and orthopyroxene.

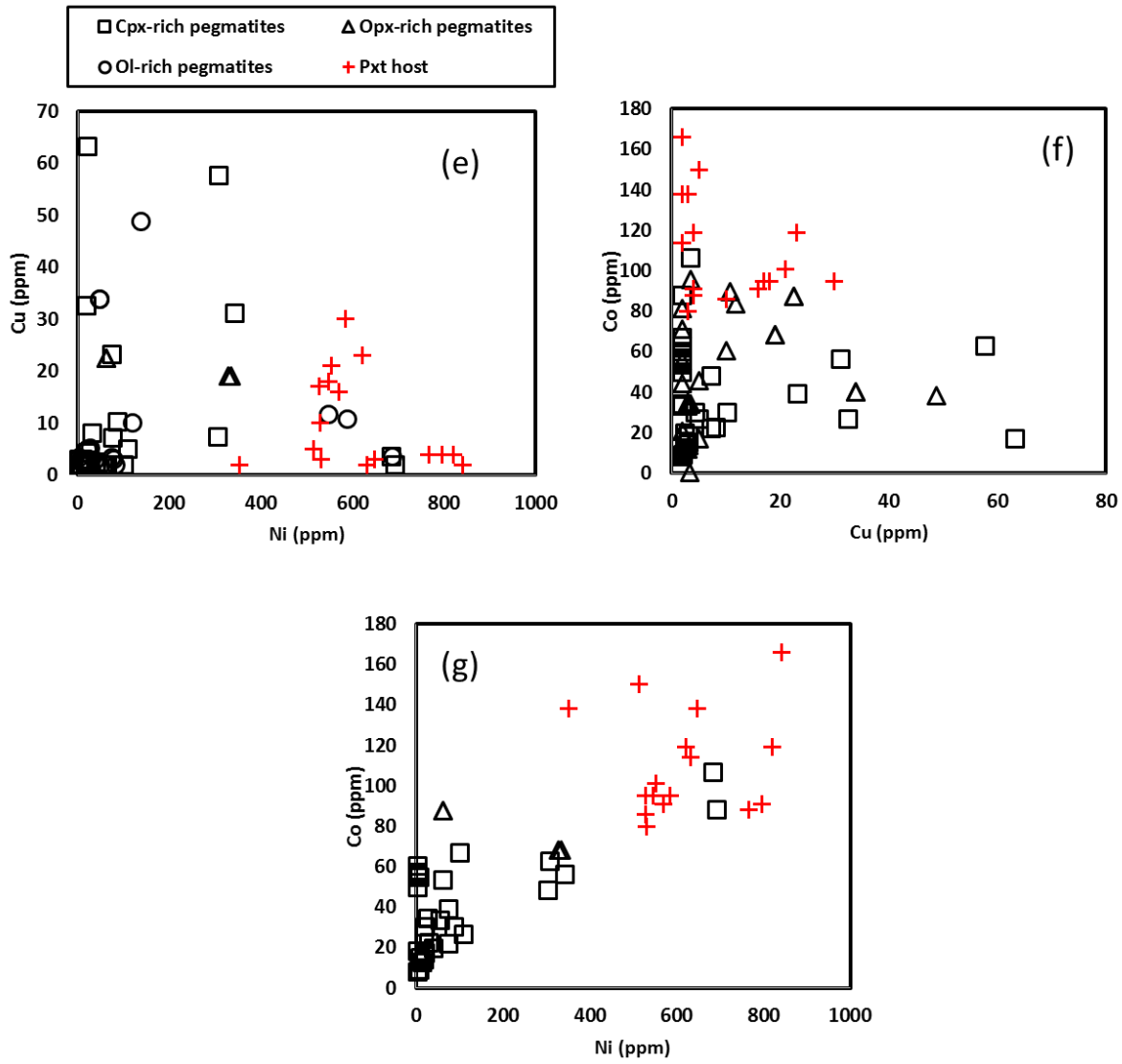

Figure 5.2 (e-g): Binary variation diagrams of (a) Cu vs Ni (b) Co vs Cu, and (c) Co vs Ni for the pegmatites and their pyroxenite host rocks. The concentration of Cu in the pegmatites is controlled by sulphides, whereas Co and Ni are closely associated with the silicate minerals.

Zinc

The elements zinc is compatible to mafic minerals due to its ability to substitute for iron (Buchanan, 1976). The Zn content of the pegmatites is overlaps with the pyroxenite host rocks (Figure 5.2h)

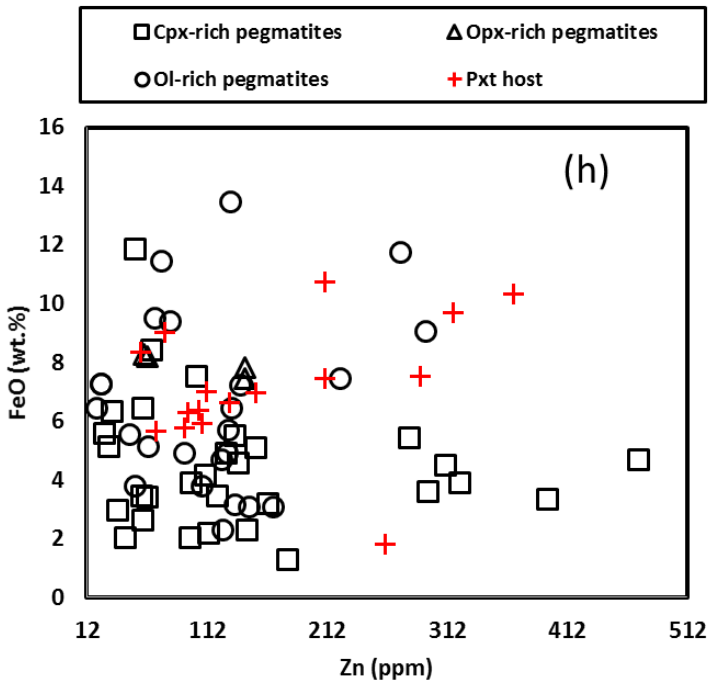

Figure 5.2 (h): Binary variation diagram of FeO and Zn for the pegmatites and their pyroxenite host rocks. The Zn concentration of the pegmatites overlaps with the pyroxenite host rocks.

Vanadium and chromite

The vanadium content of the pegmatites is generally lower than that of the pyroxenite host rocks (Figure 5.2i). Vanadium partitions readily into the cationic sites of spinel and also into orthopyroxene (Teigler, 1990). In the mafic rocks of the Bushveld Complex, vanadium is usually associated with chromite. Elevated amounts of vanadium may indicate the presence of chromite in the rocks. Vanadium also has a limited substitution into augite. A plot of V against Cr shows a strong positive correlation for the pyroxenite host rocks (Figure 5.2i). The relationship is not well defined in the pegmatites. The positive correlation of V and Cr in the pyroxenite host rocks is an indication that the vanadium content of these rocks is controlled by the presence of chromite.

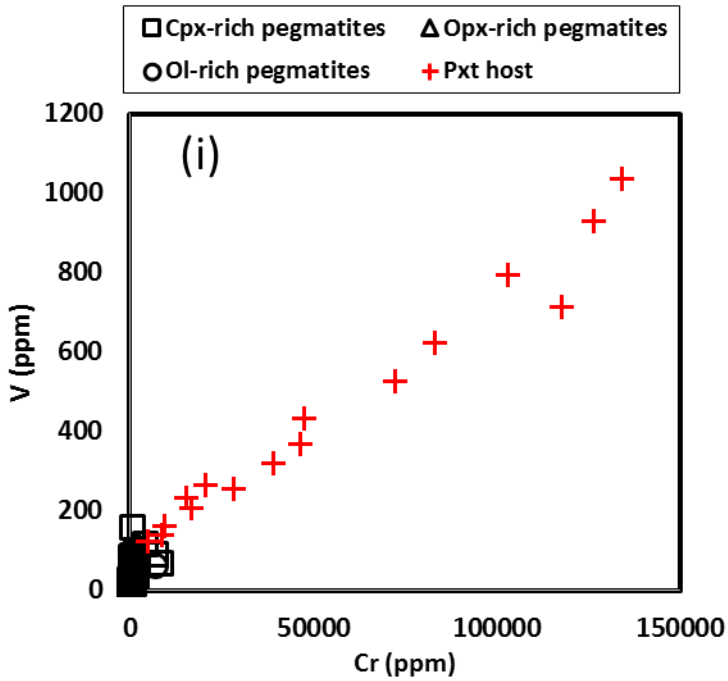

Figure 5.2i: Binary variation diagram of V and Cr for the pegmatites and their pyroxenite host rocks. The V concentration of the pyroxenite host rocks is higher than the pegmatites, and its concentration in the former is associated with the presence of chromite.

Zirconium and Yttrium

The elements Zr and Y have a small radius and tend to not readily enter the cationic sites of most common mafic minerals and therefore, they are incompatible to most mafic minerals due to their low D values in basic magmas (Pearce & Nowry, 1979). In a basic magma, the distribution coefficients ($D_Y^{Solid\text{-}liq}$) of Y in olivine, plagioclase, clinopyroxene and orthopyroxene is 0.01; 0.03; 0.50 and 0.20, respectively, whereas for Zr is 0.01; 0.01; 0.1, and 0.03, respectively (Pearce & Nowry, 1979). These elements should therefore be accommodated in the trapped liquid and accessory phases of the magma. Highly fractionated magmas would have high Zr and Y values. Hulbert (1983) observed that Y could have a limited substitution for calcium in pyroxenes. Hence, the Y is not entirely in the residual liquid of the magma. In general, there is a compositional overlap in the Zr and Y concentration of the pegmatites and the pyroxene host rocks (Figure 5.2j).

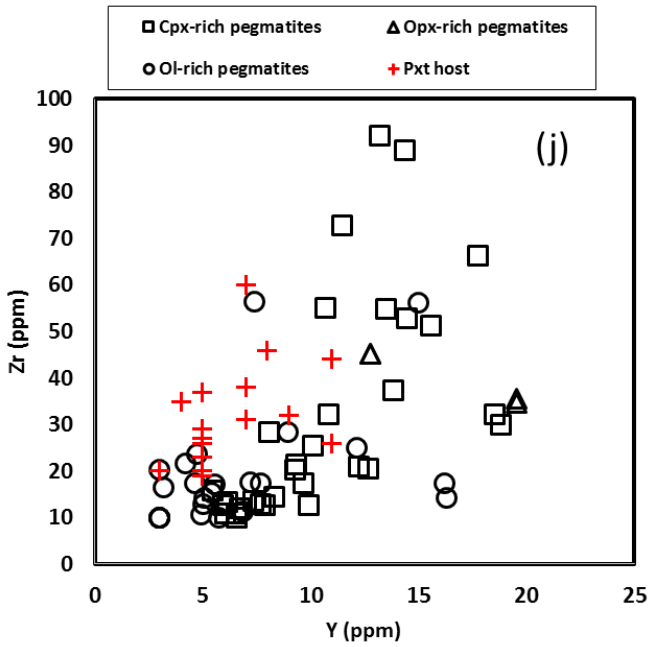

Figure 5.2j: Binary variation diagram of Zr and Y for the pegmatites and their pyroxenite host rocks. There is a compositional overlap in the Zr and Y concentrations of the pegmatites and the pyroxenite host rocks.

5.4. Trace element ratios.

Trace element ratios are useful indicators of magmatic processes such magma fractionation, magma differentiation and magma replenishment (Eales *et al.*, 1993). As has been discussed before, compatible trace elements such as Cr, V and Zn are controlled by the presence of chromite and orthopyroxene, respectively, whereas incompatible elements such as Rb, Y and Zr will be accommodated in accessory phases such as plagioclase and biotite, respectively. The following trace element ratios were calculated for both the pegmatites and pyroxenite host rocks: Mg#, Cr/V, Rb/Zr and Zr/Y. These ratios are considered petrological indicators for magma differentiation for the layered rocks of the Bushveld Complex (Eales et *al.*, 1986; Maier *et al.*, 2012).

The trace element ratios are plotted against whole rock Mg# (Mg^{2+}/ Mg^{2+}+Fe^{2+}). The Mg# of the pegmatites is generally higher than that of the pyroxenite host rocks, although there is some compositional overlap. The Mg# is influenced by the presence of chromium, and is used to indicate magma fractionation (Eales & Cawthorn, 1996). There is a general compositional overlap in the in the Zr/Y (Figure 5.2k) and Rb/Zr (Figure 5.2l) ratios of the pegmatites and their pyroxenite host rocks. The Rb/ Zr ratio is controlled by the modal abundance of plagioclase in the rock and trapped liquid. The compositional overlap in the trace element ratios of the pegmatites and the pyroxenite host rocks points

to two genetically linked magmas. The Cr/V ratios of the pegmatites are generally lower than the pyroxenite host rocks (Figure 5.2m)

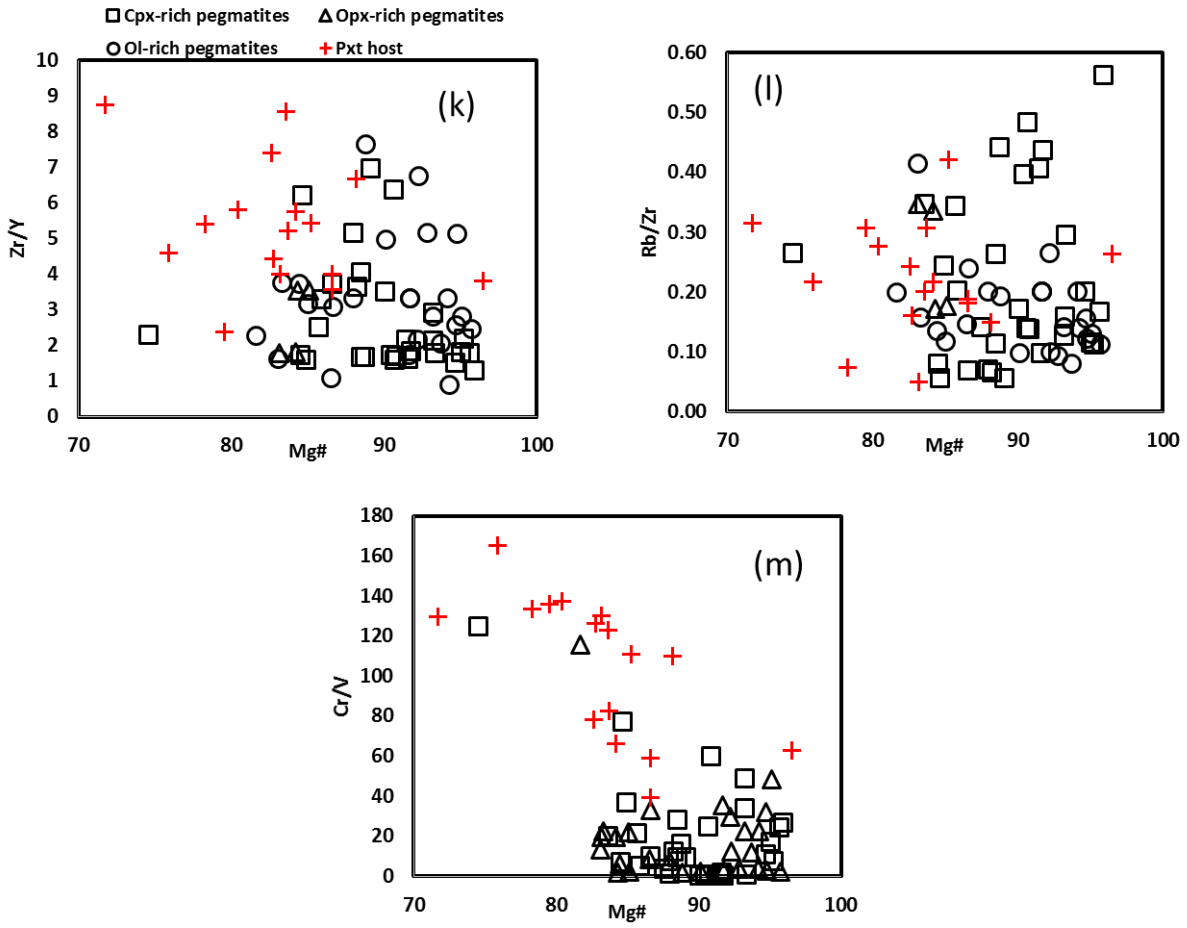

Figure 5.2(k-m): Selected ratios of the pegmatites and their pyroxenite host rocks. There is generally a compositional overlap in the Zr/Y, Rb/Zr and Mg# of the pegmatites and the pyroxenite host rocks.

5.5. Chemical variation through a layered pegmatite.

In order to illustrate the geochemical variation of major and trace elements in a vertical section through an altered pegmatite, a 1.24 m thick altered pegmatite occurring in the hanging wall of the LG-6 was chosen. This pegmatite was selected on the basis that its entire thickness was intersected by borehole DWR 155, and it offers an opportunity to investigate the variation of whole-rock chemistry with stratigraphic height. The middle part of the pegmatite is highly serpentinised and it is bounded at the top and the bottom by layers of clinopyroxene and orthopyroxene-rich pegmatite, respectively (Figure 5. 3a-l)

Selected incompatible elements such as Zr and Y are plotted against stratigraphic height. Also plotted are the trace element ratios Zr/Y, Cr/V and Rb/Zr. Trace element and trace element ratios of rocks against stratigraphic height are useful in that they may indicate whether or not there was multiple injection of magma and post cumulus migration of residual magma (Cawthorn & McCarthy, 1985). According to Figure 5.3 (a)-(e), there is a sympathetic relationship between Cr, Co, and Ni. These elements are compatible in sulphides. There is a spike in Cu and corresponding spikes in Co and Ni at the same stratigraphic position. This indicates the presence of sulphides at that stratigraphic horizon Cr correlates positively with V at a single stratigraphic level, pointing to the control of V by the presence of chromite (Figure 5.3f-h) pointing to the control on the concentration of V by chromite. However, except for that particular stratigraphic level, Cr does not correlate well with V in the intersected pegmatite, pointing to some mechanism other than Cr controlling the concentration of V. There is also a sympathetic relationship between Zr and Y (Figure 5.3i-l). Furthermore, the ratio of Zr/Y shows a large variation, pointing to the possibility of different melts that have formed the pegmatite.

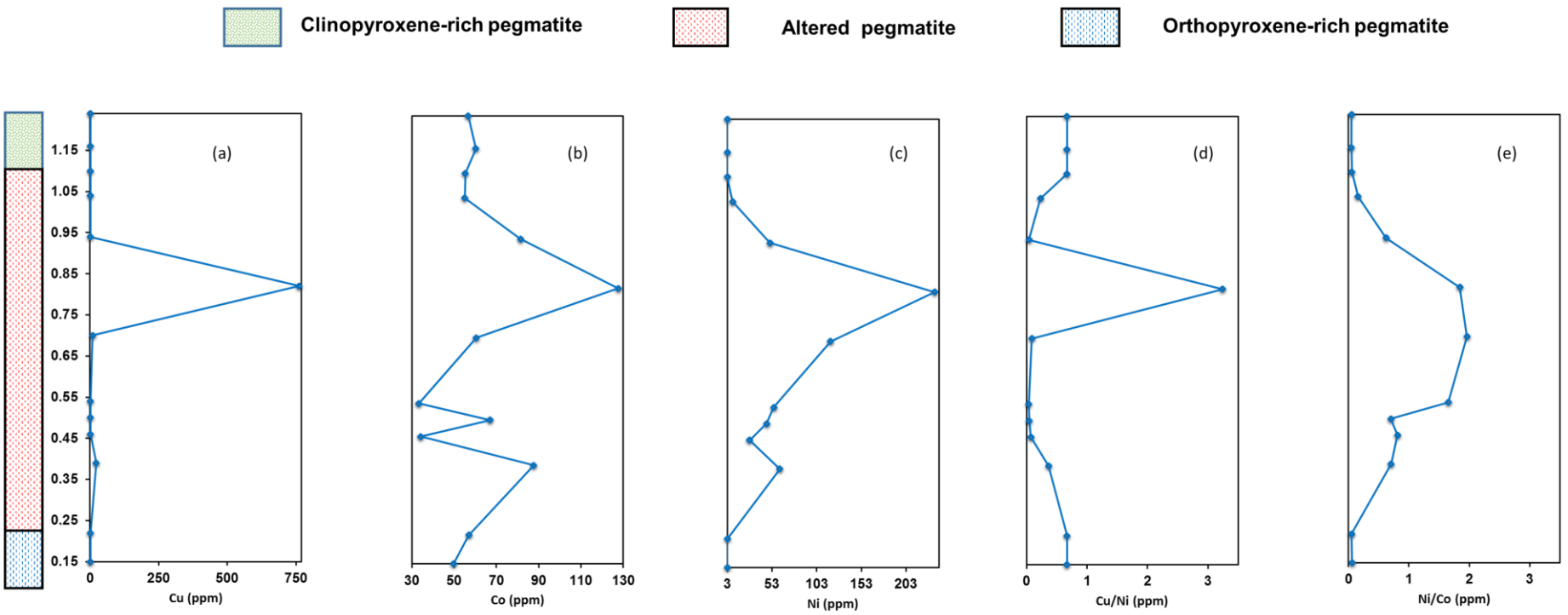

Figure 5.3: Selected trace elements variation plotted against stratigraphic height (a) Cu, (b) Co, (c) Ni, as well as trace element ratios (d) Cu/Ni, and (e) Ni/Co. There is generally a sympathetic relationship for the elements Cu, Co, and Ni. The elements Cu, Co, and Ni are compatible into sulphides. The concentration of these elements in this pegmatite is controlled by the presence of sulphides. This is also supported by the trace element ratios Cu/Ni and Ni/Co.

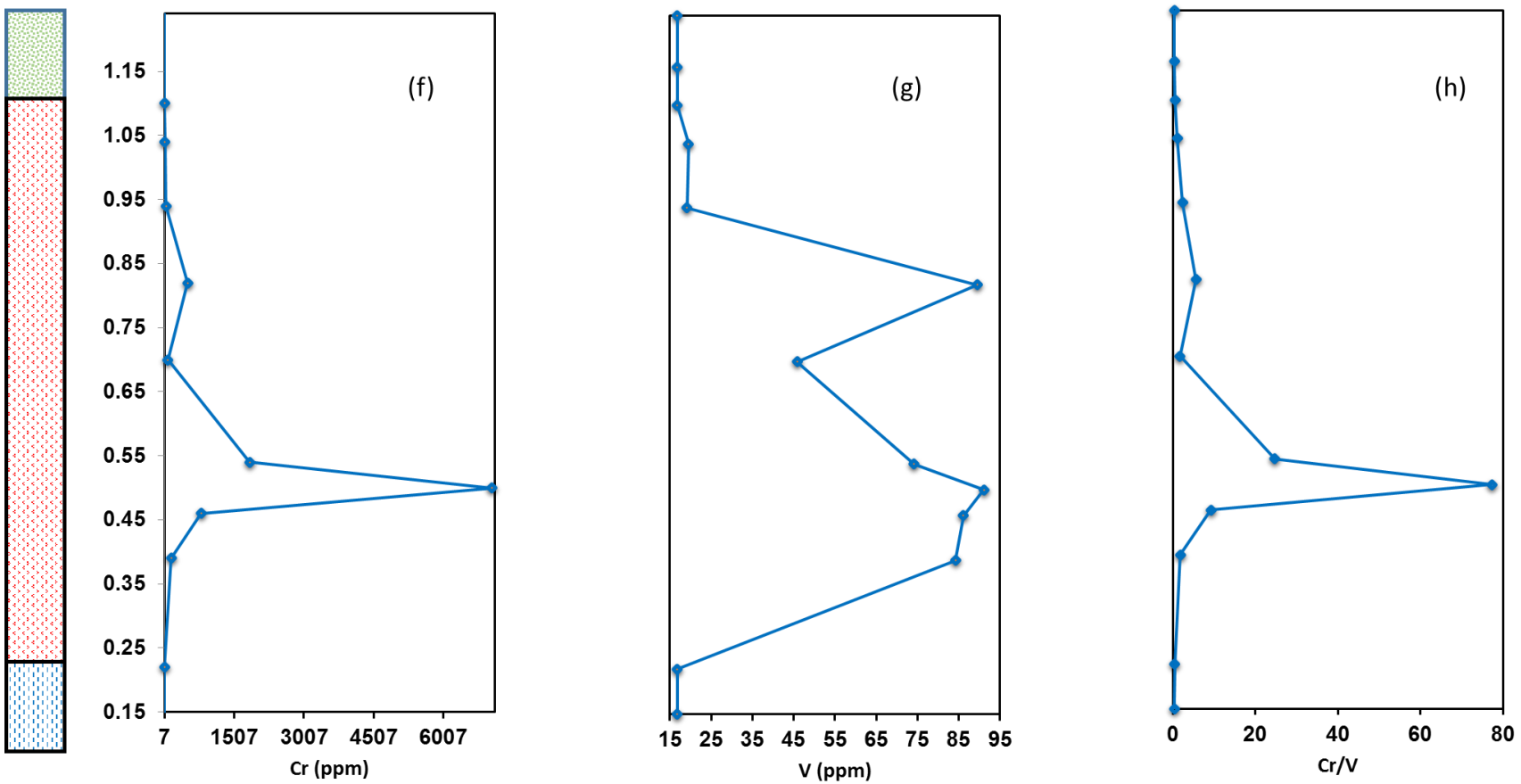

Figure 5.3 (f-h): Trace elements variation plotted against stratigraphic height (f) Cr and (g) V, and Cr/V ratio. There is generally a poor correlation between Cr and V, implying that V is mostly not controlled by Cr in this pegmatite.

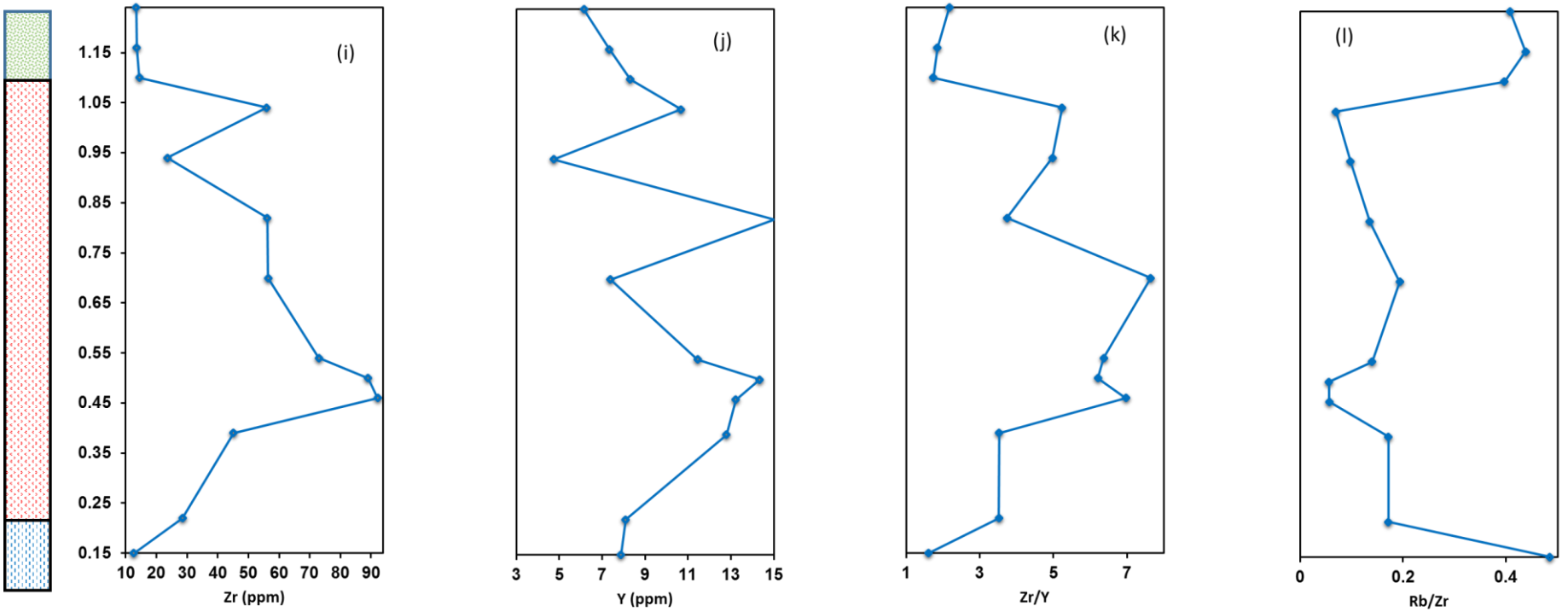

Figure 5.3 (i-l): Trace elements and trace element ratios plotted against stratigraphic height (i) Zr, (j) Y, (k) Zr/Y and (l) Ba. There is a sympathetic relationship for Zr vs Y. The elements Zr and Y are incompatible to silicate melts, and will be concentrated in the residual liquid. The pegmatite also show variation in Zr/Y, implying different melts.

5.6. Comparison of Dwarsrivier Mine pegmatites with concordant pegmatites from other locations in the Bushveld Complex: The Winterveld Mine, eastern Bushveld Complex.

Concordant pegmatites that occur similarly to the pegmatites at Dwarsrivier mine have been identified at the Winterveld mine, eastern Bushveld Complex (Bristow, 1989). The Winterveld mine occurs on the farm Winterveld 293 KT, about 35 km south of Dwarsrivier mine (Figure 1.1). The pegmatites at the Winterveld mine occur in both the silicate and chromitite rocks in the layered sequence. Bristow (1989) identified four types of pegmatites at the Winterveld Mine: orthopyroxene-, olivine-, clinopyroxene-, and amphibole-rich pegmatites. The orthopyroxene-rich pegmatites were the most ubiquitous type. The average whole rock geochemical compositions of the four types of pegmatites at Winterveld nine as reported by Bristow (1989) are listed in Table 6, together with the geochemical data for the individual samples (Table 7 and Table 8).

Table 6: Selected major element average composition of the four types of pegmatites at the Winterveld Mine, eastern Bushveld Complex (Bristow, 1989).

PEGMATITE TYPE	SiO_2 (wt%)	TiO_2 (wt%)	AL_2O_3 (wt%)	FeO (wt%)	MnO (wt%)	MgO (wt%)	CaO (wt%)	Cr_2O_3 (wt%)	Mg#
Opx-rich pegmatite	55.72	0.14	3.71	8.96	0.20	27.25	3.52	0.57	85.90
Ol-rich pegmatite	51.50	0.10	2.31	10.47	0.21	32.86	2.02	0.55	86.30
Cpx-Rich pegmatite	53.96	0.20	3.13	6.06	0.15	19.25	16.82	0.45	86.40
Amph-rich pegmatite	58.57	0.24	5.05	8.64	0.18	21.61	3.14	0.57	83.40

5.6.1. Major element comparison of the pegmatites at Dwarsrivier Mine and Winterveld Mine.

Based on the available geochemical data from the pegmatites at the Winterveld mine, the comparison between the pegmatites at Dwarsrivier mine and Winterveld mine were based on the following analyses of individual samples for the following major elements: CaO, FeO, SiO_2, Al_2O_3, MnO, TiO_2, and Cr_2O_3. Trace element comparison were based on the following elements: Rb, V, and Sr.

When plotting the major elements against MgO in bivariate plots, the pegmatites at Dwarsrivier mine are distinctly different from the pegmatites at Winterveld mine, although compositional overlaps exist with regards to certain major and trace elements (Figure 5.4a-j). Furthermore, the different pegmatite groups at Winterveld plot in different compositional fields than the pegmatites at Dwarsrivier mine. In general, the pegmatites at Winterveld have a higher SiO_2 and Cr_2O_3, with lower CaO than the pegmatites at Dwarsrivier mine.

Table 7: Major element geochemistry for the pegmatites at Winterveld Mine (Bristow, 1989).

Analyses given in wt. %

Pegmatite type	Sample number	SiO2	TiO2	Na_2O	Al_2O_3	FeO	Cr_2O_3	MnO	MgO	CaO	Total	Mg#
CPX	MB82/52B3	54.88	0.17	0.32	3.28	5.19	0.31	0.15	18.78	17.89	100.97	86.57
CPX	MB82/52A2	54.32	0.52	0.28	2.77	6.13	0.60	0.17	21.04	14.25	100.08	85.95
CPX	MB82/78	54.15	0.18	0.32	3.65	5.92	0.79	0.17	21.59	11.93	98.70	86.66
CPX	MB82/30	56.22	0.14	0.61	4.12	7.92	0.51	0.20	27.09	3.24	100.06	85.91
OPX	MB82/46	55.80	0.14	0.61	6.13	7.05	0.51	0.17	26.11	4.61	101.14	86.84
OPX	MB82/52A5	56.31	0.10	0.24	3.35	8.30	0.43	0.21	26.68	4.22	99.84	85.14
OPX	MB82/23	54.31	0.13	0.30	4.10	7.92	1.60	0.21	26.44	4.05	99.06	85.61
OPX	MB82/53AII2	56.56	0.11	0.71	2.55	8.52	0.47	0.21	26.90	3.88	99.90	84.91
OPX	MB82/41	53.97	0.18	0.32	5.25	8.38	0.79	0.20	27.17	3.59	99.85	85.25
OPX	MB82/37	57.18	0.11	0.31	3.35	1.05	0.62	0.21	27.07	3.50	93.39	84.99
OPX	MB82/40	56.87	0.17	0.50	4.28	8.12	0.47	0.20	25.39	3.43	99.43	84.78
OPX	MB82/25	55.84	0.15	0.18	3.76	8.04	0.49	0.21	27.36	3.40	99.43	85.84
OPX	MB82/95	55.23	0.11	0.27	3.96	7.56	0.58	0.19	27.77	3.35	99.02	86.75
OPX	MB82/38	56.83	0.15	0.29	3.63	8.27	0.52	0.21	23.61	3.30	96.81	84.66
OPX	MB82/45	55.83	0.13	0.37	3.75	7.62	0.46	0.19	27.92	2.96	99.22	86.72
OPX	MB82/24III	55.48	0.11	0.16	3.06	8.23	0.57	0.21	29.58	2.59	99.99	86.50
OPX	MB82/52B1	55.92	0.18	0.32	2.44	8.62	0.31	0.22	26.90	2.42	97.32	84.76
OL	MB82/24	55.24	0.24	0.79	3.18	7.82	0.57	0.20	27.77	3.69	99.50	86.35
OL	MB82/39	50.41	0.19	0.51	4.06	9.12	3.96	0.22	22.12	3.06	93.65	83.62
OL	MB82/52C1	55.46	0.09	0.00	1.35	8.71	0.59	0.23	30.89	2.36	99.68	86.34
OL	MB82/83	51.57	0.11	0.31	2.75	9.19	0.62	0.20	32.79	1.85	99.38	86.41
AMPH	MB82/56	58.57	0.28	0.79	5.05	7.78	0.57	0.18	21.61	3.14	97.97	83.19

Table 8: Trace element geochemistry for the pegmatites at Winterveld Mine (Bristow, 1989).

Analyses given in ppm

Pegmatite type	Sample number	V	Cu	Zn	Rb	Sr	Zr
CPX	MB82/52B3	161.00	16.00	34.00	0.00	0.00	0.00
CPX	MB82/52A2	158.00	8.00	42.00	0.00	33.00	24.00
CPX	MB82/78	144.00	10.00	39.00	12.00	44.00	26.00
CPX	MB82/30	96.00	26.00	65.00	10.00	59.00	15.00
OPX	MB82/46	82.00	11.00	59.00	3.00	95.00	10.00
OPX	MB82/52A5	93.00	15.00	68.00	0.00	42.00	19.00
OPX	MB82/23	119.00	26.00	68.00	7.00	49.00	12.00
OPX	MB82/53AII2	100.00	12.00	72.00	0.00	22.00	28.00
OPX	MB82/41	87.00	11.00	15.00	6.00	24.00	15.00
OPX	MB82/37	124.00	22.00	70.00	12.00	39.00	25.00
OPX	MB82/40	114.00	13.00	65.00	18.00	50.00	30.00
OPX	MB82/25	101.00	20.00	66.00	10.00	52.00	22.00
OPX	MB82/95	26.00	18.00	62.00	5.00	57.00	10.00
OPX	MB82/38	96.00	26.00	65.00	10.00	36.00	36.00
OPX	MB82/45	86.00	16.00	62.00	9.00	49.00	15.00
OPX	MB82/24III	86.00	13.00	68.00	0.00	32.00	11.00
OPX	MB82/52B1	105.00	9.00	70.00	0.00	12.00	33.00
OL	MB82/24	99.00	14.00	66.00	0.00	43.00	19.00
OL	MB82/39	312.00	25.00	105.00	5.00	25.00	17.00
OL	MB82/52C1	81.00	9.00	70.00	0.00	1.00	1.00
OL	MB82/83	85.00	38.00	69.00	4.00	22.00	11.00
AMPH	MB82/56	110.00	12.00	57.00	33.00	50.00	82.00

CPX= clinopyroxene-rich OPX= Orthopyroxene-rich Ol= Olivine-rich AMPH= Amphibole-rich

5.6.1.1. The clinopyroxene-rich pegmatites

At the Winterveld Mine, the most dominant pegmatites are the orthopyroxene-rich pegmatites, whereas at Dwarsrivier Mine, the dominant pegmatites are the clinopyroxene-rich pegmatites. The clinopyroxene-rich pegmatites at Dwarsrivier mine have a higher CaO content than at Winterveld (Figure 5.4a). This is controlled by the variable proportions of clinopyroxene in the pegmatites at Dwarsrivier mine. Though variable, the concentrations of Al_2O_3 (Figure 5.4d), MnO (Figure 5.4e) and TiO_2 (Figure 5.4f) in the pegmatites at Dwarsrivier overlaps with the Winterveld mine pegmatites. This is controlled by the modal abundances of plagioclase and clinopyroxene. The SiO_2 concentration of the pegmatites at Dwarsrivier is generally lower than the pegmatites at Winterveld mine (Figure 5.4c).

5.6.1.2. The orthopyroxene-rich pegmatites.

The orthopyroxene-rich pegmatites at Dwarsrivier mine have a higher CaO concentration than the pegmatites at Winterveld Mine (Figure 5.4a). The concentration of CaO in the pegmatites is controlled by the modal proportion of orthopyroxene. The SiO_2 concentration of the pegmatites at Dwarsrivier is generally lower than the pegmatites at Winterveld mine (Figure 5.4a). However, there is a compositional overlap with regards to FeO (Figure 5.4b), Al_2O_3 (Figure 5.4d), MnO, (Figure 5.4e) and TiO_2 (Figure 5.4f) of the pegmatites at Dwarsrivier mine and at Winterveld mine.

5.6.1.3. The olivine-rich pegmatites.

This group of pegmatites shows the largest variability in the major element chemistry. The pegmatites at Dwarsrivier mine have a higher CaO (Figure 5.4a) and SiO_2 (Figure 5.4c) and a lower FeO (Figure 5.4b) and Al_2O_3 (Figure 5.4d) concentration than the pegmatites at Winterveld mine. The concentration of the elements MnO and TiO_2 in the pegmatites from both overlaps. The variability in the modal proportion of olivine is a major factor that controls the concentration of these elements in the pegmatites.

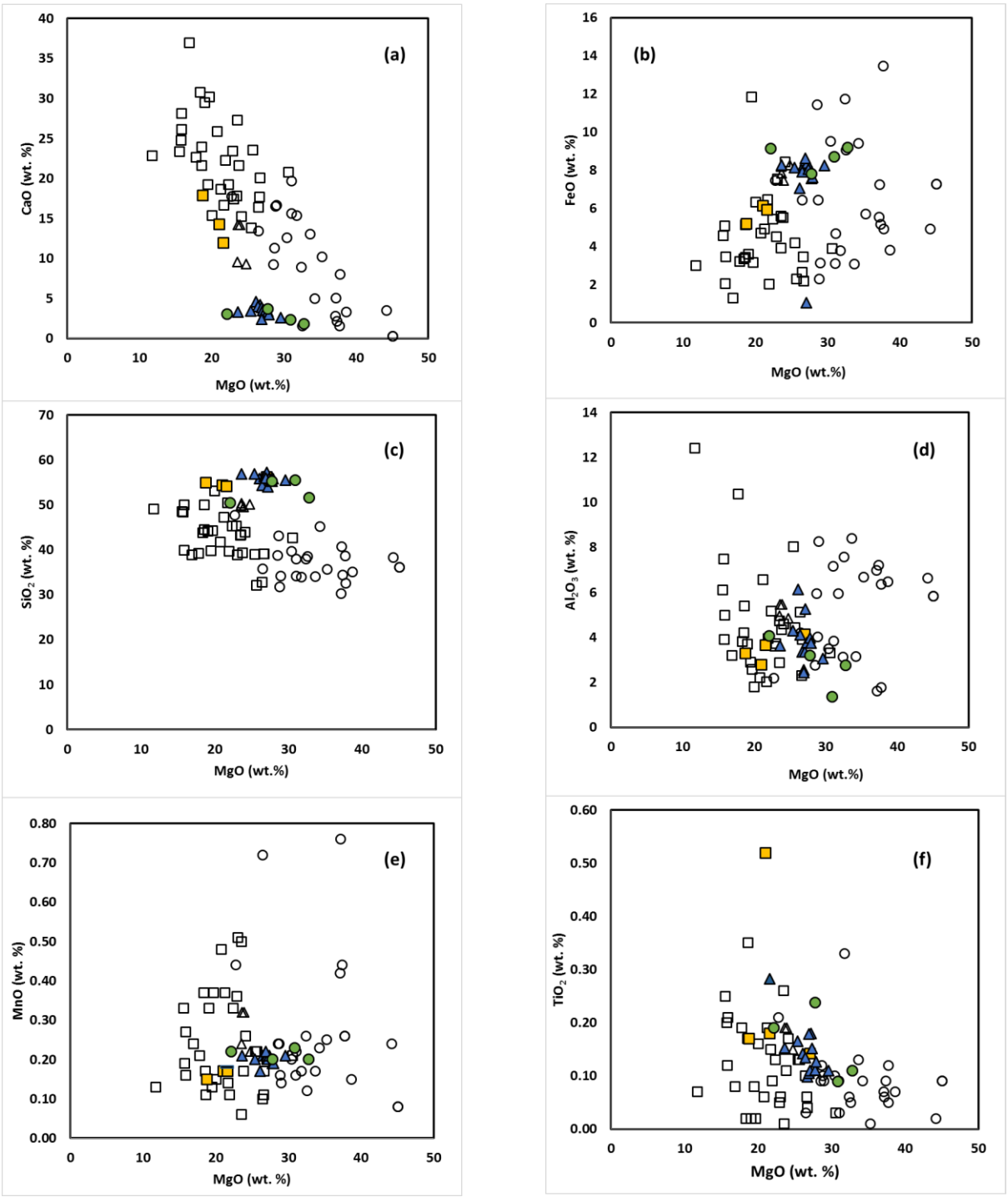

Figure 5.4: Binary variation plots of major elements (a) CaO, (b) FeO, (c) SiO2, (d) Al_2O_3, (e) MnO and (f) TiO_2 plotted against MgO (wt. %), for the pegmatites at Dwarsrivier Mine and at Winterveld Mine (Bristow, 1989). The pegmatites at Dwarsrivier mine are compositionally distinctly from the pegmatites at Winterveld mine with regards to CaO and SiO_2, although there is compositional overlap with regards to the elements MnO, Al_2O_3 and TiO_2. The two pegmatites are not genetically related. Cpx= Clinopyroxene, Opx= Orthopyroxene, Ol= olivine, Peg= pegmatite. Wintevld= Winterveld mine.

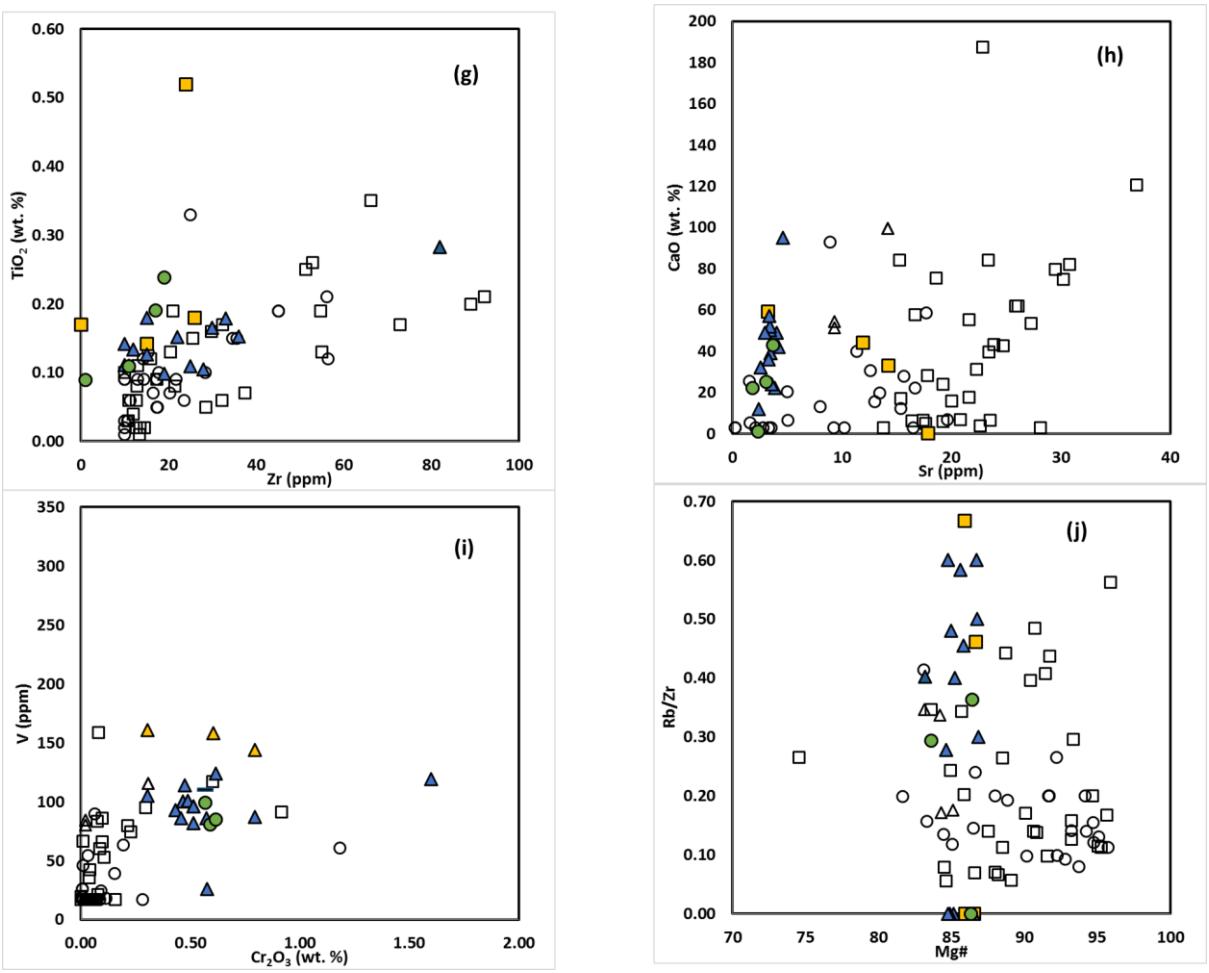

Figure 5.4 (Continued): Binary variation plots of major elements (g)TiO_2 vs Zr, (h) CaO vs Sr,(i) V vs Cr_2O_3 and Rb/Zr vs Mg# for the pegmatites at Dwarsrivier mine and at Winterveld mine. There is minimal compositional overlap between the pegmatites at Dwarsrivier Mine and Winterveld Mine (Bristow, 1989). The two pegmatites are not genetically related, although the pegmatites at Winterveld are enriched in Cr_2O_3 than the pegmatites at Dwarsrivier mine. Cpx=Clinopyroxene, Opx= Orthopyroxene, Ol= olivine, Peg= pegmatite. Wintevld= Winterveld mine.

5.6.2. Trace elements and trace element ratios comparison of the pegmatites at Dwarsrivier Mine and Winterveld Mine.

Generally, the pegmatites at Dwarsrivier mine have a high Zr (Figure 5.4g) and Sr (Figure 5.4h) concentration than the pegmatites at Winterveld mine. They also have a low concentration of Cr_2O_3 (Figure 5.4i) than their counterparts at Winterveld Mine. There is however, one olivine-rich pegmatite sample that shows enrichment in Cr_2O_3 (Figure 5.4i). The pegmatites at Winterveld Mine show a strong positive correlation between Sr and CaO, due to the presence of plagioclase (Bristow, 1989). Plagioclase accounts for up to 50 % in modal abundance in the pegmatites at Winterveld Mine (Bristow, 1989).

When the trace element trace element ratio (Rb/Zr) is plotted against Mg#, the following relationships are observed:

The Zr and Rb concentration of the pegmatites at both location is similar, although the pegmatites at Winterveld have a slightly high Rb/Zr ratio than those at Dwarsrivier mine (Figure 5.4j). This is due to the amount of trapped liquid, as well as the modal proportion of plagioclase. Plagioclase is modally more abundant in the pegmatites at Winterveld than at Dwarsrivier Mine (Bristow, 1989). The Mg# of the pegmatites at Dwarsrivier mine is higher that the pegmatites at Winterveld mine. This is interpreted as the pegmatites at Dwarsrivier mine having crystallized from a liquid that is slightly less fractionated than the pegmatites at Winterveld mine. When plotting the geochemical data of the pegmatites at Dwarsrivier and Winterveld mine on a ternary plot of FeO-(Na_2O+K_2O+CaO)-MgO, it can be seen that the pegmatites at Winterveld mine plot in a field that is compositionally different from the pegmatites at Dwarsrivier Mine (Figure 5.5). The clinopyroxene-rich pegmatites at Dwarsrivier mine plot in a field that extends towards the Na_2O+K_2O+CaO apex.

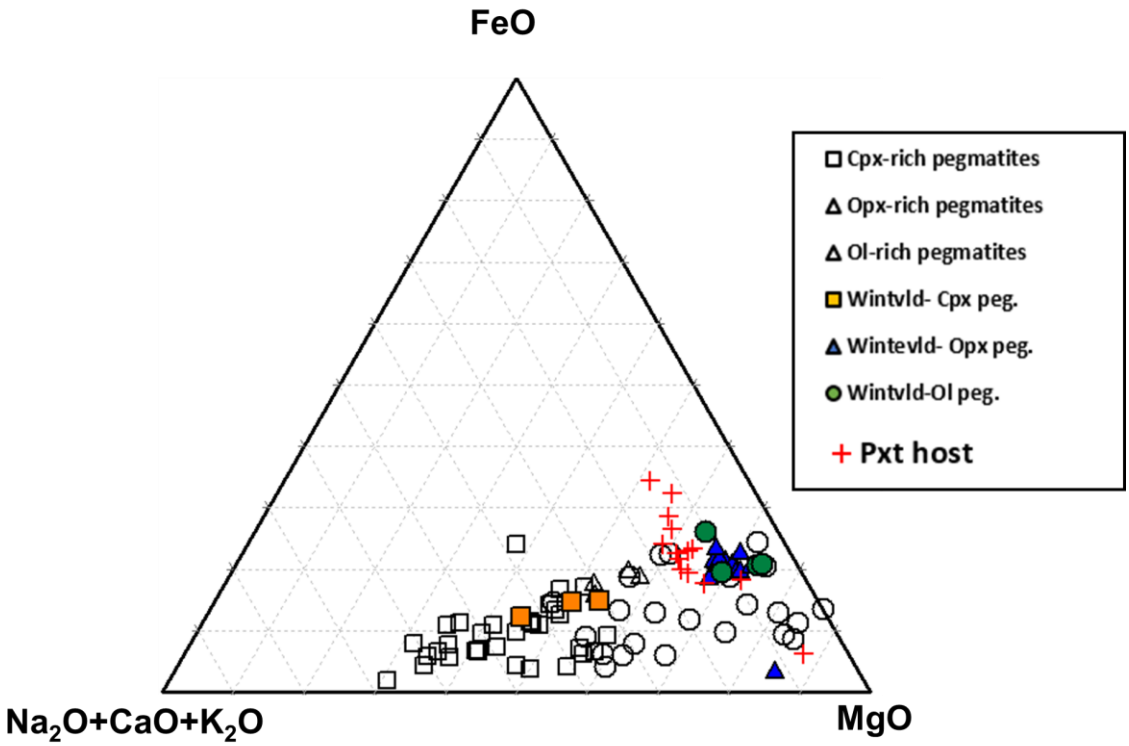

Figure 5.5: A FeO-(Na_2O+K_2O+CaO)-MgO ternary diagram for the comparison of the pegmatites at Dwarsrivier Mine and those at Winterveld Mine (Bristow, 1989). Also plotted are the pyroxenite-host rocks at Dwarsrivier. The pegmatites at Winterveld are different from the pegmatites at Dwarsrivier mine, suggesting no genetic link between the pegmatites at both locations. Also plotted are the pyroxenite host rocks (Pxt) at Dwarsrivier Mine. Cpx= Clinopyroxene, Opx= Orthopyroxene, Ol= olivine, Peg= pegmatite. Wintevld= Winterveld mine.

The major and trace element geochemistry of the pegmatites at Winterveld and Dwarsrivier indicates that the pegmatites at both locations are different in their geochemical compositions, though subtle compositional overlaps exist within individual pegmatite groups.

5.7. Comparison of the Dwarsrivier pegmatites with discordant pegmatites from the Bushveld Complex.

Discordant, transgressive pegmatites have been reported to exist in the Lower Critical Zone of the Bushveld Complex (Reid & Basson, 2002; Scoon & Mitchel, 1994; Viljoen & Scoon, 1985). They occur in both the eastern and western Bushveld Complex. These pegmatites are iron-rich, and characterized by Fe-Ti oxide such as magnetite and ilmenite. The pegmatites are collectively called iron-rich ultramafic pegmatites (IRUPs). Viljoen & Scoon (1985) described the IRUPs as follows:

- The IRUPs are highly fractionated
- They show textural variability especially in crystal size
- The IRUPs may occur in a variety of forms, ranging from small, pod-like bodies and veins to large, pipe-like masses with diameters of over a kilometre.

The IRUPs are compared with the pegmatites at Dwarsrivier Mine in a ternary diagram of FeO-Na_2O+K_2O+CaO-MgO in order to determine any genetic relationship(s) (Figure 5.6). Data for the IRUP samples are from the western Bushveld Complex at Northam (Reid & Basson, 2002).

The IRUPs are compositionally different from the pegmatites at Dwarsrivier mine, as can be seen in Figure 5.6 and Figure 5.7 (a)-(k). The major and trace element geochemistry of the pegmatites is different from, and unrelated to, the pegmatites at Dwarsrivier mine. This is controlled mainly by the difference in mineralogy, in that the pegmatites at Dwarsrivier mine do not comprise the Fe-Ti oxides that are characteristic of the IRUPs. The Mg# of the IRUPs and the trace element ratios Zr/Y; Rb/Zr and Cr/V indicate that they have crystalized from a highly fractionated magma, than the pegmatites at Dwarsrivier mine. It is therefore concluded that there is no genetic link between the pegmatites at Dwarsrivier mine and the IRUPs.

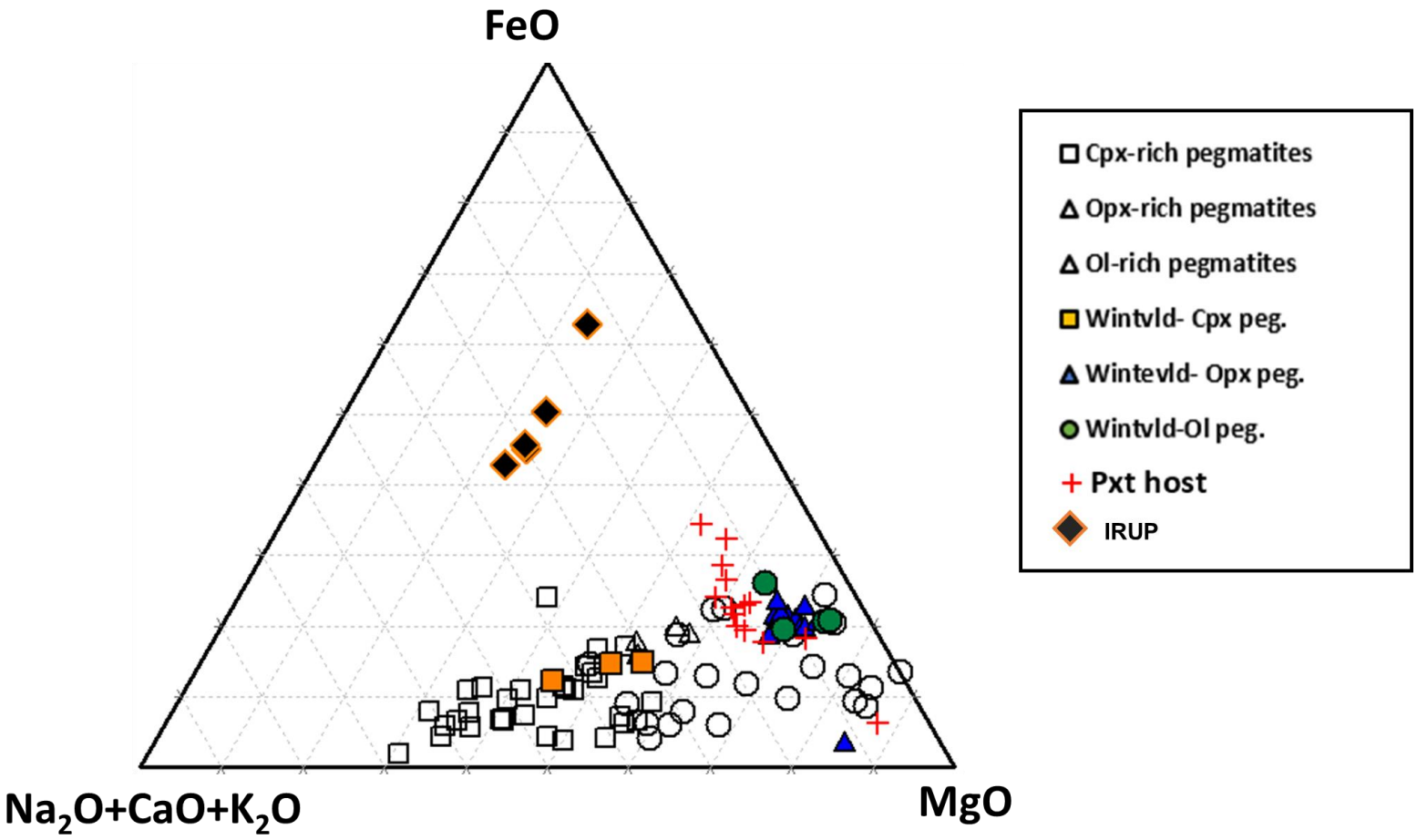

Figure 5.6: A FeO-(Na_2O+K_2O+CaO)-MgO ternary diagram for the comparison of the pegmatites at Dwarsrivier Mine and Winterveld Mine (Bristow, 1989) and the iron-rich ultramafic pegmatites (IRUPs) (Reid & Basson, 2002). Also plotted are the pyroxenite-host rocks at Dwarsrivier. Pxt=Pyroxenite, Cpx= Clinopyroxene, Opx= Orthopyroxene, Ol= olivine, Peg= pegmatite. Wintevld= Winterveld mine.

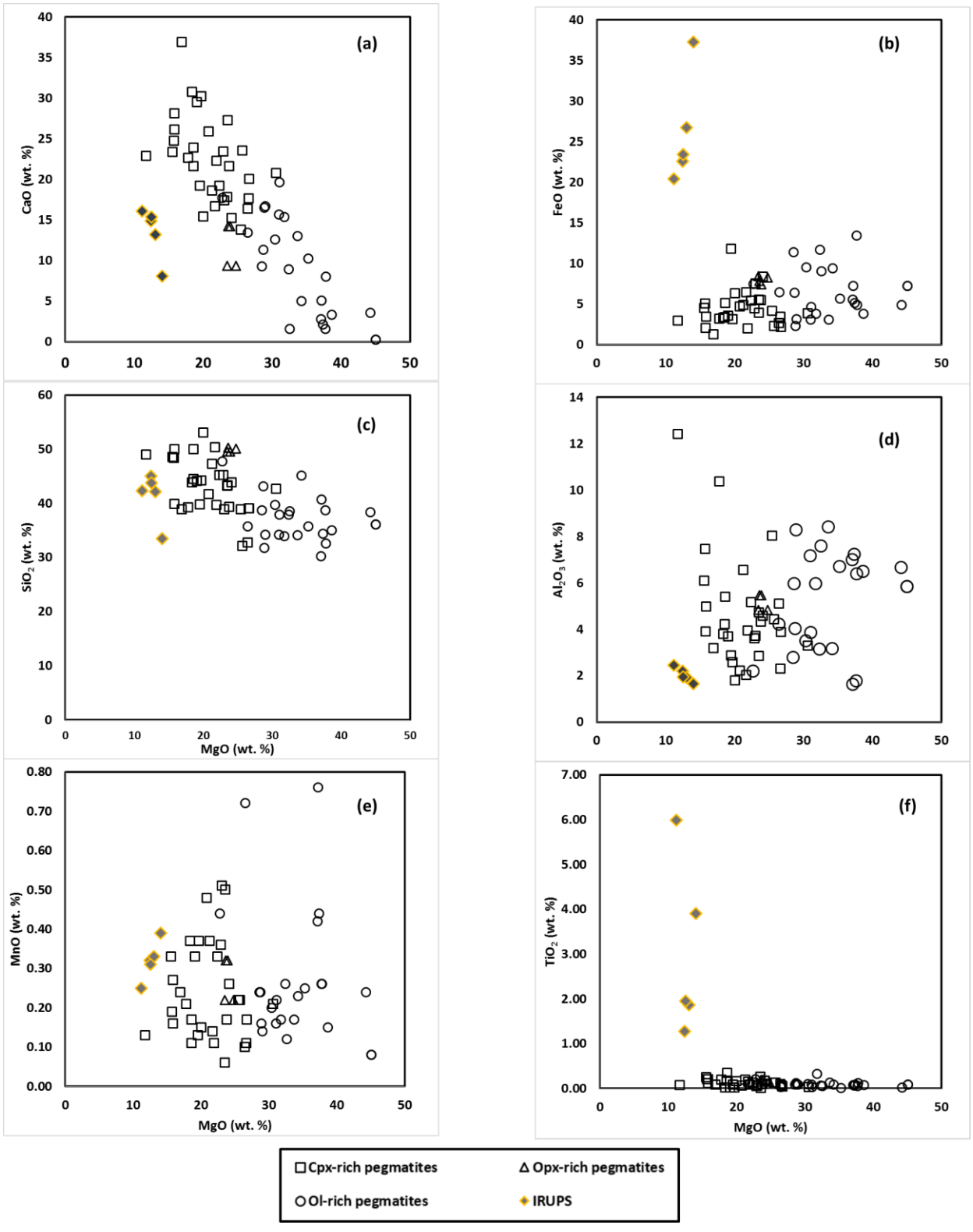

Figure 5.7: Binary variation plots of (a) CaO, (b) FeO, (c) SiO_2, (d) Al_2O_3, (e) MnO, (f) TiO_2 plotted against MgO (wt. %) for the pegmatites at Dwarsrivier mine and the IRUPs. The geochemistry of the IRUPs (Reid & Basson, 2002) is different from the pegmatites at Dwarsrivier mine. There is no genetic link between these two types of pegmatites. Cpx= Clinopyroxene, Opx= Orthopyroxene, Ol= olivine, Peg= pegmatite. Wintevld= Winterveld mine.

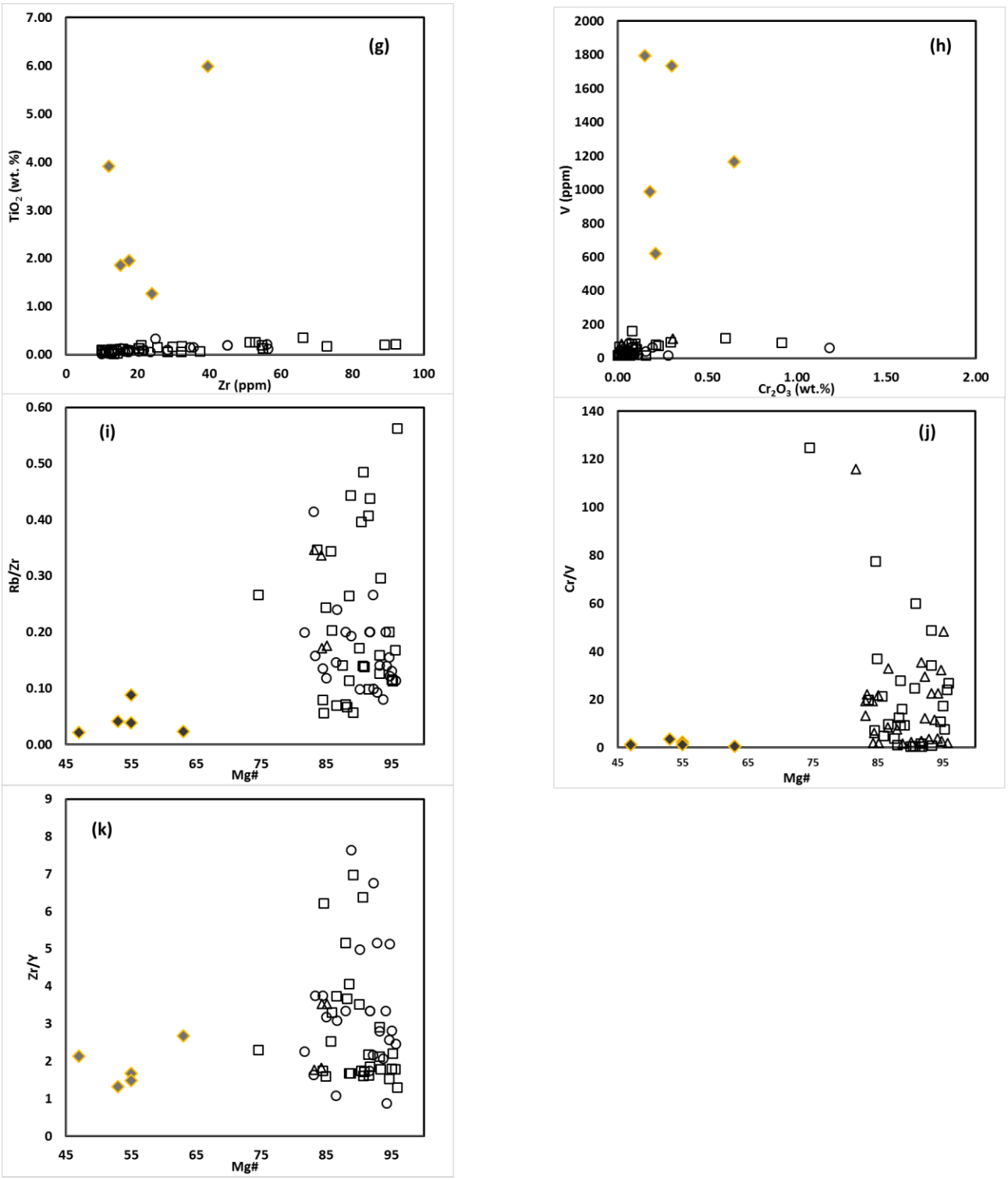

Figure 5.7 (Continued): Binary variation plots of (g) TiO_2 vs Zr, (h) V vs Cr_2O_3, (i) RB/Zr vs Mg#, (j) Cr/V vs Mg# and (k) Zr/Y vs Mg# for the pegmatites at Dwarsrivier mine and the IRUPs. The geochemistry of the IRUPs (Reid & Basson, 2002) is different from the pegmatites at Dwarsrivier mine. There is no genetic link between the pegmatites.

From the comparison of the Bushveld Complex IRUPs and the pegmatites at Dwarsrivier Mine, it can be observed that the two pegmatites are completely different with regards to their geochemical characteristics. The IRUPs contain Fe-Ti oxides. In the pegmatites at Dwarsrivier, no Fe-Ti oxides were encountered. It can therefore be concluded, based on the geochemical characteristics of the pegmatites at Dwarsrivier Mine that they are not similar to the IRUPs.

CHAPTER 6: DISCUSSION.

6.1. Introduction.

Numerous investigations into the occurrence of discordant and concordant pegmatites in the Bushveld Complex have revealed that these enigmatic features contribute to the understanding of the magmatic evolution of the Bushveld Complex, more especially, in the understanding of processes that took place post the formation of the layered sequence. Whilst most studies have focused on the discordant pegmatites, fewer studies have been undertaken to investigate the concordant pegmatites. This may be due to lack of outcrops or that they may not exist in many parts of the Bushveld Complex. This study was aimed at documenting the occurrence of concordant pegmatites at Dwarsrivier Mine, and to compare these pegmatites to other known occurrences in the Bushveld Complex. These concordant pegmatites have crystallized contemporaneously with the layered sequence, and understanding the process with which they have formed, will further our understanding of how the Bushveld Complex has formed.

Mining activities has exposed numerous pegmatites within the LG-6 chromitite. Although most of the pegmatites were found associated with the LG-6 chromitite layer, boreholes have intersected some pegmatites several tens of meters above and below the LG-6 chromitite layer. This suggests the pegmatites do not occur exclusively in association with the LG-6 chromitite layer, but are also prevalent elsewhere in the stratigraphy.

The pegmatites at Dwarsrivier mine can be subdivided, based on their mineralogy, into clinopyroxene–, orthopyroxene- and olivine-rich pegmatites, with the clinopyroxene-rich pegmatites being the most common. Several conclusions can be made regarding the occurrence of the pegmatites, their petrography as well as geochemistry.

6.2. Field occurrences

The pegmatites contained within the LG-6 chromitite layer disrupt, brecciate, and deform the LG-6, without materially changing the thickness of the host LG-6 chromitite layer. Most of the pegmatites investigated were concordant to the LG-6 chromitite layer; although the contacts of the pegmatite and the chromitite layer are irregular, non-planar and rugged. In contrast, the ‘normal’ pyroxenite fragments (from the surrounding silicate host rock) contained within the LG-6 chromitite layer have planar contacts with the chromitite layer.

When the pegmatites occur within the chromitite layer, the following features are observed:

- The host chromitite layer is deformed (brittle deformation)
- Centimetre-scale chromitite stringers are interlayered with the pegmatites. These chromitite stringers are still connected to the host chromitite layer
- Patches of chromitite occur within the pegmatites
- Fragments of the host chromitite layer are found as xenoliths within the pegmatites

The above mentioned feature imply that the pegmatites postdate the formation of the LG-6 chromitite layer. The contacts of the pegmatite and the host chromitite layer are irregular and not sharp. The LG-6 chromitite layer is deformed (brittle and plastic deformation) by the pegmatites, although it retains its composite thickness. For the chromitite layer to be deformed, it has to predate the formation of the pegmatites.

Furthermore, there are chromitite fragments that occur within the pegmatites. These fragments are found at a stratigraphic position lower than the host chromitite layer. The entrainment of the chromitite xenoliths is further evidence of the intrusion of the pegmatites into the LG-6 chromitite layer. These fragments subsequently sagged in the pegmatite under gravity, hence they are usually found some distances away from the host chromitite layer. These chromitite fragments are interpreted to have been broken off from the main chromitite layer, and incorporated into the pegmatites during the intrusion of the pegmatites melt(s).

There is also evidence of the partial assimilation of the LG-6 chromitite layer into the pegmatites. This is evidenced by the presence of centimetre-scale chromitite stringers and patches within the pegmatites. Similar features were also observed in the pegmatites at the Winterveld Mine (Bristow, 1989). Furthermore, tooth-like structures formed by the host chromitite layer were observed protruding into the pegmatites indicating the collapse of the chromitite layer into the underlying pegmatite due to gravity. From these observations, it can be suggested that the intrusion of the pegmatites into the LG-6 chromitite layer occurred when the chromitite layer was already rigid, but still consolidating.

6.3. Mineralogy and Petrography.

The mineralogy of the pegmatites is similar to the pyroxenite host rocks, with some pegmatites displaying “igneous layering” similar to the silicate host rocks. Texturally, the pegmatites are different from the pyroxenite-host rocks in that they exhibit larger textural and mineralogical variability than the pyroxenite host rocks. The occurrence of coarse-grained pyroxenes typical of the pegmatites is uncommon in the pyroxenite host rocks of the layered sequence. Furthermore, the occurrence of cumulus olivine at the stratigraphic level of the Lower Critical Zone is also uncommon.

The presence of olivine, and ultimately, olivine-rich layers within the pegmatites, is uncharacteristic of the Lower Critical Zone of the Bushveld Complex (Eales & Cawthorn, 1996). Olivine is a major rock forming mineral in the rocks of the C-unit of the Lower Critical Zone (Cameron, 1978; Cameron, 1982; Viljoen & Schürmann, 1998), where there is a dominance of dunites, and subordinate harzburgites. The C unit of the Lower Critical Zone is tens of meters below the stratigraphic position where the pegmatites occur. The stratigraphic position where the pegmatites occur is predominantly characterised by orthopyroxene (Teigler & Eales, 1996). It is therefore unusual to find olivine rich layers in the rocks above this position of the Lower Critical Zone.

Coarse-grained pyroxenes are a common feature of pegmatites that occur in ultramafic complexes. This texture has been reported in the pegmatites of the J-M Reef in the Stillwater Complex (Boudreau, 1999; Braun *et al.*, 1994) and in the pegmatites associated with the Merensky Reef and the UG-2 chromitite layer in the Bushveld Complex (Cawthorn & Boerst, 2006; Voordouw & Beukes, 2009, Bristow, 1989). Experimental studies have highlighted the effect of volatiles such H_2O and CO_2 on the olivine-orthopyroxene liquidus boundary (Eggler, 1978; Fraser, 2005; Green, 1973b; Kushiro 2007). According to Eggler (1978) and Fraser (2005) in the system Fo-Di-Qtz (Figure 6.1), the presence of water significantly shifts the olivine-orthopyroxene liquidus boundary, and expands the diopside field towards the SiO_2 apex. The expansion of the diopside field allows for the crystallization of olivine and clinopyroxene, which are the dominant minerals in the pegmatites at Dwarsrivier Mine. Therefore, the presence of coarse pyroxenes in the pegmatites can be explained by the recrystallization or sub-solidus enlargement of the pyroxenes in a volatile-rich environment (Voordouw & Beukes, 2009; Bristow, 1989). The presence of micas such as phlogopite also points to a volatile-rich environment in which the pegmatites have formed. The phlogopite is found in association with plagioclase. The pyroxenes in the pegmatites at Dwarsrivier Mine show partial replacement by amphibole. The alteration of pyroxenes to amphibole can be as a result of the presence of a $H_2O + CO_2$ rich medium.

The interlayered nature in the pegmatites, where olivine-rich layers are interlayered with clinopyroxene layers can also be explained using the Fo-Di-Qtz phase ternary diagram (Figure 6.1). The melt(s) that crystallizes the pegmatite will initially crystallize olivine. Once olivine is unstable, clinopyroxene and orthopyroxene will follow. This also explains the presence of thin orthopyroxene layers that separate the dunite layers from the clinopyroxene layers in layered pegmatites. It is envisaged that there is a continuous shift in the system Fo-Di-Qtz that produces the complex layering in some pegmatites.

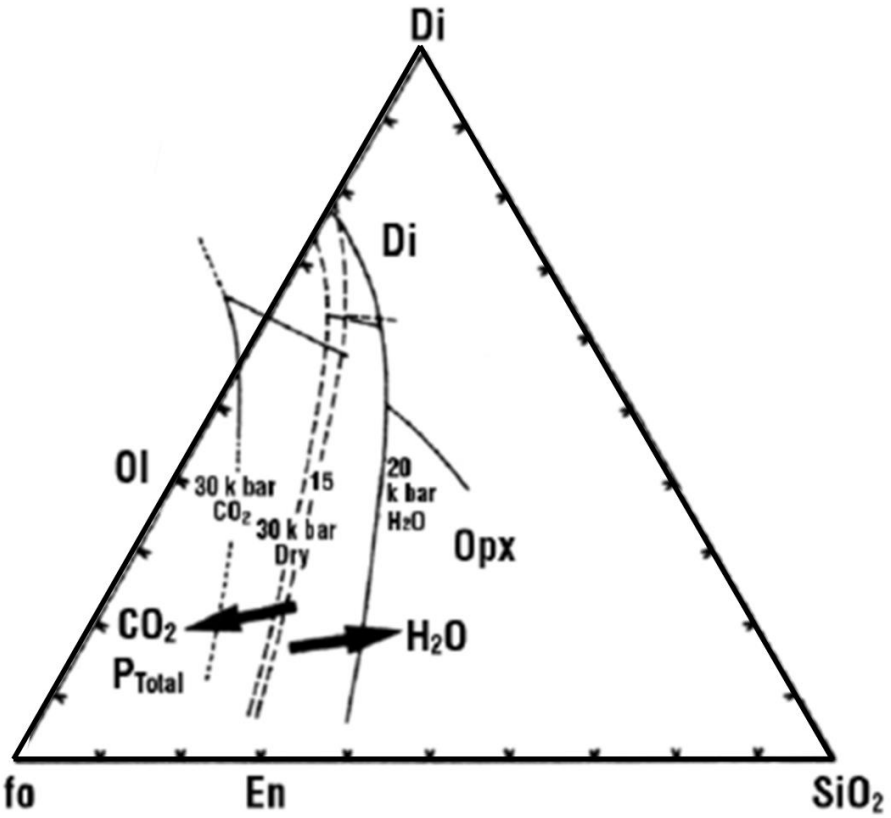

Figure 6.1: A Fo-Di-Qtz ternary phase diagram showing the effects of H_2O and CO_2 on the olivine-liquidus boundary (Fraser, 2005). Olivine crystalizes first from the liquid, and clinopyroxene crystalizes due to the shift of the olivine-orthopyroxene liquidus boundary towards the diopside field.

The orthopyroxene and clinopyroxene crystals in the pegmatites poikilitically enclose rounded olivine grains i.e. the olivine occur as "islands" within the pyroxene grains (Figure 4.8). The olivine contained within the pyroxenes are interpreted as having formed earlier, and pyroxenes subsequently crystallized around them (Bristow, 1989). A similar texture was also described Cawthorn *et al.* 2000 in the pegmatites below the Merensky Reef.

6.4. Whole rock geochemistry

The major and trace element geochemistry of the pegmatites is different from the pyroxenite host rocks, although compositional overlaps exists in some major elements (Figure 5.1a-z). Differences in the concentration of the elements CaO, Al_2O_3 and Na_2O are controlled by the modal variation of plagioclase and clinopyroxene. The Mg# of the pegmatites shows a wide variation, and in general, it is higher than

that of the pyroxene host rocks, although the Mg# of the orthopyroxene pegmatites is similar to that of the pyroxenite host rocks. The Mg# is an important parameter in basic magmas, and can be used to indicate magma fractionation (Cawthorn, 1996; Eales, *et al.*, 1990). These observations suggest that the altered pegmatites were derived from a melt that is slightly less fractionated than the pyroxenite host rocks.

The concentration of compatible elements in the pegmatites and their pyroxenite host rocks is also worth noting. In general, compositional overlaps in compatible elements Sr, Ni, Co, Cu is observed between the pegmatites and their pyroxenite host rocks. The V concentration of the pegmatites is lower than the pyroxenite host rocks. The element Sr is controlled by plagioclase in the rocks, while V and Ni are controlled by chromite and sulphides, respectively.

Furthermore, the pegmatites show a compositional overlap with the pyroxenite host rocks with regards to the Y and Zr concentrations. These elements have low D values in mafic magmas, and would increase in concentration, in the residual liquid with increased fractionation. The D values of Zr in basic magmas for olivine, plagioclase, clinopyroxene and orthopyroxene are 0.01, 0.03, 0.50 and 0.20, while those of Y are 0.01;0.01; 0.1and 0.03, respectively (Pearce & Nowry, 1979). The compositional overlap in the trace element concentration of the pegmatites and the pyroxenite host rocks may imply that the pegmatites are genetically linked (although compositionally different) to the pyroxenite host rocks, and that the pegmatites have crystallized from a melt that was possibly derived from the cumulates in the layered sequence (RLS).

The trace element ratios Zr/Y and Rb/Zr for the pegmatites also overlap with the pyroxenite host rocks. These ratios also indicate that the pegmatites are genetically linked to the pyroxenite host rocks. However, the ratio Cr/V for the pegmatites is lower than the pyroxenite host rocks, pointing to the pegmatites having crystallized from a less fractionated liquid (Bristow, 1989; Maier, 1991).

6.5. Serpentinisation

The timing of the serpentinisation of the pegmatites is presently unknown. The altered pegmatites are generally associated with areas of structural complexities, characterised by geological discontinuities such as faults and joints. These structures crosscut and displace the pegmatites and the LG-6 chromitite layer, as well as the silicate layers above and below the LG-6. It is possible that the geological discontinuities may have acted as channel ways for fluids that eventually serpentinised the pegmatites. It is also possible that the pegmatites were serpentinised by a later event, postdating the geological discontinuities. The serpentinised pegmatites are locally not connected to each other, nor continuous in

any direction, unlike their pyroxenite host rocks. The serpentinisation is localised and restricted to the pegmatites. The surrounding silicate rocks do not show pronounced signs of alteration. The source of the fluids could be residual magmatic fluids that are a result of the crystallization of the surrounding cumulate rocks (Voordouw & Beukes, 2009).

One key observation made is that lithologies consisting mainly of olivine show a high degree of serpentinisation, whereas the lithologies made up of orthopyroxene and orthopyroxene show moderate alteration. The olivine alters primarily along crystal fractures, to form a mineral assemblage dominated by serpentine and magnetite. The hydration of olivine to produce serpentine and magnetite is represented by the following reactions (Frost & Beard, 2007):

$$2Mg_2SiO_4 + 3\,H_2O = Mg_3Si_2O_5(OH)_4 \quad (1)$$

Olivine **Fluid** **Serpentine**

$$6(Mg,Fe)_2SiO_4 + 7H_2O = 3(Mg,Fe)_3Si_2O_5(OH)_4 + Fe_3O_4 + H_2 \quad (2)$$

Olivine **Fluid** **Serpentine** **Magnetite** **Hydrogen**

The orthopyroxenes in pegmatites are replaced by serpentine. This is typical when orthopyroxene is altered in an Mg-rich environment characterised by the hydration of olivine (Allen & Seyfried, 2003). The alteration of orthopyroxene to produce serpentine can be represented by the following reaction (Frost & Beard, 2007):

$$6MgSiO_3 + 3H_2O = Mg_3Si_2O_5(OH)_4 \quad (3)$$

Orthopyroxene **Fluid** **Serpentine**

Other accessory minerals present within the altered pegmatites as a result of alteration are clinozoisite and carbonate minerals. The clinozoisite occurs in association with carbonates such as calcite and dolomite. The calcite occurs as interstitial crystals to the orthopyroxene. The calcite also appears to be in textural equilibrium with orthopyroxene, and is interpreted as having formed at a late stage as a result of the alteration of the pyroxenes. The presence of carbonate possibly indicates that CO_2 rich fluids interacted with the pegmatites during or after serpentinisation (Coleman & Keith, 1971, Frost & Beard, 2007, Shervais *et al*,. 2005). Clinozoisite and calcite are Calcium-rich minerals, and are interpreted to have formed at a later stage, possibly due to a Ca-metasomatic overprinting.

6.6. Comparisons of the pegmatites at Dwarsrivier mine with their pyroxenite host rocks, the iron-rich ultramafic pegmatites (IRUPs) and pegmatites from elsewhere in the Bushveld Complex.

The pegmatites at Dwarsrivier Mine were compared with the concordant pegmatites at Winterveld Mine (Bristow, 1989), eastern Bushveld Complex, as well as the discordant pegmatites from Amandelbult (Reid & Basson, 2002), western Bushveld Complex. The pegmatites at Dwarsrivier Mine are compositionally different from the pegmatites at Winterveld Mine with regards to major and trace elements. Subtle variations in major elements such as MgO, CaO and FeO are controlled by the modal abundance of clinopyroxene and olivine. Furthermore, the pegmatites at Dwarsrivier have low Cr_2O_3 than the pegmatites at Winterveld mine due to the lack of chromite.

These differences do not necessarily indicate the differences in modal mineralogy, but may indicate the difference in the composition of the melt from which the pegmatites have crystallized, though there are compositional overlap in some major and trace elements between the pegmatites at Dwarsrivier and Winterveld Mine. The association of the pegmatites at the Winterveld mine with the chromitite and silicate rocks is similar to the occurrence of the pegmatites at Dwarsrivier Mine. The major difference is that the pegmatites at the Winterveld section are not serpentinised and altered in a similar manner as the pegmatites at Dwarsrivier Mine. It can therefore be concluded based on mineralogy and geochemistry that the processes that led to the formation of the pegmatites at the Winterveld section are different from Dwarsrivier Mine.

The pegmatites at Dwarsrivier mine are also distinctly different from the discordant, iron-rich ultramafic pegmatites (Reid & Basson, 2002; Scoon & Mitchel, 1994; Viljoen & Scoon, 1985). This is observed when comparing the major and trace elements of the pegmatites at Dwarsrivier Mine and the IRUPs. The pegmatites at Dwarsrivier mine lack the Fe-Ti oxide that are characteristic to the IRUPs. It can therefore be concluded, on the basis of mineralogy, geochemistry and occurrence that these two pegmatite types are not genetically related.

6.7. Conclusions.

The occurrences of the fresh and altered pegmatites and their associated enveloping coarse-grained pyroxenites is unique and different from the host magmatic rocks. Although the pegmatites have a similar mineralogy as, and may be genetically related to, the surrounding pyroxenite host rocks, they have a different geochemistry than the pyroxenite host rocks. The pegmatites have possibly crystallized from a volatile-rich liquid, hence the crystal size variability than the pyroxenite host rocks.

The occurrence of the pegmatites within the LG-6 chromitite layer suggest that they are intrusive. The LG-6 chromitite layer is deformed by the pegmatites, and parts of it are assimilated into the pegmatite.

The mineralogy and the geochemistry of the pegmatites at Dwarsrivier mine indicate that they are not related to the discordant IRUPs as well as the pegmatites at the Winterveld mine, in the eastern Bushveld Complex (Bristow, 1989).

The pegmatites are less fractionated than their pyroxenite host rocks. Some of the pegmatites are highly serpentinised, in a process that occurred after their crystallization. Although the pegmatites were serpentinised, they still retain their original magmatic texture. Their proximity to geologically disturbed areas does not suggest any structural control in their formation but points to these structures having possibly acted as passageways of fluids that serpentinised the pegmatites.

7. REFERENCES.

1. Allen, D.E. and Seyfried, W.E. (2003). Compositional control on vent fluids from ultramafic-hosted hydrothermal systems at mid-ocean ridges: An experimental study at 400ºC, 500 bars. *Geochimica et Cosmochica Acta*, **67**, p 1531-1542.

2. Barnes, S-J. (1986). The effect of trapped liquid shift on the cumulus mineral compositions in layered intrusions. *Contributions to Mineralogy and Petrology*, **93**, p 524-531.

3. Barnes, S.-J. and Campbell, I.H. (1988). Role of late magmatic fluids in Merensky - type platinum deposits: a discussion. *Geology*, **16**, p 488-491.

4. Barnes, S.-J. and Maier, W.D. (2002). Platinum-group element distributions in the Rustenburg Layered Suite of the Bushveld Complex, South Africa. *In*: Cabri, L.J. (Ed.), *The Geology, Geochemistry, Mineralogy and Mineral Beneficiation of Platinum-Group Element*s. Canadian Institute of Mining, Metallurgy and petroleum, Special Volume, **54**, p 431-458.

5. Bennett, H. and Oliver, G. (1992). XRF Analysis of Ceramics, Minerals and Applied Materials. John Wiley and Son, New York, United States of America, p 67-93.

6. Billhaus, C.G. and Stumpfl, E.F. (1986). Sulfide and platinum mineralization in the Merensky Reef: evidence from hydrous silicate and fluid inclusions. *Contributions to Mineralogy and Petrology*, **94,** p 193-204.

7. Boudreau, A. (1999). Fluid Fluxing of Cumulates: the J-M Reef and Associated Rocks of the Stillwater Complex, Montana. *Journal of Petrology*, **40**, p 755–772.

8. Braun, K., Maurer, W., Boudreau, A.E. and McCallum, I.S. (1994). Compositions of pegmatoids beneath the J-M Reef of the Stillwater Complex, Montana, U.S.A. *Chemical Geology*, **113**, p 245-257.

9. Bristow, D.M. and Wilson, A.H. (1983). Some aspects of pegmatite development in the Winterveld mine-eastern Bushveld Complex (Abstr.). *Symposium on Bushveld Complex, University of Pretoria, Oct 31- Nov 2. Programme with Abstracts*, p 1-2.

10. Bristow, D.M. (1989). The petrology and the geochemistry of the Lower Critical Zone, Winterveld Chrome Mine- eastern Bushveld Complex, with particular reference to the disruptive pegmatites. *Unpublished PhD Thesis*, University of Natal, 305pp.

11. Buchanan, D.L. (1979). A combined transmission electron microprobe and electron microprobe study of Bushveld pyroxenes from the Bethal area. *Journal of Petrology*, **20**, p 327-354.

12. Cameron, E.N. and Emerson, M.E. (1959). The origin of certain chromite deposits of the Eastern Bushveld Complex. *Economic Geology*, **59**, p 1151-1213.

13. Cameron, E.N. and Desborough, G.A. (1969). Occurrence and characteristics of chromite deposits- eastern Bushveld Complex. *Economic Geology*, **4,** p 23-40.

14. Cameron, E.N. (1977a). Chromite in the central sector of the Eastern Bushveld Complex, South Africa. *American Mineralogist*, **62**, p 1082-1096.

15. Cameron, E.N. (1977b). The Lower Zone of the eastern Bushveld Complex in the Olifants River trough. *Journal of Petrology*, **19,** p 437-462.

16. Cameron, E.N. (1978). An unusual titanium-rich oxide mineral from the Eastern Bushveld Complex. *American Mineralogist*, **63**, p 37-39.

17. Cameron, E.N. (1980). Evolution of the Lower Critical Zone, Central Sector, Eastern Bushveld Complex, and its Chromite deposits. *Economic Geology*, **75**, p 845-871.

18. Cameron, E.N. (1982). The Upper Critical Zone of the eastern Bushveld Complex-Precursor of the Merensky Reef. *Economic Geology*, **77**, p 1307-1327.

19. Cawthorn, RG. And McCarthy, T. S. (1985). Incompatible trace element behaviour in the Bushveld Complex. *Economic Geology*, **80,** p 1016-1026.

20. Cawthorn, R.G. and Molyneux, T.G. (1986). Vanadiferous magnetite deposits of the Bushveld Complex. In: Anhaeusser, C.R. and Maske, S. (Eds.), Mineral Deposits of Southern Africa. . Geological Society of South Africa. Johannesburg/ Council for Geoscience, Johannesburg, p 1251-1266.

21. Cawthorn, R.G. and Walraveren, F. (1998). Emplacement and crystallization time for the Bushveld Complex. *Journal of Petrology*, **39**, p 1669-1687.

22. Cawthorn, R.G. (1999). The platinum and palladium resources of the Bushveld Complex. *South African Journal of Science*, **95**, p 481-489.

23. Cawthorn, R.G., Harris, C. and Kruger, F.J. (2000). Discordant ultramafic pegmatite pipes in the Bushveld Complex. *Contributions to Mineral Petrology*, **140**, p 119-133.

24. Cawthorn, R.G. and Webb, S.J. (2001). Connectivity between the western and eastern limbs of the Bushveld Complex. *Tectonophysics*, **330**, p 195-209.

25. Cawthorn, R.G. and Boerst, K. (2006). Origin of the pegmatitic pyroxenite in the Merensky Unit, Bushveld Complex, South Africa. *Journal of Petrology*, **47**, p 1509-1530.

26. Cawthorn, R.G., Eales, H.V., Walraveren, F., Uken, R. and Watkeys, M.K. (2006). The Bushveld Complex. *In*: Johnson, M.R., Anhaeusser, C.R. and Thomas, R.J. (Eds.), *The Geology of South Africa*. Geological Society of South Africa. Johannesburg/ Council for Geoscience, Pretoria, p 261-281.

27. Clarke, B.M., Uken, K., Watkeys, M.K. and Reinhardt, J. (2005.). Folding of the Rustenburg Layered Suite adjacent to the Steelpoort pericline: Implications for syn-Bushveld tectonism in the eastern Bushveld Complex. *South African Journal of Geology*, **108**, p 397-412.

28. Clark-Halkett, C.E. (2010). An investigation into the formation of the Lower Main Zone in the eastern Limb of the Bushveld Complex, South Africa. *Unpublished MSc. Thesis,* University of Pretoria, Pretoria, 112pp.

29. Coleman, R.G. (1971). Petrologic and geophysical nature of serpentinites. *Geological Society of America Bulletin*, **82**, p 897-918.

30. Cousins, C.A. (1959). The structure of the mafic portion of the Bushveld Igneous Complex. *Transactions of the Geological Society of South Africa*, **62**, p 179-189.

31. Cousins, C.A. (1964). Additional notes on the chromite deposits of the eastern part of the Bushveld Complex. *In*: Haughton S.H. (Ed.), *The geology of some Ore Deposits in Southern Africa*. Special Publications, Geological Society of South Africa, **2**, p 169-182.

32. Cousins, C.A. and Ferringa, G. (1964). The chromite deposits of the western belt of the Bushveld Complex. *In*: Haughton S.H. (Ed.), *The geology of some Ore Deposits in Southern Africa*. Special Publications, Geological Society of South Africa, **2**, p 183-202.

33. Curl, E.A. (2001). Parental magmas of the Bushveld Complex, South Africa. *Unpublished PhD Thesis, Monash University, Australia,* 140pp.

34. Daly, R.A. and Molengraaf, G.A.F. (1924). Structural relations of the Bushveld Igneous Complex. *Journal of Geology*, **32**, p 1-35.

35. Davies, G., Cawthorn, R.G., Barton, J.M. and Morton, M. (1981). Parental magmas to the Bushveld Complex. *Nature*, **287**, p 33-35.

36. Du Plessis, A. and Kleywegt, R.J. (1987). A dipping sheet model for the mafic lobes of the Bushveld Complex. *South African Journal of Geology*, **90**, p 1-6.

37. Eggler, D.H. (1978). The effect of CO_2 upon partial melting of peridotite in the system Na_2O-CaO-Al_2O_3-MgO-SiO_2-CO_2 to 35kb, with an analysis of melting in a peridotite-H_2O-CO_2 system. *American Journal of Science*, **278**, 315-343.

38. Eales, H.V. and Reynolds, I.M. (1986). Cryptic variations within chromitites of the Upper Critical Zone, Northwestern Bushveld Complex. *Economic Geology*, **81**, p 1056-1066.

39. Eales, H.V., Marsh, J.S., Mitchell, A.A., De Klerk, W.J., Kruger, F.J. and Field, M. (1986). Some geochemical constraints upon models for the crystallization of the upper critical zone-main zone interval, northwestern Bushveld Complex. *Mineralogical Magazine*, **50**, p 567-582.

40. Eales, H.V., Field, M., De Klerk, W.J. and Scoon, R.N. (1988). Regional trends of chemical variation and thermal erosion in the Upper Critical Zone, western Bushveld Complex. *Mineralogical Magazine*, **52**, p 63-79.

41. Eales, H.V., de Klerk, W.J., Butcher, A.R. and Kruger, F.J. (1990). The cyclic unit beneath the UG1 chromitite (UG1FW unit) at RPM Union Section Platinum Mine-Rossetta Stone of the Bushveld Upper Critical Zone. *Mineralogical Magazine*, **54**, p 23-43.

42. Eales, H.V., Teigler, B. and Maier, W.D. (1993). Cryptic variations of minor elements Al, Cr, Ti and Mn in Lower and Critical Zone orthopyroxenes of the western Bushveld complex. *Mineralogical Magazine*, **57**, p 257-264.

43. Eales, H.V. and Cawthorn, R.G. (1996). The Bushveld Complex. *In:* Cawthorn, R.G. (Ed.), *Layered Intrusions*, Elsevier Science, p 181-230.

44. Eales, H.V. (2000). Implications of the chromium budget of the western limb of the Bushveld complex. *South African Journal of Geology*, **103**, p 141-150.

45. Ford, C.E., Russell, D.G., Craven, J.A. and Fisk, M.R. (1983). Olivine-liquid equilibria: temperature, pressure and composition dependence of the crystal/liquid cation partition coefficients for Mg, Fe2+, Ca and Mn. *Journal of Petrology*, **24**, p 256-265.

46. Franz, G. and Selverstone, J. (1992). An empirical phase diagram for the clinozoisite-zoisite transformation in the system $Ca_2Al_2Fe^{3+}Si_3O1_2(OH)$. *American Mineralogist*, **77**, p 631-642.

47. Fraser, D.G. (2005). Acid-base properties and structons: towards a structural model for predicting the thermodynamic properties of silicate melts. *Annals of Geophysics*, **48**, p 549-559.

48. Frost, B.R. and Beard, J.S. (2007). On silica activity and serpentinisation. *Journal of Petrology*, **48**, p 1351-1368.

49. Gain, S.B. (1985). The geologic setting of the platiniferous UG-2 chromitite layer on the farm Maandagshoek, Eastern Bushveld Complex. *Economic Geology*, **80**, 925-943.

50. Green, D. H. (1973b). Experimental melting studies on model upper mantle compositions at high pressure under both water-saturated and water-undersaturated conditions. *Earth Planetary Science Letters*, **19**, p 37-53.

51. Gauert, C. D. (1998). The petrogenesis of the Uitkomst Complex, Mpumalanga Province, South Africa. *Unpublished Ph.D. Thesis*, University of Pretoria, Pretoria, South Africa. 315pp.

52. Hall, A.L. (1932). The Bushveld Igneous Complex of the central Transvaal. *Geological Survey of South Africa Memoirs*, **28,** 560pp.

53. Harmer, R.E. and Sharpe, M. (1985). Field relations and Strontium isotope systematics of the marginal rocks of the eastern Bushveld Complex. *Economic Geology*, **80**, p 813-837.

54. Harney, D.M.W., Merkle, R.K.W. and Von Gruenewaldt, G. (1990). Platinum-Group element behaviour in the Lower part of the Upper Critical Zone, Eastern Bushveld Complex-Implications for the formation of the Main Magnetite Later. *Economic Geology*, **85**, p 1777-1789.

55. Hatton, C.J. and Von Gruenewaldt, G. (1985). The geological setting and petrogenesis of the Bushveld chromitite layers. *Research Report. Institute of Geological Research on the Bushveld Complex*, University of Pretoria, **57**, p 1-48.

56. Hatton, C.J. and Von Gruenewaldt, G. (1987). The geological setting and petrogenesis of the Bushveld chromitite layers. *In*: Stowe, C.W. (Ed.), *Evolution of Chromium Ore Fields*. New York: Van Nostrand Reinhold, p 109-143.

57. Hornsey, R. and van der Merwe, P. (2003). Optimization of geological lead-time in a feasibility study drill out- Two Rivers Platinum Mine, Mpumalanga, South Africa. Applications of Computer

and Operations Research in the Minerals Industries, *South African Institute of Mining and Metallurgy*, p 335-344.

58. Hulbert, L.J. (1983). A petrological investigation of the Rustenburg Layered Suite and associated mineralization south of Potgietersrus. *Unpublished PhD Thesis*, University of Pretoria, South Africa, 512pp.
59. Kinnaird, J.A., Kruger, F.J., Nex, P.A.M. and Cawthorn, R.G. (2002): Chromitite formation – a key to understanding processes of platinum enrichment. Transactions of the Institution of Mining and Metallurgy (Section B: Applied Earth Sciences.) **111**, B23-B35.
60. Kinloch, E.D. (1982). Regional trends in the Platinum-Group mineralogy of the Critical Zone of the Bushveld Complex, South Africa. *Economic Geology*, **77,** p 1328-1347.
61. Klemm, D.D., Henckel, J., Dehm, R. and von Gruenewaldt, G. (1985). The geochemistry of titanomagnetite in magnetite layers and their host rocks of the Eastern Bushveld Complex. *Economic Geology***, 80**, p 1075-1088.
62. Klemm, D.D., Ketterer, S., Reichhardt, F., Steindl, J. and Weber-Diefenbach, K. (1985). Implication of vertical and lateral compositional variations across the Pyroxene marker and its associated rocks in the Upper part of the Main Zone in the eastern Bushveld Complex. *Economic Geology*, **80**, p 1007-1015.
63. Kottke-Levin, J. (2011). A geochemical study of the Middle Group chromitites, Helena mine, Bushveld complex, South Africa. . *Unpublished PhD Thesis*, University of the Free State, South Africa, 339pp.
64. Kruger, F.J. and Marsh, J.S. (1982). Significance of $^{87}Sr/^{86}Sr$ ratios in the Merensky cyclic unit of the Bushveld Complex. *Nature*, **298**, p 53-55
65. Kruger, F.J. (2005). Filling the Bushveld Complex magma chamber: lateral expansion, roof and floor interaction, magmatic unconformities, and the formation of giant chromitite, PGE and Ti-V magnetite deposits. *Mineralium Deposita*, **40**, p 451-472.
66. Kushiro, M.J.A. (2007). Origin of magmas in subduction zones: a review of experimental studies. *Proceedings of the Japan Academy Ser B Physical and Biological Sciences*, **83**, p 1-15.
67. Lee, C.A. and Fesq, H.W. (1986). Au, Ir, Ni and Co in some chromitites of the eastern Bushveld Complex South Africa. Chemical Geology, **62**, p 227-237.

68. Lee, C.A. and Tredoux, M. (1986). Platinum Group Element abundances in the Lower and the Lower Critical Zones of the Eastern Bushveld complex. *Economic Geology*, **81**, p 1087-1095.

69. Lee, C.A. and Parry, S.J. (1988). Platinum-Group element geochemistry of the Lower and Middle Group chromitites of the Eastern Bushveld Complex. *Economic Geology*, **83**, p 1127-1139

70. Loubser, M. and Verryn, S. (2008). Combining XRF and XRD analyses and sample preparation to solve mineralogical problems. *South African journal of Geology*, **111**, p 229-238

71. Lundgaard, K.T., Tegner, C., Cawthorn, R.G., Kruger, F.J. and Wilson, J.R. (2006). Trapped intercumulus liquid in the Main Zone of the Eastern Bushveld Complex, South Africa. *Contributions to Mineral Petrology*, **151**, p 352-369.

72. Mabuza, M. (2007). Two Rivers Platinum Mine: the orebody, the mining method- a perfect match. *The Journal of the Southern African Institute of Mining and Metallurgy*, **107**, p 43-50.

73. Maier, W.D. (1991). Geochemical and petrological trends in the UG-2-Merensky interval of the Upper Critical Zone in the Western Bushveld Complex. *Unpublished PhD Thesis*, Rhodes University, South Africa, 354pp.

74. Maier, W.D. and Barnes, S.-J. (1998). Concentrations of rare earth elements in silicate rocks of the Lower, Critical and Main Zones of the Bushveld Complex. *Chemical Geology*, **150**, p 85-103.

75. Maier, W.D. and Barnes, S.-J. (1999). Platinum-Group Elements in the Silicate rocks of the Lower, Critical and main Zones at Union Section, western Bushveld Complex. *Journal of Petrology*, **40**, p 1647-1671.

76. Maier, W.D., Barnes, S.-J. and Groves, D.I. (2012). The Bushveld Complex, South Africa: formation of platinum-palladium, chrome- and vanadium-rich layers via hydrodynamic sorting of a mobilized cumulate slurry in a large, relatively slowly cooling, subsiding magma chamber. *Mineralium Deposita*, **48**, p 1-56

77. Manyeruke, T.D., Maier, W.D. and Barnes, S.-J. (2005). Major and trace element geochemistry of the Platreef on the farm Townlands, northern Bushveld Complex. *South African Journal of Geology*, **108**, p 381-396.

78. McDonald, I., Harmer, R.E., Holwell, D.A., Hughes, H.S.R. and Boyce, A.J. (2017). Cu-PGE mineralisation at the Aurora project and potential for a new PGE province in the Northern Bushveld Main Zone. *Ore Geology Reviews*, **80**, p 1135-1159.

79. Meyer, R. and de Beer, J.H. (1987). Structure of the Bushveld Complex from resistivity measurements. *Nature*, **325**, p 610-612.

80. Mitchell, A.A. (1990). The stratigraphy, petrography, and mineralogy of the Main Zone of the northwestern Bushveld Complex. *South African Journal of Geology*, **93**, p 818-831.

81. Mitchell, A.A. (1996). Compositional cyclicity in a pyroxenite layer from the Main Zone of the western Bushveld Complex: evidence for repeated magma influx. *Mineralogical Magazine*, **60**, p 149-161.

82. Mitchell, A.A. and Manthree, R. (2002). The Giant mottled Anorthosite: a transitional sequence at the top of the Upper Critical Zone of the Bushveld Complex. *South African Journal of Geology*, **105**, p 15-24.

83. Molyneux, T.G. (1970). The geology of the area in the vicinity of Magnet Heights, Eastern Transvaal, with special reference to the magnetite iron ore. *Geological Society of South Africa*, Special Publication, **1**, p 228-241.

84. Naldrett, A.J., Wilson, A., Kinnaird, J., Yudovskaya, M. and Chunnett, G. (2012). The origin of chromitites and related PGE mineralization in the Bushveld Complex: new mineralogical and petrological constraints. *Mineralium Deposita*, **47**, p 209–232.

85. Nex, P.A. (1998). A new stratigraphy for the Main Zone of the Bushveld Complex, in the Rustenburg area. *South African Journal of Geology*, **101(3),** 215-219

86. Pawley, A.R., Redfern, S.A.T. and Holland, T.J.B. (1996). Volume behaviour of hydrous minerals at high pressure and temperature: I. Thermal expansion of lawsonite, zoisite, clinozoisite, and diaspora. *American Mineralogist*, **81,** p 335-340.

87. Perreira, D., Yenes, M., Blanco, J.A. and Peinado, M. (2007). Characterisation of serpentinites to define their appropriate use as dimension stone. *In:* Prikryl, R. and Smith, B.L. (Eds.), *Building Stone Decay: From Diagnosis to Conservation*. Geological Society of London, Special Publications, **271**, p 55-62.

88. Perrit, S. and Roberts, M. (2007). Flexural-slip structures in the Bushveld Complex, South Africa. *Journal of Structural Geology*, **29,** p 1422-1429.

89. Phillipotts, J.A. and Schnetzler, C.C. (1970). Phenocryst-matrix coefficients for K, Rb, Sr, and Ba with application to anorthosite and basalt genesis. *Geochimica et Cosmochica Acta*, **34**, 307-322.

90. Rajamani, V. and Naldrett, A.J. (1978). Partitioning of Fe, Co, Ni, and Cu between Sulfide Liquid and Basaltic Melts and Composition of Ni-Cu Sulfide Deposits. *Economic Geology*, **73**, p 82-93.

91. Reid, D.L. and Basson, I.J. (2002). Iron-rich ultramafic pegmatite replacement bodies within the Upper Critical Zone, Rustenburg Layered Suite, Northam Platinum Mine, South Africa. *Mineralogical Magazine*, **66**, p 895-914.

92. Reynolds, I.M. (1985a). Contrasted mineralogy and textural relationships in the uppermost titaniferous magnetite layers of the Bushveld Complex in the Bierkraal area north of Rustenburg. *Economic Geology*, **80**, p 1027-1045.

93. Reynolds, I.M. (1985b). The nature and origin of the titaniferous magnetite –rich layers in the Upper Zone of the Bushveld Complex: A review and synthesis. *Economic Geology*, **80**, p 1069-1108.

94. Reynolds, I.M. (1986a). The mineralogy and ore petrology of the Bushveld titaniferous magnetite-rich layers. In: Anhaeusser C.R. and Maske,S.(Eds.). Mineral Deposits of Southern Africa. Geological Society of South Africa, Johannesburg, **2**, p 1267–1286.

95. Reynolds, I.M. (1986b).The mineralogy and ore petrography of some vanadium-bearing titaniferous magnetite-rich layers. In: Anhaeusser C.R. and Maske,S.(Eds.). Mineral Deposits of Southern Africa. Geological Society of South Africa, Johannesburg, **2**, p 1267–1286.

96. Rollinson, H. (1993). Using geochemical data: evaluation, presentation, interpretation. Pearson Education Ltd., Essex, England.

97. Rose, D.H. (2010). The Merensky reef at Dwarsrivier 372KT with reference to the mineral chemistry and the platinum group minerals in the Merensky reef chromitite stringers. *Unpublished MSc. Thesis*, University of Johannesburg, Johannesburg, 184pp.

98. Seabrook, C.L. (2005). The Upper Critical and Main Zones of the eastern Bushveld Complex. *Unpublished PhD Thesis*, University of the Witwatersrand, South Africa, 211pp.

99. Scoates, J.S. and Friedman, R. M. (2008). Precise Age of the Platiniferous Merensky Reef, Bushveld Complex, South Africa, by the U-Pb Zircon Chemical Abrasion ID-TIMS Technique. *Economic Geology*, **103**, p 1037-1049.

100. Scoates, J.S, Wall, C.J, Friedman, R.M. and Chamberlain, K.R. (2011). Revisiting the age of the Merensky Reef, Bushveld Complex. Abstr, Goldschmidt Conference 2011.

101. Scoon, R.N. and Mitchell, A.A. (1994). Discordant Iron-rich Ultramafic Pegmatites in the Bushveld Complex and their relationship to Iron-rich intercumulus and residual liquids. *Journal of Petrology*, **35**, p 881-917.

102. Scoon, R.N. and Teigler, B. (1995). A new LG-6 chromite reserve at Eerste Geluk in the boundary zone between the Central and Southern Sectors of the Eastern Bushveld Complex. *Economic Geology*, **90**, p 969-982.

103. Scoon, R.N. and Mitchell, A.A. (2004). The platiniferous pipes in the eastern limb of the Bushveld Complex: Review and comparison with un-mineralized discordant ultramafic bodies. *South African Journal of Geology*, **107**, p 505-520.

104. Scoon, R.N. and Mitchell, A.A. (2011). The principal geological features of the Mooihoek platiniferous dunite pipe, eastern Bushveld Limb of the Bushveld Complex, *South African Journal of Geology*, **114**, p 15-40.

105. Schmidt, M.W. and Poli, S. (1994). The stability of lawsonite and zoisite at high pressures: Experiments in CASH to 92 kbar and implications for the presence of hydrous phases in subducted lithosphere. *Earth and Planetary Sciences Letters*, **124**, p 105-118.

106. Schouwstra, R., Kinloch, D. and Lee, C.A. (2000). A short geological review of the Bushveld Complex. *Platinum Metals Review*, **44**, p 33-39.

107. Schürmann, L.W., Grabe, P.J. and Steenkamp, C.J. (1998). Chromium. *In*: Wilson, M.G.C. and Anhaeusser, C.R. (Eds.), *The Mineral Resources of South Africa*. Handbook, Council for Geosciences, **16**, p 40-45.

108. Sharpe, M.R. (1981). The chronology of magma influxes to the eastern compartment of the Bushveld Complex, as exemplified by its marginal border group. *Journal of the Geological Society of London*, **138**, p 307-326.

109. Sharpe, M.R. (1985). REE and isotopic evidence for multiple parental magmas to the Bushveld Complex. *University of Pretoria, Institute for Geological Research on the Bushveld Complex, Annual Report* 1985/6, p 56-62.

110. Sharpe, M.R. and Hulbert, L.J. (1985). Ultramafic sills beneath the eastern Bushveld Complex: Mobilized suspensions of early Lower Zone cumulates in a parental magma with boninitic affinities. *Economic Geology*, **80**, p 849-871.

111. Shervais, J.W., Kolesar, P. and Anderson, K. (2005). A field and chemical study of serpentinisation-Stontford, California: Chemical flux and mass balance. *International Geology Review*, **47**, p 1-28.

112. SACS (South African Committee for Stratigraphy) (1980). Stratigraphy of South Africa. *Geological Survey of South Africa*. *Handbook*, **8,** 690pp.

113. Tankard, A.J., Jackson, M.P.A., Eriksson, K.A., Hobda, D.K., Hunter, D.R. and Minter, W.E.L. (1982). Crustal Evolution of South Africa-3.8 billion years of earth history. Springer Verlag, New York, p 175-199.

114. Tegner, C., Cawthorn, R.G. and Kruger, F.J. (2006). Cyclicity in the Main and Upper Zones of the Bushveld Complex, South Africa: Crystallization from a Zoned Magma Sheet. *Journal of Petrology*, **47**, p 2257-2279.

115. Teigler, B. (1990). Mineralogy, Petrology and geochemistry of the Lower and Lower Critical Zones, Northwestern Bushveld Complex. *Unpublished PhD thesis*, Rhodes University, Grahamstown, 247pp.

116. Teigler, B. and Eales, H.V. (1996). The Lower and Critical Zones of the western limb of the Bushveld Complex, as indicated by the Nooitgedacht boreholes. *Bulletin of the Geological Survey of South Africa*, **95**, p 17-28.

117. Uken, R. (1998). The geology and structure of the Bushveld Complex metamorphic aureole in the Olifants River area. *Unpublished. PhD Thesis*, University of Natal, Durban, South Africa, 311pp.

118. Van der Merwe, M.J. (1978). The layered sequence of the Potgietersrus limb of the Bushveld Complex. *Unpublished PhD Thesis*, University of Witwatersrand, Johannesburg, 176pp.

119. Vermaak, C.F. (1986). Summary aspects of the economics of chromium with special reference to Southern Africa. *In*: Anhausser, C.R. and Maske, S. (Eds.), *Mineral Deposits of Southern Africa*. Geological Society of South Africa, **2**, p 1156-1181.

120. Vermaak, C.F. (1997). A brief overview of South Africa's mineral industry: world context and changing local circumstances. *Mineralium Deposita*, **32**, p 312-322.

121. Viljoen, M.J. and Scoon, R.N. (1985). The Distribution and main geologic features of discordant bodies of Iron-rich ultramafic pegmatite in the Bushveld Complex. *Economic Geology*, **80**, p 1109-1128.

122. Viljoen, M.J., de Klerk, W.J., Coetzer, P.M., Hatch, N.P., Kinloch, E. and Peyerl, W. (1986). The Union section of Rustenburg Platinum Mines Ltd with reference to the Merensky Reef. In: Anhaeusser,C.R. and Maske, S. (Eds.), Mineral Deposits of Southern Africa. Geological Society of South Africa, Johannesburg, p 1061–1090.

123. Viljoen, M.J. and Schürmann, L.W. (1998). Platinum group metals. *In*: Wilson, M.G.C. and Anhaeusser, C.R. (Eds.), *The Mineral Resources of South Africa*. Handbook, Council for Geoscience, **16**, p 523-568.

124. Voordouw, R.J. and Beukes, N.J. (2009a). Alteration and metasomatism of the UG2 melanorite and its stratiform pegmatites, Bushveld Complex, South Africa -characteristics, timing and origins. *Geological Society of South Africa*, **112**, p 47-64.

125. Voordouw, R.J., Gutzmer, J. and Beukes, N.J. (2009b). Intrusive origin for the Upper Group (UG1, UG2) stratiform chromitite seams in the Dwars River area, Bushveld Complex, South Africa. *Mineralogy and Petrology*, **97**, p 75-94

126. Von Gruenewaldt, G. (1973). The Main and Upper Zones of the Bushveld Complex in the Roossenekal area eastern Transvaal. *Transactions of the Geological Society of South Africa*, **76,** p 207-227.

127. Von Gruenewaldt, G. and Weber-Diefenbach, K. (1977). Co-existing Ca-poor pyroxenes in the Main Zone of the Bushveld Complex. *Contributions to Mineralogy and Petrology*, **65**, 11-18.

128. Von Gruenewaldt, G., Klemm, D.D. and Dehm, R.M. (1985). Exsolution features from the massive layers and their host rocks of the Upper Critical Zone, eastern Bushveld Complex. *Economic Geology*, **80**, p 1049-1061.

129. Von Gruenewaldt, G., Sharpe, M.R. and Hatton, C.J. (1985). The Bushveld Complex: Introduction and review. *Economic Geology*, **80**, p 803-812.

130. Von Gruenewaldt, G., Hatton, C.J., Merkle, R.K.W. and Gain, S.B. (1986). Platinum-Group element-chromitite associations in the Bushveld Complex. *Economic Geology*, **81**, p 1067-1079.

131. Wagner, P.A. (1929). The platinum deposits and mines of South Africa. Oliver and Boyd, Edinburgh, 326pp.

132. Walraven, F., Amstrong, R.A. and Kruger, J.F. (1990). A chronostratigraphic framework for the north-central Kaapvaal Craton, the Bushveld Complex, and Vredefort structure. *Tectonophysics*, **173**, p 23-48.

133. Watson, J.S. (1996). Fast, Simple Method of Powder Pellet Preparation for X-Ray Fluorescence Analysis. *X-Ray Spectrometry*, **25**, p 173-174.

134. Webb, S.J., Cawthorn, R.G., Nguuri, T. and James, D. (2004). Gravity modelling of the Bushveld Complex connectivity supported Southern African seismic experiment results. *South African Journal of Geology*, **107**, p 207-218.

135. Wicks, F. and Whittacker, E.J.W. (1977). Serpentine texture and serpentinisation. *Canadian Mineralogist*, **13**, p 227-243.

136. Willemse, J. and Bensch, J.J. (1964). Inclusions of original carbonate rocks in gabbro and norite of the eastern part of the Bushveld Complex. *Transactions of the Geological Society of South Africa*, **67**, p 1-87.

8.APPENDICES

APPENDIX 1: SAMPLE PREPARATION, ANALYTICAL PROCEDURE, ANALYTICAL CONDITIONS.

Appendix 1a: Sample collection.

Detailed underground mapping and sampling was carried out on the underground panels at Dwarsrivier Mine. Samples were collected manually from different underground exposures across the mine for analysis of whole rock geochemistry and for thin sections. Other samples were collected from borehole core DWR155. A total number of 77 samples, comprising of underground face samples and borehole core samples were collected. The samples are grouped in the following manner:

1. 16 pyroxenite host rock samples.
2. 28 fresh, unaltered pegmatitic mafic/ultramafic rocks.
3. 33 altered (serpentinised) pegmatitic mafic/ultramafic rocks.

Appendix 1b: Sample preparation.

Borehole core sampling was carried out on borehole core DWR155. The core was quartered, with one quarter analysed for whole rock geochemistry and the other quarter was used for thin sections. Samples collected from the underground workings and from the borehole core were crushed in a jaw crusher. The samples were ground in a tungsten-carbide milling pot to achieve particle sizes of <75 micron. In order to minimise cross contamination, after every sample was milled, the mill was cleaned by milling clean quartz, and washing the mill pots with acetone.

Appendix 1c: X-Ray analysis

The samples were dried at 100°C overnight and roasted at 1000°C for a period of 24 hours to determine percentage loss on ignition (LOI). Major elements were determined on fused beads, which were prepared following the standard method used in the XRD/XRD laboratory of the University of Pretoria, as adapted from Bennet and Oliver (1992). A 1g aliquot was mixed with 6g lithium tetraborate ($Li2B_4O_7$) flux and fused at 1050°C to make a stable fused glass bead (Loubser & Verryn, 2008). For trace element analysis, the samples were prepared after the method adapted from Watson (1996). Approximately 16-20 ml of sample powder was mixed with a PVA binder and pressed into a pellet using a 10-ton press. QA/QC is done by frequent drift corrections and analyses of standard with each

batch. The Thermo Fisher ARL9400XP+ Sequential XRF, equipped with a Rhodium tube, LiF200, LiF220, GER, AXO6 (a 50 Å synthetic multilayer). Analyses were executed using the WinXRF and Quantas softwares.

Appendix 1d: XRF calibration

The XRF Spectrometer was calibrated with certified reference materials, specpure oxides and in-house standards. The detection limits are listed in the Tables below:

Table 1: Standard deviation and lower limits of detection of the XRF method (Major elements)

	Std dev. (%)	LOD (wt. %)
SiO_2	0,4	0,02
TiO_2	0,03	0,0032
Al_2O_3	0,3	0,01
Fe_2O_3	0,3	0,0097
MnO	0,0065	0,0013
MgO	0,1	0,0118
CaO	0,07	0,01
Na_2O	0,11	0,0265
K_2O	0,06	0,005
P_2O_5	0,08	0,01
Cr_2O_3	0,0053	0,0006
NiO	0,01	0,0013
V_2O_5	0,0018	0,0008
ZrO_2	0,005	0,0009
CuO	0,0037	0,0003

Table 2: Standard deviation and lower limits of detection of the XRF method (Trace elements)

	Std dev.(ppm)	LOD (ppm)
Cu	3	2
Ga	2	2
Mo	1	1
Nb	3	2
Ni	6	3
Pb	3	3
Rb	4	2
Sr	4	3
Th	2	3
U	2	3
Y	4	3
Zn	4	4
Zr	6	10
Co	6	3
Cr	40	15
Sc	5	1
V	10	1
Cs	5	10
Ba	14	5
La	24	5
Ce	14	6

LOD= Limit of Detection, Std dev = Standard deviation, ppm= parts per million

APPENDIX 2: DIMENSIONS OF SOME OF THE PEGMATITIC MAFIC/ULTRAMAFIC ROCKS AT DWARSRIVIER MINE.

Outcrop	X-Coordinate	Y-Coordinate	Length	Breadth	Height	Area (m^2)	Volume (m^3)	Cluster
1	89266.892	-60112.151	23.48	12.92	2.2	303.36	667.4	South
2	89219.981	-60305.591	39.98	18.1	2.1	723.64	1519.64	South
3	89153.054	-60205.652	10.95	7.34	2	80.37	160.75	South
4	89111.939	-60219.402	56.97	14.08	1.9	802.14	1524.06	South
5	89120.577	-60263.811	41.17	27.66	1.78	1138.76	2027	South
6	89144.201	-60292.712	34.63	23.48	1.85	813.11	1504.26	South
7	89075.587	-60281.267	57.63	17.28	2.24	995.85	2230.7	South
8	89099.2	-60422.627	17.32	12.84	2.5	222.39	555.97	South
9	89077.03	-60464.513	33.93	23.59	2.1	800.41	1680.86	South
10	89030.392	-60474.493	36.46	30	1.9	1093.8	2078.22	South
11	88997.914	-60417.607	24.68	21.9	2.2	540.49	1189.08	South
12	88946.41	-60520.243	40.4	27.58	1.95	1114.23	2172.75	South
13	88860.528	-60557.642	15.26	15.26	1.89	232.87	440.12	South
14	88898.571	-60723.719	32.93	23.85	1.87	785.38	1468.66	South
15	89132.231	-60625.504	24.56	17.22	2.03	422.92	858.53	South
16	89075.826	-60672.693	18.92	15.61	2.17	295.34	640.89	South
17	-88746.21	-60683.23	90.25	79.85	1.8	7206.46	12971.63	South
18	-89487.57	59493.2	22	15	1.5	330	495	North
19	-89353.63	-59050.81	64	32	1.8	2048	3686.4	North
20	-89403.44	-59465.216	34.6	22.1	0.4	764.66	305.86	North
21	-89412.93	-59411.3	48.18	36.17	0.5	1742.67	871.34	North
22	-89339.44	-59434.52	54.53	35.26	0.3	1922.73	576.82	North
23	-89338.71	-59465.612	8.81	7.25	0.14	63.87	8.94	North
24	-89866.71	-59499.31	15	25	1.62	0	0	DWR155
25	-88957.71	-60685.61	18			0	0	AM58
26	-88915.8	-60387.72						AM60
27	-89404.81	-59422.81						AM68
28	-88847.38	-58484.332						North

NOTE: the pegmatites that do not have volume calculation is because there was no full exposure to complete the calculations.

APPENDIX 5: MAJOR ELEMENT GEOCHEMISTRY OF THE ALTERED PEGMATITES.

			Analyses are given in wt %													
SAMPLE NAME	ALTERATION	PEGMATITE TYPE	SiO_2	TiO_2	Al_2O_3	FeO	MnO	MgO	CaO	Na_2O	K_2O	P_2O_5	Cr_2O_3	LOI	Total	Mg#
CS20	ALTERED	CPX	39.74	0.08	2.88	11.85	0.13	19.49	19.21	0.01	0.00	0.00	0.01	6.78	100.17	74.56
2	ALTERED	CPX	45.22	0.05	3.61	4.50	0.36	22.91	23.41	0.01	0.00	0.00	0.00	1.17	101.24	90.07
3	ALTERED	CPX	43.82	0.02	3.80	3.35	0.37	18.37	30.78	0.01	0.00	0.03	0.00	0.90	101.45	90.71
4	ALTERED	CPX	43.33	0.01	2.86	3.92	0.50	23.55	27.29	0.01	0.00	0.00	0.00	1.21	102.68	91.46
5	ALTERED	CPX	44.19	0.02	2.57	3.16	0.37	19.70	30.21	0.01	0.03	0.00	0.00	1.50	101.76	91.74
6	ALTERED	CPX	44.12	0.02	3.70	3.59	0.33	19.06	29.49	0.01	0.00	0.00	0.00	2.33	102.65	90.44
7	ALTERED	CPX	45.24	0.13	5.16	5.44	0.33	22.37	19.22	0.01	0.00	0.00	0.00	2.38	100.28	87.99
CL6B1(2)	ALTERED	CPX	39.04	0.06	2.30	3.44	0.11	26.61	17.67	0.01	0.01	0.01	0.06	10.67	99.98	93.23
CL6B2-1	ALTERED	CPX	39.09	0.04	3.89	2.17	0.17	26.69	20.04	0.01	0.01	0.01	0.05	7.82	99.98	95.64
CL6B2-2	ALTERED	CPX	39.71	0.09	3.95	2.03	0.11	21.92	22.28	0.01	0.01	0.01	0.03	9.87	100.01	95.06
CS7-2	ALTERED	CPX	42.65	0.03	3.30	3.89	0.21	30.60	20.80	0.01	0.00	0.00	0.00	0.20	101.69	93.34
CL02	ALTERED	CPX	38.88	0.08	3.18	1.28	0.24	16.90	36.93	0.01	0.01	0.02	0.06	2.34	99.92	95.92
CL22	ALTERED	CPX	38.91	0.13	8.03	4.17	0.22	25.47	13.80	0.01	0.01	0.01	0.05	9.91	100.70	91.58
CL34	ALTERED	CPX	39.24	0.19	10.38	3.20	0.21	17.80	22.64	0.01	0.01	0.01	0.16	6.08	99.91	90.83
CL39	ALTERED	CPX	39.87	0.12	3.90	2.05	0.27	15.83	28.13	0.01	0.01	0.01	0.04	9.82	100.04	93.22
CS39	ALTERED	OL	38.71	0.09	2.76	11.43	0.24	28.55	9.25	0.01	0.00	0.00	1.18	9.03	101.25	81.65
CL46	ALTERED	OL	37.93	0.06	3.12	11.73	0.26	32.39	8.91	0.01	0.01	0.01	0.28	5.19	99.89	83.11
CS7-1	ALTERED	OL	38.32	0.02	6.64	4.90	0.24	44.24	3.53	0.01	0.00	0.00	0.01	5.08	102.99	94.15
CL35B	ALTERED	OL	30.23	0.07	6.98	5.54	0.42	37.12	2.80	0.01	0.01	0.01	0.02	16.09	99.29	92.27
CL6B2(3)	ALTERED	OL	31.71	0.10	4.01	2.29	0.16	28.85	16.53	0.01	0.01	0.01	0.02	16.28	99.97	95.73
CL6B3(1)	ALTERED	OL	34.15	0.09	7.15	3.09	0.16	31.03	15.65	0.01	0.01	0.01	0.05	8.58	99.97	94.71
CL6B3(2)	ALTERED	OL	34.08	0.13	8.39	3.08	0.17	33.67	13.01	0.01	0.01	0.01	0.09	7.34	99.97	95.12
CL6B3-1	ALTERED	OL	34.20	0.09	8.27	3.14	0.14	28.99	16.68	0.01	0.01	0.01	0.07	8.39	99.99	94.27
CS35-01	ALTERED	OL	34.38	0.09	7.21	5.15	0.44	37.38	2.12	0.01	0.00	0.00	0.01	15.78	102.56	92.82
CS35-02	ALTERED	OL	35.04	0.07	6.48	3.80	0.15	38.66	3.30	0.01	0.00	0.00	0.01	12.00	99.51	94.77
CL21B	ALTERED	OL	37.92	0.03	3.84	4.67	0.22	31.09	19.66	0.01	0.01	0.01	0.06	2.35	99.86	92.22
CL29	ALTERED	OL	33.93	0.33	5.94	3.79	0.17	31.78	15.37	0.01	0.01	0.01	0.04	8.53	99.89	93.73
CL44	ALTERED	OL	32.54	0.12	6.36	4.90	0.26	37.77	8.02	0.01	0.01	0.01	0.04	9.97	100.00	93.21
1	ALTERED	OPX	49.50	0.19	5.46	7.45	0.32	23.90	14.19	0.01	0.06	0.01	0.02	0.50	101.61	85.11
CL53A	ALTERED	OPX	50.10	0.15	4.84	8.28	0.22	24.78	9.32	0.10	0.37	0.01	0.31	3.18	101.65	84.21

APPENDIX 6: TRACE ELEMENT GEOCHEMISTRY OF THE ALTERED PEGMATITES.

			Analysis are given in ppm													
SAMPLE NAME	ALTERATION	PEGMATITE TYPE	Nb	Cu	Ni	Rb	Sr	Y	Zn	Zr	Co	Cr	V	Ba	La	Zr/Y
CS20	ALTERED	CPX	2.00	2.00	692.08	5.69	5.87	9.35	52.05	21.40	88.05	8317.35	66.71	8.49	26.25	2.29
2	ALTERED	CPX	2.00	2.00	3.00	4.87	39.71	8.09	310.86	28.46	56.99	8.25	16.81	16.54	30.48	3.52
3	ALTERED	CPX	2.00	2.00	3.00	6.13	82.01	7.88	395.78	12.66	49.70	6.84	16.81	19.71	43.08	1.61
4	ALTERED	CPX	2.00	2.00	3.00	5.45	53.30	6.16	322.20	13.38	56.62	6.84	16.81	15.16	33.68	2.17
5	ALTERED	CPX	2.00	2.00	3.00	5.92	74.73	7.33	976.57	13.53	60.26	6.84	16.81	21.15	37.72	1.85
6	ALTERED	CPX	2.00	2.00	3.00	5.72	79.50	8.31	296.41	14.43	55.24	9.31	16.81	18.90	42.48	1.74
7	ALTERED	CPX	2.00	2.00	8.72	3.88	23.83	10.67	280.98	55.01	55.03	21.42	19.53	12.61	31.94	5.16
CL6B1(2)	ALTERED	CPX	2.00	23.16	74.91	2.00	5.08	5.95	120.99	12.63	39.27	573.15	16.81	26.03	4.26	2.12
CL6B2-1	ALTERED	CPX	2.00	3.10	11.13	2.00	15.90	6.71	113.15	11.92	15.23	404.47	16.81	32.82	4.26	1.78
CL6B2-2	ALTERED	CPX	2.00	2.12	7.62	2.00	31.05	9.66	97.83	17.39	9.03	290.81	16.81	32.96	20.11	1.80
CS7-2	ALTERED	CPX	2.00	2.00	61.40	3.20	6.77	6.06	98.51	10.81	53.65	14.43	16.81	18.18	27.49	1.78
CL02	ALTERED	CPX	2.00	2.00	3.00	7.19	120.60	9.93	179.16	12.78	8.29	450.95	16.81	47.20	16.45	1.29
CL22	ALTERED	CPX	2.00	2.47	39.50	2.00	3.00	12.67	110.46	20.49	19.69	27.34	16.81	19.61	9.16	1.62
CL34	ALTERED	CPX	2.00	2.38	18.72	2.89	3.69	12.24	163.00	20.98	15.77	1006.57	16.81	29.27	13.00	1.71
CL39	ALTERED	CPX	2.00	3.53	684.81	2.00	3.00	5.46	44.27	15.86	106.49	1735.55	35.56	12.91	4.26	2.90
CS39	ALTERED	OL	2.00	3.53	685.94	3.46	3.00	7.68	74.14	17.35	95.87	7008.90	60.49	6.75	16.91	2.26
CL46	ALTERED	OL	2.00	3.33	3.00	4.65	92.94	6.88	273.05	11.23	0.52	224.22	16.81	61.42	12.98	1.63
CS7-1	ALTERED	OL	2.00	2.00	82.13	2.00	3.00	3.00	128.79	10.00	71.04	63.71	16.81	10.40	19.19	3.33
CL35B	ALTERED	OL	2.00	2.00	64.11	2.00	3.00	3.00	47.79	20.26	44.41	205.80	16.81	15.02	4.26	6.75
CL6B2(3)	ALTERED	OL	2.00	2.00	12.34	2.00	3.00	7.21	125.12	17.70	10.76	32.72	16.81	24.29	6.04	2.45
CL6B3(1)	ALTERED	OL	2.00	3.02	13.98	2.00	27.84	5.02	147.18	12.89	11.90	540.94	16.81	26.96	8.19	2.57
CL6B3(2)	ALTERED	OL	2.00	3.06	16.40	2.00	15.60	5.44	167.23	15.31	13.98	813.29	16.81	29.36	4.87	2.81
CL6B3-1	ALTERED	OL	2.00	2.00	13.14	2.00	22.25	16.29	135.62	14.31	11.47	378.42	16.81	26.16	5.18	0.88
CS35-01	ALTERED	OL	2.00	2.00	60.95	2.00	3.00	4.21	63.50	21.67	55.38	58.58	16.81	4.77	16.28	5.15
CS35-02	ALTERED	OL	2.00	2.00	23.48	2.00	3.00	3.21	52.56	16.46	20.89	45.61	16.81	8.42	19.85	5.13
CL21B	ALTERED	OL	2.00	3.46	74.83	2.85	6.64	4.95	124.82	10.72	34.16	498.27	16.92	31.45	5.07	2.17
CL29	ALTERED	OL	2.00	5.11	27.94	2.00	12.24	12.12	108.03	25.02	16.94	194.56	16.81	30.38	15.67	2.06
CL44	ALTERED	OL	2.00	2.90	37.33	2.00	13.24	5.07	93.41	14.20	34.88	379.67	16.81	48.78	977.00	2.80
1	ALTERED	OPX	43.23	22.43	61.72	7.94	99.51	12.79	143.55	45.15	87.60	158.79	80.27	99.10	33.00	3.53
CL53A	ALTERED	OPX	5.27	19.07	333.51	12.00	54.39	19.55	59.87	35.64	68.20	2256.25	115.70	145.33	13.20	1.82

APPENDIX 7: MAJOR ELEMENT GEOCHEMISTRY OF THE HOST ROCKS AT DWARSRIVIER MINE.

		Analyses are given in wt %													
SAMPLE NAME	**ROCK TYPE**	**SiO_2**	**TiO_2**	**Al_2O_3**	**FeO**	**MnO**	**MgO**	**CaO**	**Na_2O**	**K_2O**	**P_2O_5**	**Cr_2O_3**	**LOI**	**Total**	Mg#
DWR 74/06	Pyroxenite	41.25	0.44	16.11	8.36	0.22	23.21	4.79	0.68	0.12	0.07	5.22	1.20	101.66	83.19
DWR 74/09	Pyroxenite	50.18	0.28	12.48	7.53	0.23	21.75	4.49	0.62	0.14	0.05	3.45	0.20	101.40	83.73
DWR 74/11	Pyroxenite	52.17	0.22	11.68	6.30	0.22	22.84	3.98	0.48	0.16	0.11	3.26	0.20	101.64	86.59
DWR 74/ 13	Pyroxenite	42.50	0.44	17.89	9.02	0.19	19.68	4.69	0.35	0.05	0.03	4.56	1.20	100.58	79.55
DWR 74/21	Pyroxenite	45.29	0.32	13.98	9.68	0.19	19.57	4.56	0.66	0.10	0.03	4.89	1.80	101.06	78.28
DWR 74/27	Pyroxenite	47.60	0.45	15.33	10.75	0.20	18.98	3.13	0.59	0.09	0.03	3.13	0.96	101.24	75.89
DWR 74/33	Pyroxenite	52.52	0.18	13.62	1.82	0.27	28.33	1.93	0.03	0.11	0.02	1.93	0.20	100.98	96.51
DWR 74/34	Pyroxenite	45.74	0.32	14.70	5.78	0.25	24.26	3.01	0.08	0.12	0.02	3.01	2.70	99.98	88.19
DWR172/01	Pyroxenite	35.95	0.51	17.19	10.32	0.20	14.68	2.82	0.61	0.17	0.03	17.43	1.20	101.11	71.72
DWR172/06	Pyroxenite	54.27	0.27	12.75	6.37	0.22	19.06	3.73	0.74	0.35	0.08	2.10	1.30	101.24	84.21
DWR172/07	Pyroxenite	52.46	0.29	13.38	7.00	0.23	18.65	3.91	0.83	0.22	0.06	2.90	0.90	100.83	82.60
DWR172/09	Pyroxenite	55.91	0.18	11.96	5.64	0.23	20.46	4.13	0.53	0.20	0.05	0.65	1.30	101.24	86.60
DWR172/27	Pyroxenite	49.66	0.35	13.65	6.97	0.22	18.75	2.91	0.89	0.25	0.07	6.22	1.50	101.43	82.75
DWR172/28	Pyroxenite	52.93	0.28	12.42	5.93	0.21	19.22	3.97	0.69	0.38	0.06	3.84	1.60	101.54	85.24
DWR172/29	Pyroxenite	45.51	0.43	14.40	7.46	0.21	17.18	4.08	0.78	0.20	0.04	9.65	0.60	100.53	80.40
DWR172/30	Pyroxenite	50.78	0.30	12.98	6.63	0.21	19.00	3.72	0.72	0.25	0.08	5.28	0.50	100.44	83.61

APPENDIX 8: TRACE ELEMENT GEOCHEMISTRY OF THE HOST ROCKS AT DWARSRIVIER MINE.

		Analyses are given in ppm													
SAMPLE NAME	ROCK TYPE	Cu	Ni	Rb	Sr	Y	Zn	Zr	Co	Cr	S	V	Ba	La	Zr/Y
DWR 74/06	Pyroxenite	2	352	1	191	5	57	20	138	103155	61	794	40	15	4.00
DWR 74/09	Pyroxenite	4	767	8	60	5	290	26	88	16980	0	206	15	11	5.20
DWR 74/11	Pyroxenite	3	531	6	66	9	96	32	80	9555	371	162	59	9	3.56
DWR 74/ 13	Pyroxenite	5	514	8	55	11	77	26	150	126382	0	929	23	12	2.36
DWR 74/21	Pyroxenite	4	820	2	51	5	317	27	119	83051	57	622	21	17	5.40
DWR 74/27	Pyroxenite	3	647	5	68	5	210	23	138	117702	61	712	29	23	4.60
DWR 74/33	Pyroxenite	4	796	5	57	5	260	19	91	8702	27	139	50	-2	3.80
DWR 74/34	Pyroxenite	2	632	3	6	3	93	20	114	47495	130	433	61	4	6.67
DWR172/01	Pyroxenite	2	841	11	62	4	367	35	166	134301	80	1037	48	14	8.75
DWR172/06	Pyroxenite	18	547	10	61	8	105	46	95	15363	71	233	124	5	5.75
DWR172/07	Pyroxenite	16	570	9	59	5	112	37	91	20713	67	265	66	1	7.40
DWR172/09	Pyroxenite	10	529	8	49	11	70	44	86	4784	31	122	68	0	4.00
DWR172/27	Pyroxenite	30	585	5	50	7	153	31	95	46380	162	368	66	8	4.43
DWR172/28	Pyroxenite	17	528	16	43	7	108	38	95	28199	76	254	98	4	5.43
DWR172/29	Pyroxenite	23	621	8	53	5	210	29	119	72356	128	527	60	8	5.80
DWR172/30	Pyroxenite	21	553	12	50	7	131	60	101	39134	92	319	72	13	8.57